

FABRICATION OF NANOSTRUCTURED ZINC OXIDE VIA  
ELECTRODEPOSITION AND HEAT TREATMENT

Miss Thanyalux Wanotayan



จุฬาลงกรณ์มหาวิทยาลัย

CHULALONGKORN UNIVERSITY

บทคัดย่อและแฟ้มข้อมูลฉบับเต็มของวิทยานิพนธ์ตั้งแต่ปีการศึกษา 2554 ที่ให้บริการในคลังปัญญาจุฬาฯ (CUIR)  
เป็นแฟ้มข้อมูลของนิสิตเจ้าของวิทยานิพนธ์ ที่ส่งผ่านทางบัณฑิตวิทยาลัย

The abstract and full text of theses from the academic year 2011 in Chulalongkorn University Intellectual Repository (CUIR)  
are the thesis authors' files submitted through the University Graduate School.

A Dissertation Submitted in Partial Fulfillment of the Requirements  
for the Degree of Doctor of Philosophy Program in Nanoscience and Technology  
(Interdisciplinary Program)  
Graduate School  
Chulalongkorn University  
Academic Year 2016  
Copyright of Chulalongkorn University

การสังเคราะห์สังกะสีออกไซด์โครงสร้างนาโนโดยการชุบเคลือบด้วยไฟฟ้าและกระบวนการทาง  
ความร้อน



วิทยานิพนธ์นี้เป็นส่วนหนึ่งของการศึกษาตามหลักสูตรปริญญาวิทยาศาสตรดุษฎีบัณฑิต  
สาขาวิชาวิทยาศาสตร์นาโนและเทคโนโลยี (สหสาขาวิชา)  
บัณฑิตวิทยาลัย จุฬาลงกรณ์มหาวิทยาลัย  
ปีการศึกษา 2559  
ลิขสิทธิ์ของจุฬาลงกรณ์มหาวิทยาลัย

Thesis Title	FABRICATION OF NANOSTRUCTURED ZINC OXIDE VIA ELECTRODEPOSITION AND HEAT TREATMENT
By	Miss Thanyalux Wanotayan
Field of Study	Nanoscience and Technology
Thesis Advisor	Associate Professor Yuttanant Boonyongmaneerat
Thesis Co-Advisor	Associate Professor Joongjai Panpranot

---

Accepted by the Graduate School, Chulalongkorn University in Partial  
Fulfillment of the Requirements for the Doctoral Degree

..... Dean of the Graduate School  
(Associate Professor Sunait Chutintaranond)

#### THESIS COMMITTEE

..... Chairman  
(Associate Professor Vudhichai Parasuk)

..... Thesis Advisor  
(Associate Professor Yuttanant Boonyongmaneerat)

..... Thesis Co-Advisor  
(Associate Professor Joongjai Panpranot)

..... Examiner  
(Dr. Jiaqian Qin)

..... Examiner  
(Assistant Professor Sukkaneste Tungasmita)

..... External Examiner  
(Dr. Sittha Sukkasi)

..... External Examiner  
(Dr. Wannipha Amatyakul)

ชื่อย่อ : วโนทยาน : การสังเคราะห์สังกะสีออกไซด์โครงสร้างนาโนโดยการชุบเคลือบด้วยไฟฟ้าและกระบวนการทางความร้อน (FABRICATION OF NANOSTRUCTURED ZINC OXIDE VIA ELECTRODEPOSITION AND HEAT TREATMENT) อ.ที่ปรึกษาวิทยานิพนธ์หลัก: รศ. ดร. ยุทธนันท์ บุญยมณีรัตน์, อ.ที่ปรึกษาวิทยานิพนธ์ร่วม: รศ. ดร. จุงใจ ปั่นประจวบ, หน้า.

สังกะสีออกไซด์เป็นวัสดุที่มีแนวโน้มในการใช้เป็นตัวเร่งปฏิกิริยาแบบใช้แสงในการบำบัดสารปนเปื้อนอินทรีย์ในน้ำ ในงานวิจัยนี้จะทำการศึกษาอย่างเป็นระบบของกระบวนการสังเคราะห์แผ่นฟิล์มสังกะสีออกไซด์โครงสร้างนาโนโดยการชุบเคลือบด้วยไฟฟ้าและกระบวนการทางความร้อน เพื่อวิเคราะห์ความสัมพันธ์ระหว่างกระบวนการผลิต โครงสร้าง และ คุณสมบัติของฟิล์มสังกะสีและสังกะสีออกไซด์ งานวิจัยนี้ถูกแบ่งออกเป็นสามส่วน ในส่วนแรกมีการศึกษาถึงผลกระทบของความหนาแน่นกระแสไฟฟ้าและสารเติมแต่งต่อโครงสร้างและสมบัติของฟิล์มสังกะสี ได้พบว่าทั้งความหนาแน่นกระแสไฟฟ้าและสารเติมแต่งมีบทบาทสำคัญในการควบคุมโครงสร้างของฟิล์มสังกะสีและการเกิดของสังกะสีออกไซด์ สารเติมแต่งมีผลต่อการพัฒนาโครงสร้างและความต้านทานการกัดกร่อนของชั้นเคลือบ เมื่อใช้กระแสไฟฟ้าตรงที่  $2 \text{ A/dm}^2$  โดยไม่มีสารเติมแต่ง พบโครงสร้างสังกะสีรูปทรงแท่งขนาดเล็กที่มีการพันกันและประกอบกันเป็นกลุ่มผลึกขนาดเล็ก ส่วนที่สองศึกษาถึงผลกระทบของอุณหภูมิต่อโครงสร้างและสัณฐานวิทยาบนพื้นผิวของฟิล์มสังกะสีออกไซด์ ได้ทำการศึกษาปฏิกิริยาการเกิดออกซิเดชันทั้งที่อุณหภูมิต่ำกว่าและสูงกว่าจุดหลอมเหลวของสังกะสี สำหรับอุณหภูมิที่ต่ำกว่าจุดหลอมเหลว สังกะสีออกไซด์รูปทรงแท่งขนาดนาโนถูกสร้างและเติบโตขึ้น โดยใช้โครงสร้างของสังกะสีเป็นแม่แบบ แต่อนุภาคสังกะสีทรงกลมถูกสร้างขึ้นสำหรับอุณหภูมิสูงกว่าจุดหลอมเหลว ส่วนที่สาม ฟิล์มบางสังกะสีออกไซด์ที่มีลักษณะสัณฐานวิทยาบนพื้นผิวที่แตกต่างกัน ได้ถูกนำมาทดสอบเพื่อหาคุณสมบัติโฟโตแคตาไลติก จากการทดสอบพบว่าฟิล์มบางที่ผ่านการอบด้วยความร้อนที่อุณหภูมิ 500 องศาเซลเซียสแสดงให้เห็นถึงประสิทธิภาพในการย่อยสลายสีเมทิลีนบลูภายใต้การฉายรังสียูวีได้ดีที่สุด และนี่เป็นผลมาจากพื้นที่ผิวที่สูงของชั้นฟิล์ม ผลสรุปในงานนี้พบว่าฟิล์มบางสังกะสีออกไซด์โครงสร้างนาโนที่มีคุณสมบัติโฟโตแคตาไลติกที่ดีสามารถสังเคราะห์ขึ้นได้จากการชุบเคลือบด้วยไฟฟ้าและกระบวนการทางความร้อน

สาขาวิชา วิทยาศาสตร์นาโนและเทคโนโลยี ลายมือชื่อนิพนธ์ .....

ปีการศึกษา 2559 ลายมือชื่อ อ.ที่ปรึกษาหลัก .....

ลายมือชื่อ อ.ที่ปรึกษาร่วม .....

# # 5487772020 : MAJOR NANOSCIENCE AND TECHNOLOGY

KEYWORDS: ZINC OXIDE / ELECTRODEPOSITION / HEAT TREATMENT / PHOTOCATALYST

THANYALUX WANOTAYAN: FABRICATION OF NANOSTRUCTURED ZINC OXIDE VIA ELECTRODEPOSITION AND HEAT TREATMENT.  
ADVISOR: ASSOC. PROF. YUTTANANT BOONYONGMANEERAT, CO-ADVISOR: ASSOC. PROF. JOONGJAI PANPRANOT, pp.

Zinc oxide is a promising material used as a photocatalyst to treat organic contaminants in water. To obtain good photocatalytic activity in the film, porosity and high surface area are often promoted. In this work, a systematic study of the fabrication process of nanostructured zinc oxide thin film via electrodeposition and heat treatment is carried out. The process-structure-property relationship of both zinc and zinc oxide films are investigated. This research is divided into three parts. In the first part, the effects of current density and additives on the structure and property of zinc film are studied. Both current density and additives play an important role in controlling the structure of the zinc film and also in the formation of zinc oxide. Additives influence the texture development of the deposits and in turn influence the corrosion resistance in the coatings. Upon applying a direct current of 2 A/dm<sup>2</sup> with no additive, sub-micron zinc rods that are intertwined and formed clusters of granules is observed. In the second part, the effect of heat treatment temperature on the structure and surface morphology of zinc oxide thin films are analyzed. The oxidation reaction both below and above the melting point of zinc metal are studied. For temperature below the melting point, ZnO nanoneedle is formed and grown using the zinc deposit structure as a template. However, spherical ZnO particles agglomerate as parts of the rod structure for temperature above the melting point. In the third part, ZnO thin film with different surface morphologies is tested for the photocatalytic property. ZnO thin film annealed at 500°C shows the best photocatalytic activity in degrading MB dyes under UV light irradiation. This may be attributed to the higher surface area of the film. In conclusion, nanostructured ZnO thin film with good photocatalytic property can be synthesized from electrodeposition and heat treatment method.

Field of Study: Nanoscience and Technology Student's Signature .....

Academic Year: 2016

Advisor's Signature .....

Co-Advisor's Signature .....

## ACKNOWLEDGEMENTS

First and foremost, I would like to express my deepest gratitude to my thesis advisor, Associate Professor Dr. Yuttanant Boonyongmaneerat, and co-advisor, Associate Professor Dr. Joongjai Panpranot, for their continuous support and guidance. Associate Professor Dr. Yuttanant Boonyongmaneerat motivates, encourages, and steers me in the right direction whenever I have problems.

I am grateful to my thesis committee Associate Professor Dr. Vudhichai Parasuk, Assistant Professor Dr. Sukkaneste Tungasmita, Dr. Jiaqian Qin, Dr. Sittha Sukkasi, and Dr. Wannipha Amatyakul for the valuable advices and comments.

I sincerely thank Professor Atsushi Nishikata and Associate Professor Dr. Eiji Tada for giving me the opportunity to do research at Tokyo Institute of Technology, Japan. Their guidance and support are greatly appreciated.

I would also like to thank my colleagues from PORETEGE research group and all my friends for their suggestions and encouragement.

I would like to acknowledge the financial support from the Graduate School for the tuition fees (5 years), Nanoscience and Technology Program, the 90th Anniversary of Chulalongkorn University (Ratchadaphiseksomphot Endowment Fund), and Overseas Research Experience Scholarship for Graduate Student.

Last but not the least, I would like to express my profound gratitude to my parents and family for providing me with unfailing support, understanding and continuous encouragement throughout my years of study and research.

## CONTENTS

	Page
THAI ABSTRACT .....	iv
ENGLISH ABSTRACT.....	v
ACKNOWLEDGEMENTS .....	vi
CONTENTS.....	vii
List of Figures .....	9
List of Tables .....	11
CHAPTER I INTRODUCTION.....	12
1.1 Motivation.....	12
1.2 Objective.....	14
1.3 Scope of Research.....	14
1.3.1 Influenced of processing variables on the structure and properties of zinc .....	15
1.3.2 Heat treatment of zinc .....	15
1.3.3 Photocatalytic Property of ZnO.....	15
1.4 Outcome of the research .....	16
1.5 Outline of the thesis .....	16
CHAPTER II LITERATURE REVIEW .....	17
2.1 Photocatalyst.....	17
2.2 Fabrication process of ZnO photocatalyst .....	19
2.2.1 Powder photocatalyst .....	19
2.2.2 Thin Film photocatalyst.....	20
2.3 Electrodeposition and Heat Treatment .....	21
2.3.1 Electrodeposition.....	22
2.3.1.1 Bath composition.....	22
2.3.1.2 Current Density .....	23
2.3.1.3 Additives .....	23
2.3.1.4 Post treatment .....	24
2.3.1.5 Electroplated zinc .....	25

	Page
2.3.1.6 Hull Cell .....	26
2.3.2 Heat treatment .....	28
CHAPTER III EXPERIMENTAL PROCEDURE.....	30
3.1 PART I: Electrodeposition of Zinc.....	30
3.1.1 Sample Preparation.....	30
3.1.2 Hull Cell .....	32
3.1.3 Electrodeposition.....	33
3.1.4 Conversion Coatings .....	34
3.1.6 Characterization.....	35
3.2 PART II: Heat treatment of Zinc .....	36
3.2.1 Thermal Annealing.....	37
3.2.2 Characterization.....	37
3.3 PART III: Photocatalytic Test .....	37
3.3.1 Photocatalytic Experiments.....	37
3.3.2 Photoelectrochemical Measurements .....	38
CHAPTER IV RESULTS AND DISCUSSION.....	40
4.1 PART I: Influence of process variables on structure and properties of zinc.....	40
4.1.1 Sample Characteristics .....	40
4.1.2 Corrosion Behaviors.....	50
4.1.3 Discussions.....	56
4.2 PART II: Heat treatment of Zinc .....	58
4.2.1 Sample Characteristics .....	58
4.2.2 Discussions.....	61
4.3 PART III: Photocatalytic Zinc Oxide.....	64
CHAPTER V CONCLUSION.....	75
REFERENCES .....	78
APPENDIX.....	86
VITA.....	98



## List of Figures

Figure 1 The mechanism of a photocatalyst .....	18
Figure 2 Electrodeposition process setup .....	25
Figure 3 Schematic diagram of Hull cell .....	27
Figure 4 Sample preparation process .....	31
Figure 5 Sample after pretreatment.....	31
Figure 6 Hull Cell setup.....	32
Figure 7 Experimental conditions.....	34
Figure 8 Sample subjected to corrosion test. ....	35
Figure 9 Electrochemical cell setup.....	36
Figure 10 Photocatalytic setup.....	38
Figure 11 Hull cell test of zincate bath without additives. ....	40
Figure 12 Electrodeposited zinc at (a) 2 A/dm <sup>2</sup> and (b) 4 A/dm <sup>2</sup> .....	41
Figure 13 Defect sample .....	42
Figure 14 SEM image of electrodeposited zinc at 2 A/dm <sup>2</sup> (a) 200x and (b) 10000x and at 4 A/dm <sup>2</sup> (c) 200x and (d) 10000x.....	42
Figure 15 Effects of current density (a) 2 A/dm <sup>2</sup> and (b) 4 A/dm <sup>2</sup> on nucleation and growth .....	43
Figure 16 Electrodeposited zinc samples with additives. ....	43
Figure 17 Effects of additives on nucleation and growth. ....	44
Figure 18 SEM micrographs of electrogalvanized samples: (a) EZ1, (b) EZ2, and (c) EZ3. ....	45
Figure 19 XRD profiles of the zinc samples (a) before and (b) after completion of the 6-week corrosion test. ....	47
Figure 20 XRD profiles of the chromated samples (a) before and (b) after completion of the 6-week cyclic exposure corrosion test. ....	48
Figure 21 Cross-sectional SEM micrograph of electrogalvanized sample with steel substrate, zinc layer and chromium conversion layer. ....	49
Figure 22 OM images of the samples following each week of the cyclic exposure corrosion test.....	50

Figure 23 Coating thickness loss of the electrogalvanized samples in each week of the cyclic exposure corrosion test .....	51
Figure 24 Nyquist, Bode and phase shift plots of the zinc samples from the EIS analysis following the 1st and 6th week of the cyclic exposure test .....	53
Figure 25 Nyquist, Bode and phase shift plots of the chromated samples from the EIS analysis following the 1st and 6th week of the cyclic exposure test .....	54
Figure 26 Electrical equivalent circuits of the samples without (a) and with (b) passive oxide film in a saline solution based on the electrochemical impedance spectroscopy (EIS).....	55
Figure 27 Heat treatment at 500°C of samples (a) EZ2, (b) EZ0, and (c) EZ0' .....	58
Figure 28 SEM images of heat treated samples (a) EZ2, (b) EZ0, and (c) EZ0' .....	58
Figure 29 EZ0 samples at different heat treatment temperature (a) 300°C, (b) 400°C, (c) 500°C, and (d) 600°C.....	59
Figure 30 SEM images of heat treated zinc without additive at (a) 300°C, (b) 400°C, (c) 500°C, and (d) 600°C.....	60
Figure 31 XRD pattern.....	62
Figure 32 DRS of ZnO at different heat treatment temperature. ....	63
Figure 33 SEM image of ZnO photocatalyst (a) 400°C, (b) 500°C, and(c) 600°C after photocatalytic test. ....	65
Figure 34 XRD patterns of ZnO after photocatalytic test.....	66
Figure 35 Photolysis test.....	66
Figure 36 Photocatalytic activity of ZnO powder.....	67
Figure 37 Photocatalytic test of ZnO with and without additives .....	68
Figure 38 Typical absorbance spectrum of MB solution with sintered ZnO photocatalyst (a) 400°C, (b) 500°C, and (c) 600°C. ....	69
Figure 39 MB solution sampling with ZnO photocatalyst (a) 400°C, (b) 500°C, and (c) 600°C. ....	70
Figure 40 Concentration of MB with respect to irradiation time.....	71
Figure 41 Nyquist plot of EIS for ZnO under UV light irradiation.....	73
Figure 42 Repeated experiments of ZnO photocatalyst sintered at 500°C.....	74

## List of Tables

Table 1 The additives for non-chromated and chromated electrodeposited zinc samples.....	33
Table 2 XRF chromium to zinc content ratio in the top-coat vicinity of the deposit samples.....	49
Table 3 Numerical data of equivalent circuit elements of the non-chromated and chromated electrogalvanized samples from the EIS analysis following the 1st and 6th week of the cyclic exposure test .....	55



# CHAPTER I

## INTRODUCTION

### 1.1 Motivation

Industrialization is the root cause to environmental pollution and one of the main reasons is the industrial waste. The discharge of waste from factories into the rivers contained untreated effluents and they are toxic and hazardous. From the environmental viewpoint, the removal of color from wastewater is necessary. Various techniques have been applied to degrade the organic contaminants and photocatalysis appeared to be one of the most promising methods as it can both decolorize and degrade the textile dye.

Semiconducting oxide photocatalysts, such as zinc oxide (ZnO), titanium dioxide (TiO<sub>2</sub>), iron oxide (Fe<sub>2</sub>O<sub>3</sub>), and tungsten oxide (WO<sub>3</sub>), have increasingly received high attentions, as the materials offer great potentials to treat organic contaminants in water and air [1-4]. While TiO<sub>2</sub> is now being employed relatively widely, ZnO is of increasing interest, owing to its band gap comparable to TiO<sub>2</sub>, relatively low cost and non-toxic in nature. ZnO is a promising material due to its unique properties such as strong oxidation ability, wide band gap, and large exciton binding energy at room temperature [5-7].

During the photocatalysis, the semiconductor particles were employed in suspension [8-11]. However, in the practical view point, the powder form in the suspension tends to aggregate and is hard to recover and recycle [12]. Hence, researchers have been immobilizing ZnO particles or layers on a surface. A systematic study that comprehensively analyzes the relationship between

microstructure and photocatalytic properties of ZnO films is rather limited [11, 13, 14]. In the past years, interest of nanoscale materials has increased significantly. Photocatalysts in the form of nanorods, nanowires, and thin porous films were applied as they provide high surface area [13, 15].

Various techniques can be used to synthesize nanostructured ZnO films. The synthesis methods include chemical vapor deposition [16], sputtering [17], sol-gel [18, 19], thermal evaporation [20, 21] and electrodeposition [22]. Electrodeposition is an attractive method to produce nanomaterials [23]. It is a simple, rapid and cost effective process. It can be done at low temperature and controls the film thickness and morphology accurately.

Electrodeposition is a process which uses electric current to deposit thin film coating onto a conducting substrate. Various parameters including bath compositions, additives and current densities can affect the film characteristic. Electrodeposition was used to deposit zinc or zinc oxide thin film onto the substrate. The obtained films then undergo further heat treatment. The microstructure and morphology of zinc oxide can be affected by the heat treatment temperature, time and environment [24-26]. In addition, the structure of ZnO may be influenced by the structure of electrodeposited zinc.

Electrodeposition followed by heat treatment is an important approach to synthesize ZnO film. This work aims to develop ZnO film with good photocatalytic property. First, the influence of electroplating parameters on the structure and property of zinc are studied. The zinc film obtained could be an important precursor for the ZnO film under heat treatment. Different temperatures are varied to modify the structure of the ZnO film. ZnO film with high surface roughness provides high

surface area for good photocatalytic property. The photocatalytic activity and reusability of the ZnO films is tested under UV light irradiation. In addition, the process-structure-property relationships could be useful for further implementation.

## 1.2 Objective

The main objectives of this research are:

1. To investigate the fabrication of nanostructured zinc oxide via the electrodeposition and subsequent heat treatment technique
2. To study the processing parameters, structures, and property of electroplated zinc
3. To study the relationship of nanostructure and photocatalytic activity of zinc oxide

## 1.3 Scope of Research

This thesis focused on the study of fabrication of zinc oxide nanostructures via electrodeposition and heat treatment. The experiment aims to develop the process-structure-property relationship. In order to accomplish the three objectives mentioned above, the scope of this thesis is divided into three parts. First, zinc is deposited via electrodeposition method and followed by heat treatment of zinc in the second part. Then the photocatalytic property of ZnO thin films is studied. The studies of all parts are in successive order as below:

### **1.3.1 Influenced of processing variables on the structure and properties of zinc**

Zinc films are deposited by electrodeposition method. The characteristic of the film can be controlled by processing parameters like bath compositions, additives, and applied current densities. The effects of current density and additives in the plating bath on the microstructure of zinc film are studied. The structure of zinc can be one of the key factors influencing the formation of ZnO structure. The microstructures and property of zinc film are discussed to further develop the ZnO films. In addition, the corrosion property of the zinc film is studied as the structure and crystallographic texture of the electrodeposited zinc may in turn influence the corrosion behavior of the metal coating.

### **1.3.2 Heat treatment of zinc**

Heat treatment is applied to transform the zinc film obtained in the first part to ZnO film. In general, ZnO film with high surface area and surface roughness has good photocatalytic property. The film is treated at different temperatures to modify the structure of the film which in turn affects its property. In this part, the effects of the heat treatment temperature on the structure of ZnO film are investigated.

### **1.3.3 Photocatalytic Property of ZnO**

In the last part, ZnO thin films obtained at different temperature are tested for its photocatalytic activity under UV light irradiation. The effects of the structure and morphology of the ZnO film on the photocatalytic activity are discussed. The ZnO film with the best photocatalytic activity is further tested for the reusability of the film and for the photocorrosion property.

#### 1.4 Outcome of the research

- The effects of the processing parameters on the structure of zinc and zinc oxide
- The effects of the structure of zinc on corrosion behaviors
- The optimal condition of ZnO film for the photocatalytic reaction

#### 1.5 Outline of the thesis

This research focuses on the fabrication of zinc oxide via electrodeposition and heat treatment. The thesis consists of 5 chapters as listed below:

**Chapter I:** This chapter consists of the overview, scope and outcome of the research.

**Chapter II:** This chapter presents the knowledge and theory behind this thesis. The literature reviews on the processing of zinc and zinc oxide and their property are discussed.

**Chapter III:** This chapter presents the synthesis method and characterization techniques of zinc and zinc oxide films. The experimental setup of the corrosion test and photocatalytic test are described.

**Chapter IV:** The process-structure-property relationships of zinc and zinc oxide are shown and discussed.

**Chapter V:** This chapter summarizes and concludes the work in this thesis.

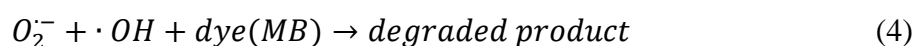
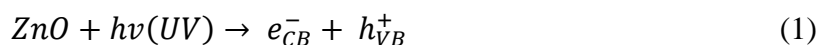


## CHAPTER II

### LITERATURE REVIEW

#### 2.1 Photocatalyst

Photocatalysis is a process which uses light to activate a substance that modifies a chemical reaction without itself being consumed in the end. The photocatalytic activity depends on the ability of the catalyst to create electron-hole pairs. When a photocatalyst is illuminated by light with energy equal to or greater than the band gap energy, electrons in the valence band can be excited to the conduction band, leaving a positive hole in the valence band. If the charged separation is maintained, the electrons and holes migrate to the surface of the semiconductor and participate in an oxidation and reduction reactions. Holes react with water to form highly reactive hydroxyl radicals while electron reacts with oxygen to form a superoxide radical anion. These radicals are the key factor for partial or complete mineralization of the organic substances. The electron-hole pairs breakdown the organic compound into carbon dioxide and water. The electron and hole could react with the absorbed reactants or it could recombine. A simplified mechanism could be presented in Fig. 1 and expressed as below:



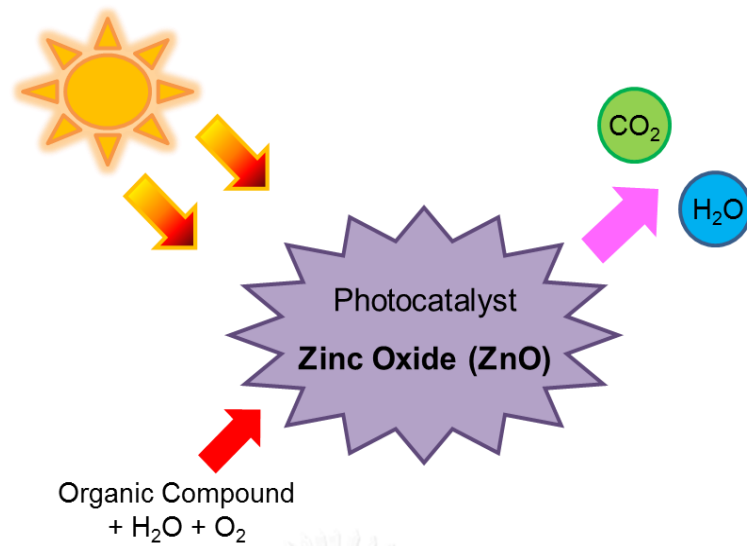
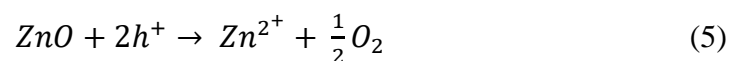


Figure 1 The mechanism of a photocatalyst

As the degradation of chemicals take place at the surface of the photocatalyst, the surface morphology plays an important role. The film with higher surface roughness has higher surface area for the activity to take place and hence a better photocatalytic activity. In a practical usage of the photocatalyst, the photocatalytic stability of the ZnO film is an important concern for the recyclability of the photocatalyst. When the ZnO photocatalyst are irradiated under UV light, the photogenerated holes can induced the photocorrosion of ZnO films. The overall photocorrosion process can be presented as



where  $h^+$  are the positive holes created by the action of UV irradiation. When photocorrosion occurred, there is a partial dissolution of Zn and the collapse of ZnO structure [27].

## 2.2 Fabrication process of ZnO photocatalyst

ZnO photocatalyst is being used both in the form of powder or thin film. Powders are usually more effective than film supported catalyst due to the higher surface area and better accessibility of the pollutants to the surface of the photocatalyst. However, the typical ZnO powder catalysts show tendency to aggregate and difficulty in recovery and recycling and is relatively expensive for scaling up [12]. Hence, ZnO film supported photocatalyst has been developed to increase the performance of the film.

### 2.2.1 Powder photocatalyst

Many research works on ZnO photocatalysts have been focusing on developments of ZnO nanoparticles to achieve high surface area and hence more superior photocatalytic activity [14, 28, 29].

The effect of particle size on the photocatalytic activity is studied. Dodd et al. produced nanoparticulate ZnO powders with a controlled particle size and minimal agglomeration from a three-stage process consisting of mechanical milling, heat treatment, and washing. By controlling the temperature of the post-milling heat treatment, the average particle size was controlled over the range of 28-57 nm. The decrease in the average particle size from 57 to 33 nm resulted in an increase in the photocatalytic activity but the photocatalytic activity slightly decreases when the average particle size is reduced to 28 nm. Hence, there is an optimum particle size (33 nm) for a maximum photocatalytic activity [28].

Morphologies can also affect the surface area and photocatalytic activity. Pung et al. successfully synthesized ZnO particles via sol-gel approach using zinc

acetate dehydrate and ammonia solution as precursors. The morphologies of the ZnO particles can be manipulated by the reaction parameters. The effectiveness of ZnO particles with different morphologies, rodlike, ricelike and disklike, on the photocatalytic activity has been studied. The rodlike ZnO particles showed the best photocatalytic efficiency, followed by ricelike and disklike ZnO particles. This may be due to a larger surface area to volume ratio of rodlike ZnO particles. However, disklike ZnO nanoparticles performed poorly and this could be attributed to the presence of ringlike ZnO particles and contamination of Al element from the complexing agent [14].

Furthermore, the structure of the particles can be developed. Ali et al. fabricated ZnO nanoparticles using a simple combustion process. A porous nonuniform size and shape of ZnO nanoparticles were obtained. The nonuniformity is due to the uncontrolled processing parameters. Proper control of the processing parameters might produce a uniform size and shape of the particles. The fabricated ZnO nanoparticles exhibit excellent catalytic properties. The porous structure provides larger surface area with an elevated active surface, hence leading to a better catalytic degradation properties of nanosized ZnO particles over commercial ZnO [29].

### **2.2.2 Thin Film photocatalyst**

The film supported catalyst comprised of immobilizing ZnO particles or layers on a surface or support. To increase the performance of the film, various morphologies and porous ZnO thin films were developed [13, 15, 30]. Wang et al. prepared different porous ZnO film on the surface of alumina substrates by a simple

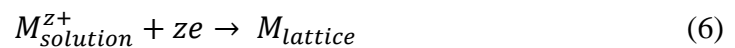
chemical bath deposition method. The porous characteristic of the films changes with increase of sintering temperature. At 300°C, the porous characteristic of the as-prepared ZnO films is kept with the flake totally decomposed of nanoparticles of an average size about 10 nm. With an increase in temperature to 500°C, the porous films are uniform and the particles are interconnected with uniform pores. The particles grow bigger with an average size about 50 nm. The flake like totally disappears at 800°C and big irregular pores are formed with an aggregation of particles of average size about 100 nm. Photocatalytic activity of ZnO films was analysed by measuring the decoloration of Methyl Orange solution. It is found that ZnO film sintered at 500°C demonstrates the highest photocatalytic activity and 300°C shows the lowest photocatalytic activity. Lower decoloration efficiency at 800°C can be due to the reduction of effective surface area for its bigger particle size and at 300°C should be due to the lower particle crystallinity [13].

### 2.3 Electrodeposition and Heat Treatment

Zinc is an important precursor for the preparation of other Zn-based semiconductors such as ZnO, ZnS, and ZnSe [31]. The structure of zinc precursor can also influence the structure of zinc oxide. Electrodeposition followed by heat treatment is an attractive approach to synthesize the ZnO film. Electrodeposition can be done at low temperature and controls the film thickness and morphology accurately. Heat treatment is then applied to modify the film's structure and property.

### 2.3.1 Electrodeposition

Electrodeposition is a process of depositing material onto a conducting surface from an electrolyte containing metal ions by applying electrical current to the system [32]. The reduction of metal ions  $M^{z+}$  in aqueous solution is represented by



The system composed of the immersion of two electrodes, positively charged electrode (anode) and negatively charged electrode (cathode), in an electrolyte and connected to an external power supply to allow current flow. The object to be coated is at the cathode and the source of metal is at the anode. The metal ions are discharged to metal atoms which eventually form the deposit on the surface.

The electroplating parameters must be controlled during electrodeposition since they have significant effect on the coating properties and deposition efficiency. Processing parameters like bath composition, current density, and addition of surfactants are taken into consideration.

#### 2.3.1.1 Bath composition

The bath solution serves as a source of metal to be deposited. It provides conductivity, a stabilizer to stabilize the solution, regulates the corporal form of the deposit and helps dissolve the anodes. Complex ions are formed to stabilize the cation, which becomes much more stable when complexed to some ligand or to metal atoms by coordinate bonding. The electrolytes should conduct electricity in their aqueous solution due to ionization and could be acid, base, or salts. The ions existing

in the electrolyte are responsible for the conduction which results in current or free electrons passing through the wires [33].

### ***2.3.1.2 Current Density***

Electrodeposition process consists of nucleation, growth mechanisms and thickening of the primary layer [34]. The nucleation is enhanced by current density during electrodeposition. Grain size decreased with larger current densities due to the increase in nucleation rate. At low current density, the zinc deposit grows in a close-packed directions in the close-packed planes producing fine dendrites while at higher current density, growth occurs in all directions of the close-packed resulting in flat deposits [35]. Moreover, the current density can have a significant impact on the thickness of the zinc coating. The higher the current density, the greater is the coating thickness. If the current density exceeds practical limits, a wrinkled substrate surface is produced. In addition, a higher current density increases the rate of hydrogen evolution and also increases the rate of hydrogen absorption in the metal substrate. Therefore, it is important to determine the current density values where hydrogen evolution does not occur together with metal deposition.

### ***2.3.1.3 Additives***

Additives are often organic compounds that can affect the growth and structure of the deposits when added to the plating bath in small amounts. The use of additives brightens the deposit, reduces grain size, promotes levelling, and increases current density range. Additives are classified as brighteners or levelers. Brighteners

consist of small molecules with specific functional groups whereas levelers are polymeric or macromolecular compounds [36].

Many researches have been done to study the effects of additives on the plating characteristic and coating appearance [37-42]. Polyamine (PA) was developed to stabilize the cyanide and non-cyanide based electrolytes and modified the morphology of the deposits. Polyvinylalcohol (PVA) helps in reducing the rate of reaction producing more compact and smaller crystals deposition [40, 43]. Aliphatic quaternary ammonium compounds (QACs) have been shown to prevent dendritic growth [44, 45]. Hsieh et al. studied the effects of polyamines on the zinc deposition behavior in an alkaline non-cyanide bath at high current density. Polyethyleneimines and ethyleneimine compounds were shown to smoothen deposit surface. The reaction product of imidazole and epihalohydrin is powerful for depressing the formation of zinc dendrites. Polyquaternary amine salt produces uniform and compact deposit [37].

#### **2.3.1.4 Post treatment**

Upon completion of the electrodeposition process, the sample undergoes post treatment. This normally involves rinsing in water to remove any remaining contaminants and plating bath remnants and thoroughly dry the plated samples. In cases where additional corrosion protection is required or for decorative purpose, the application of passivates and sealers can be included in the post-treatment process [46-48].



### 2.3.1.5 Electroplated zinc

Electrodeposition of zinc, also known as electroplating, is a process of depositing zinc onto the surface of a conducting substrate with the help of electrical current. The typical set up of the electrodeposition system is as shown in Fig.2.

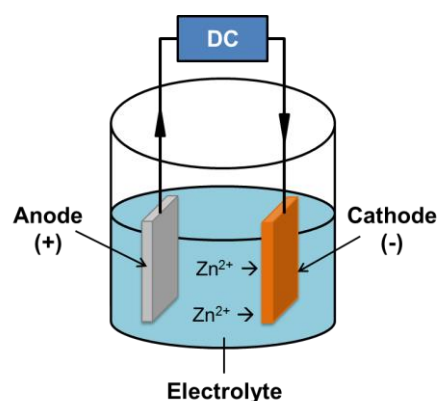


Figure 2 Electrodeposition process setup

For zinc plating, the most widely used plating solutions are categorized as alkaline cyanide zinc, alkaline non-cyanide zinc, and acid zinc [49-51]. Cyanide baths are strongly alkaline solutions containing cyanide ions and additives. The cyanide bath is easy to control as they exhibit stable performance in function of the bath composition and have high throwing power and. The deposits from cyanide baths have relatively poor brightness when compared with acid baths. Alkaline non-cyanide zinc plating baths compose of zinc, caustic soda, and organic additives. The alkaline bath is difficult to control due to a rather narrow optimum operating range of chemical composition (especially the concentration of zinc) and temperature but when properly controlled, a very bright deposit can be produced. An addition of brightener is necessary to produce bright deposit. Acid (chloride) baths have the best leveling ability, high current efficiency, and produce deposits with highest brightness of all the zinc plating baths. They also have high conductivity leading to energy savings [51].

An acid zinc bath is used where it is desirable to have a high plating rate with maximum current efficiency. However, the poor throwing power of these solutions restrict their use to plate only on regular shaped articles and acid bath requires special tank materials due to the high corrosiveness of the solution. Considering pollution hazards and high industrial effluent treatment costs, non-cyanide zinc baths have been introduced in place of cyanide solutions. Low toxicity, simple waste treatment, low make-up costs, good plate distribution and use of steel tanks, are a few practical advantages in choosing an alkaline non-cyanide zinc bath for plating [36, 52, 53].

Zinc plating can be used to significantly increase the corrosion resistance of the underlying substrate. In addition to forming a physical barrier, the zinc serves as a sacrificial coating. This means that the zinc coating will corrode instead of the metal substrate that it protects. When additional corrosion protection is required, chromate conversion coatings are commonly used as post-plating treatment [48]. The corrosion behavior of zinc with and without post treatment can be examined using potentiostat, salt spray test, or the wet-dry cyclic test. This cyclic test condition has been identified as an accelerated test protocol that closely simulates a typical non-sheltered atmospheric saline environment [54-57]. In this work, the corrosion behavior of zinc coatings with and without chromate conversion layers under wet-dry cyclic conditions are analyzed using the electrochemical impedance spectroscopy (EIS) [55, 57, 58].

#### ***2.3.1.6 Hull Cell***

The Hull cell, a simple small electrodeposition cell, is an analytical electrochemical cell used to analyse the performance of chemical bath. The schematic

diagram is shown in Fig.3. The trapezoidal geometry was designed to incorporate a range of current densities in a single experiment. The closest distance and farthest between the electrodes refer to the high current density and low current density respectively. The optimal plating conditions can be determined mainly from the study of the current distribution in the cell. It was designed to examine electroplating rather than mass production processes.

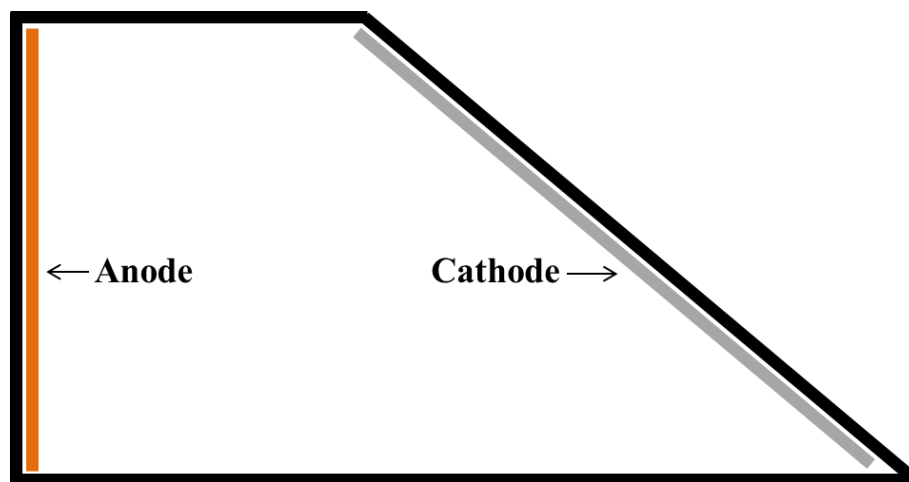


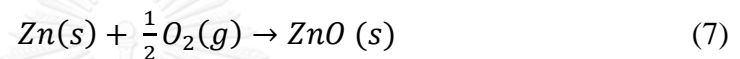
Figure 3 Schematic diagram of Hull cell

A Hull cell can be used to determine process parameters like the approximate bright range, approximate concentration of primary bath components, approximate concentration of addition agents, the throwing power, and effect of temperature and pH variations [40, 59, 60]. The cell holds 267 ml of plating solution. At that volume, there are direct correlations of milliliter or gram additions to 100 gal of plating solution. A 2-g or 2-ml addition to the 267-ml cell equal an addition of 1 oz/gal in your operating bath [61]. Therefore, Hull cell can be applied in daily maintenance, establishing operating parameters, and modifications or improvements of a plating process.

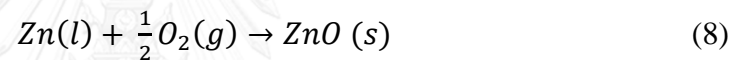
### 2.3.2 Heat treatment

Heat treatment is a controlled process used to alter the microstructure of metals and alloys. The growth condition can be controlled by temperature and time. The oxidation reaction of zinc can occur with two mechanisms, above and below the melting point of zinc metal [62]. Zinc in the liquid phase formed ZnO at temperature more than 420°C and zinc in the solid phase oxidized to form ZnO at temperature less than 420°C.

The oxidation reaction of Zn solid:

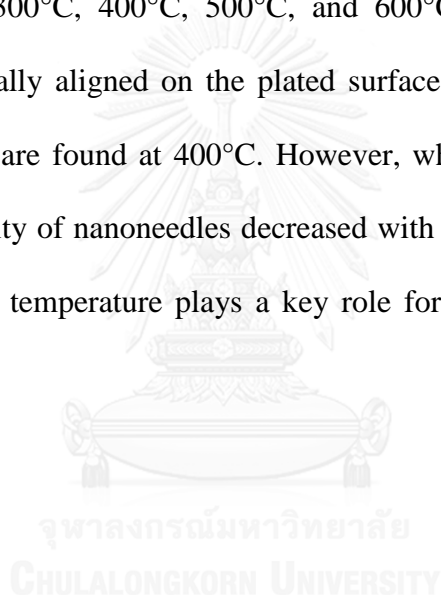


And the chemical reaction of Zn liquid:



Thermal oxidation of pure zinc films has been used to produce the ZnO both below and above the melting point of zinc. Gupta et al. oxidized the films at 250°C, 350°C, and 400°C and obtained ZnO flake like structure. In all cases, both the peaks for Zn and ZnO appeared indicating incomplete oxidation of the Zn films. The results also show that by controlling the texture of Zn film, the texture of ZnO can be controlled by oxidation technique [24]. Ren et al. controlled the oxidation temperature to be below the melting point of zinc and selected 200°C, 250°C, 300°C, 350°C, and 400°C. They successfully synthesized 1-D ZnO nanowires arrays when oxidized in oxygen or in air environment at 350°C and 400°C but no nanowires observed when oxidized below 300°C [63]. Rusu et al. heated the film at various temperatures ranging between 300K and 650K. The complete oxidation of Zn film occurred for the heating temperature at 650K. The increase of heating temperature determines the increase of the surface clusters size and surface roughness [64]. Wen et al. grows

ZnO nanobelt arrays from and on zinc substrates by controlling the thermal oxidation in the presence of oxygen. At 400°C, only sparse and short nanobelts are formed. Increasing the temperature to 550°C, more nanobelts are formed on the substrate and at 600°C, dense and long nanobelt arrays are found. At temperature above melting point of zinc, zinc foils are roughened and distorted and a non-uniform growth of ZnO nanobelt are formed on the substrate [65]. Liu et al. synthesized one-dimensional ZnO nanoneedles by thermal oxidation of zinc nanocrystalline layer by pulse plating technique in air at 300°C, 400°C, 500°C, and 600°C. At 300°C the needle-like materials exist vertically aligned on the plated surface and a well-aligned and high density ZnO needles are found at 400°C. However, when the temperature increases over 400°C, the density of nanoneedles decreased with few nanoneedles. Hence, it is shown that oxidation temperature plays a key role for the synthesis and density of ZnO nanoneedle [66].



## **CHAPTER III**

### **EXPERIMENTAL PROCEDURE**

In this work, zinc oxide is fabricated via electrodeposition and heat treatment. First, zinc film is being deposited as a precursor. The effects of the processing parameters, additives and applied current densities, on the structure and property of zinc films are being investigated. In addition, the corrosion properties of zinc film are tested. Then, the zinc films undergo heat treatment to obtain ZnO thin films. Different nanostructured ZnO thin films are then tested for its photocatalytic property.

#### **3.1 PART I: Electrodeposition of Zinc**

In this part zinc film is electrodeposited onto a substrate. First, Hull cell is used to study the processing parameters. The influence of process parameters on the microstructure and property of zinc film are studied. The corrosion property of the zinc film is studied as the structure and crystallographic texture of the electrodeposited zinc may in turn influence the corrosion behavior of the metal coating. The results from this experiment will be used to further develop the ZnO film. The electrodeposition of zinc process involves sample preparation, plating process, and post treatment.

##### **3.1.1 Sample Preparation**

It is necessary to clean the surface of the substrate thoroughly before the plating process. Sample preparation helps provide the surface for proper adhesion of the zinc coating. The steel substrates ( $5 \times 7 \times 0.1 \text{ cm}^3$ ) were pretreated by soak

cleaning in 50% NaOH at 50°C for 30 mins, rinsed with water, electrocleaning in 5% NaOH at 5V for 30 secs, rinse with water, acid dipping in 5% HCl for 10 secs, and rinse with water as shown in Fig.4.

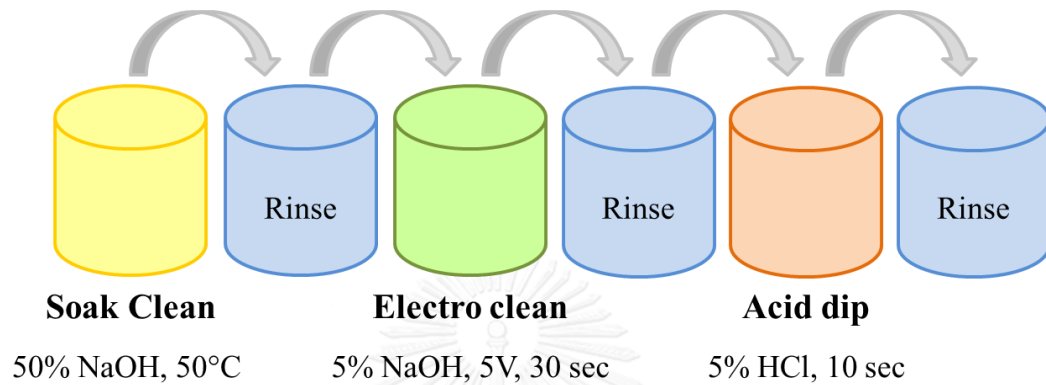


Figure 4 Sample preparation process

The copper substrates ( $2 \times 2.5 \text{ cm}^2$ ) were mounted with resin and polished to a mirror-like finish as seen in Fig.5. The copper plate were ground with SiC paper from coarse to fine (#180, #240, #400, #800, #1200, #2500) and then diamond grinding ( $6 \mu\text{m}$  and  $3 \mu\text{m}$ ).



Figure 5 Sample after pretreatment

### 3.1.2 Hull Cell

Before the plating process, a standard hull cell test was performed to study the current distribution in the cell. The Hull cell setup is as shown in Fig.6. The cell was filled with 267 ml of solution from each bath as indicated in Table 1. The electrodeposition was carried out using a direct current of 1 A for 10 mins at room temperature (25°C). This provides current densities ranging from 0.5 A/dm<sup>2</sup> to 5 A/dm<sup>2</sup> for each sample.



Figure 6 Hull Cell setup

In addition, the hull cell test is also used to study the effects of the processing parameter, such as concentration of additives in the zincate bath, on the appearance of the coatings. The electrodeposition was carried out using a direct current of 2 A/dm<sup>2</sup> for 10 mins at room temperature (25°C).



### 3.1.3 Electrodeposition

The electrodeposition was carried out in an alkaline non-cyanide zincate baths ( $\text{Na}_2\text{Zn}(\text{OH})_4$ ), containing 10 g/L of Zn and 120 g/L of NaOH denoted as bath1, and some selected additives. The three groups of polyamine additives commonly used in the zinc plating process were added to the plating bath. The additives added include imidazole and epihalohydrin for bath 2, polyquaternary amine salt for bath 3, and polyethyleneimine for bath 4 as shown in Table 1. A summary of the experimental conditions is summarized as in Fig.7. Upon deposition, a direct current was applied for 30 mins at 25°C to the plating cell. For bath without additive, a direct current of 2 and 4  $\text{A}/\text{dm}^2$  were applied and the specimens are termed EZ0 and EZ0' respectively. For baths with additives, a direct current of 2  $\text{A}/\text{dm}^2$  was applied and the specimens from the three baths are designated EZ1, EZ2, and EZ3, respectively.

Table 1 The additives for non-chromated and chromated electrodeposited zinc samples

Bath	Sample Set	Additives for Zn deposit	$\text{Cr}^{3+}$
1	EZ0	-	-
2	EZ1	imidazole and epihalohydrin	-
3	EZ2	polyquaternary amine salt	-
4	EZ3	polyethyleneimine	-
2	EZP1	imidazole and epihalohydrin	$\text{Cr}^{3+}$
3	EZP2	polyquaternary amine salt	$\text{Cr}^{3+}$
4	EZP3	polyethyleneimine	$\text{Cr}^{3+}$

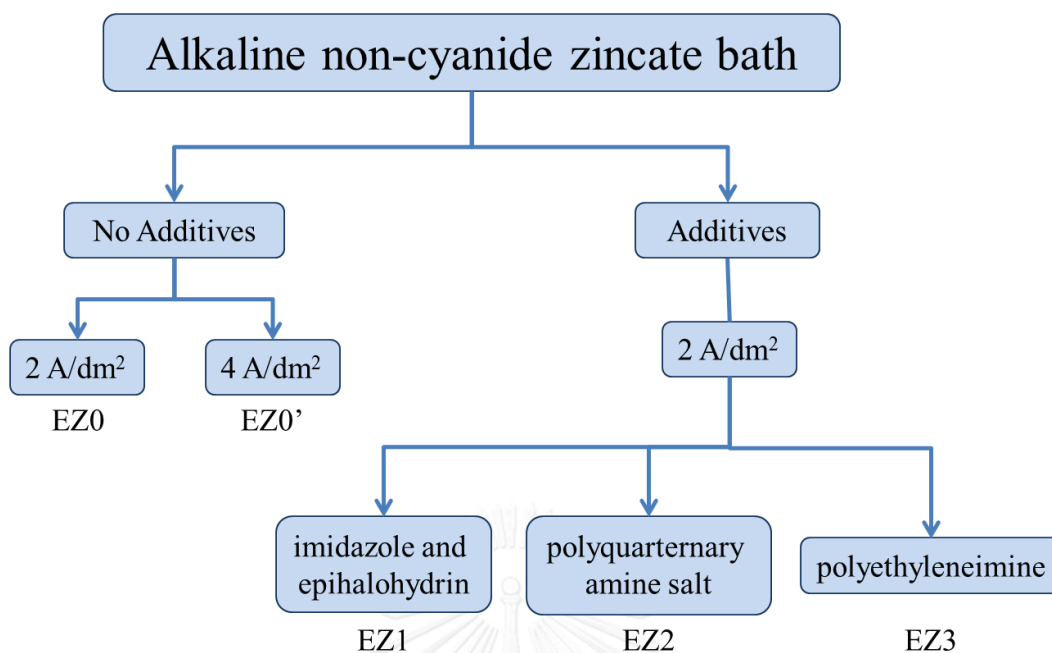


Figure 7 Experimental conditions

### 3.1.4 Conversion Coatings

Subsequent to the deposition, a separate set of samples from each bath was passivated with a commercial trivalent chromium-based solution (ES Coat Black SOP, OKUNO). The chromate conversion process consisted of surface activation in 1%  $\text{HNO}_3$  for 10 secs, dipping in the  $\text{Cr}^{3+}$ -based solution at  $30^\circ\text{C}$  with controlled pH of 2.2 for 45 secs, applying a top coat, rinse with water and oven-drying at  $80^\circ\text{C}$  for 30 mins. With respect to the number of their zinc baths, the samples are named EZP1, EZP2, and EZP3 respectively as presented in Table 1.

### 3.1.5 Corrosion Test

For the corrosion test, 7 samples of each group (EZ1, EZ2, EZ3, EZP1, EZP2, and EZP3) were used in the experiments. The samples were masked with tape as

shown in Fig.8 leaving an exposed area of  $3.14 \text{ cm}^2$ . The exposed area was deposited with  $5 \text{ g/m}^2$  NaCl droplet. The samples were subjected to wet-dry cycles in a chamber for six weeks. The wet-dry cycle was conducted by exposing the samples to alternating conditions of 2 h drying (40 %RH) and 2 h wetting (95 %RH) at  $25^\circ\text{C}$ .

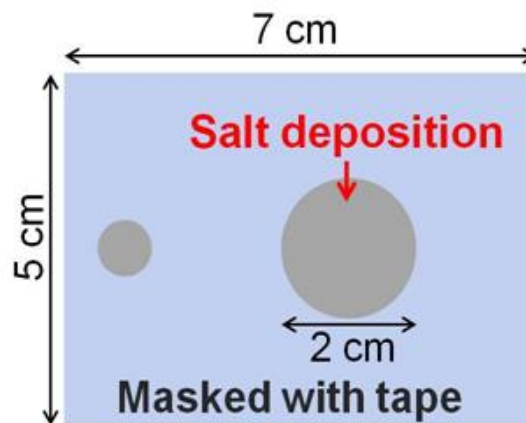


Figure 8 Sample subjected to corrosion test.

### 3.1.6 Characterization

Optical and scanning electron microscopy (OM, Keyence VHX and SEM, Hitachi SU-8030) were used to analyze surface appearance and cross-sectional structure of the coatings, respectively. To characterize chemical and phase compositions, X-ray fluorescence (XRF, Fischerscope X-ray XUV 773) and X-ray diffractometry (XRD, Philips X'Pert MPD-OEC) were applied on the outer surface of the specimen.

An optical microscope (OM) was used to observe the corrosion products on the samples' surface every week. A sample of each group was then removed from a chamber each week for an anodic stripping thickness measurement. Additionally, one sample of each group in the corrosion session was reserved for the weekly EIS measurement for impedance monitoring.

All electrochemical analyses were conducted in a three-electrode cell (Fig.9) with silver/silver chloride (Ag/AgCl, sat. KCl) electrode as a reference electrode, platinum wire as a counter electrode, and sample as a working electrode. The samples were immersed in 10 mM NaCl solution at room temperature. Using a potentiostat (Bio-Logic VSP), EIS measurements were performed at open-circuit potential (OCP) with a 10 mV amplitude and the impedance spectra were recorded in the frequency range of 10 kHz to 1 mHz. For anodic stripping, a constant current of  $200 \mu\text{A}/\text{cm}^2$  was applied to the system.

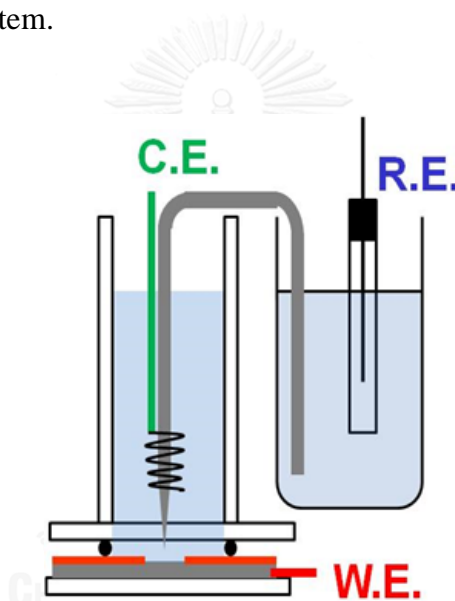


Figure 9 Electrochemical cell setup.

### 3.2 PART II: Heat treatment of Zinc

Heat treatment is applied to transform the zinc film obtained in the first part to ZnO film. In general, ZnO film with high surface area and surface roughness has good photocatalytic property. The film is treated at different temperatures to modify the structure of the film which in turn affects its property. The effects of the processing parameters on the formation of the ZnO film are investigated.

### 3.2.1 Thermal Annealing

Three zinc specimens (EZ0, EZ0', and EZ2) obtained from part I were selected based on their surface roughness and will undergo further heat treatment process. The oxidation reaction of both below and above the melting point of zinc metal is considered. The specimens were annealed at different temperature from 300 °C to 600 °C for 4 hours in air to form the zinc oxide thin films.

### 3.2.2 Characterization

Morphology and composition of the zinc and zinc oxide films were analyzed by a scanning electron microscopy with energy dispersive X-ray spectroscopy (SEM/EDX, Hitachi S3400N). The crystal structures of the films were identified by an x-ray diffractometer (XRD, Philips PW3710 X'Pert). Moreover, UV-vis diffuse reflectance spectra (UV-DRS) were performed using a UV-vis spectrophotometer (Hitachi UV-3100) equipped with an integrated sphere attachment and the spectra were recorded in the range of 300-4000 nm.

## 3.3 PART III: Photocatalytic Test

### 3.3.1 Photocatalytic Experiments

Methylene Blue (MB) was selected as the model dye to test the photocatalytic activity of ZnO thin films. The ZnO thin films were immersed in a 50 mL methylene blue solution (5 ppm). The photocatalytic setup is as shown in Fig.10. A 300W xenon lamp was use as the light source and the average light intensity was 83 mW/cm<sup>2</sup>. The distance between the lamp and the sample was 20 cm. The experiment was conducted using MB solution under UV light irradiation with and without the ZnO photocatalyst.

The experiment without ZnO photocatalyst was done as a blank experiment. For the photocatalytic test, the sample was kept in dark for 30 mins to obtain the adsorption-desorption equilibrium and then irradiated under UV light for 3 h. At 30 mins interval, 2 mL of solution was collected. The dye solution was measured using UV-vis spectrophotometer and the absorption of MB at 664 nm is used to evaluate the photocatalytic performance. In a practical usage of the photocatalyst, the film should be stable so a reusability experiment was done. The ZnO film annealed at 500°C was performed 3 times to determine the characteristic of the film.

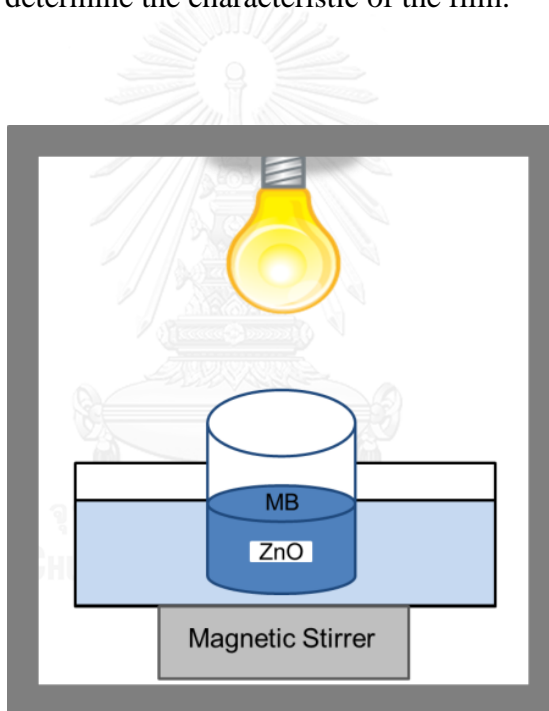


Figure 10 Photocatalytic setup

### 3.3.2 Photoelectrochemical Measurements

Photoelectrochemical tests were conducted in a three-electrode cell (Fig.9) filled with 0.1 M  $\text{Na}_2\text{SO}_4$  electrolyte with saturated calomel electrode (SCE) as a reference electrode, platinum wire as a counter electrode, and sample as a working

electrode. The mercury lamp was used an excitation light source. Electrochemical impedance spectra (EIS) were performed at open-circuit potential (OCP) with a 10 mV amplitude and the frequency ranges from 100 kHz to 0.5 mHz. All electrochemical measurements were carried out using  $\mu$ AutolabIII/FRA2 potentiostat.

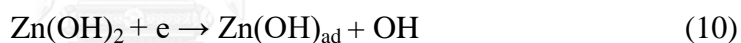


## CHAPTER IV

### RESULTS AND DISCUSSION

#### 4.1 PART I: Influence of process variables on structure and properties of zinc

The process of electroplating zinc in an alkaline non-cyanide solution is controlled by the applied current density to discharge  $\text{Zn(OH)}_4^{2-}$  onto the cathode [67]. First,  $\text{Zn(OH)}_4^{2-}$  is discharged into  $\text{Zn(OH)}_2$  in which the two charges are transfer step by step, then  $\text{Zn(OH)}_2$  is discharged into  $\text{Zn(OH)}_{\text{ad}}$ . Finally,  $\text{Zn(OH)}_{\text{ad}}$  is discharged and form a zinc layer at the cathode. Therefore, the mechanism of  $\text{Zn(OH)}_4^{2-}$  depositing in alkaline zincate solution is determined as



##### 4.1.1 Sample Characteristics



Figure 11 Hull cell test of zincate bath without additives.



Hull cell setup was used to perform a test from all zincate baths with and without additives. Fig. 11 shows the Hull cell specimen for studying the current distribution for bath without additives. From high to low current density (left to right), the visual inspection of the sample showed that the roughness of the surface decreases and the color varies from dark gray to dark gray for sample without additives. As anticipated, without using plating additives, a dull deposit with a relatively rough surface was observed. From the Hull cell study, a direct current of 2 and 4 A/dm<sup>2</sup> were selected for zincate bath without additive. At 2 A/dm<sup>2</sup>, a compact and uniform coating can be seen as in Fig.12(a) while for 4 A/dm<sup>2</sup>, thick layers of zinc deposits with surface irregularities was found (Fig.12(b)). The pores in the coating at 4 A/dm<sup>2</sup> can be attributed to the higher rate of hydrogen evolution at higher current density. As hydrogen evolution occur together with the metal deposition, making the coating layer less dense. The thick porous layer protruding from the surface of the coatings occurred as a result of no additives and high current density. The protruding part can be easily detached (Fig.13) as the coating layer is not compact and has low adhesion to the substrate.

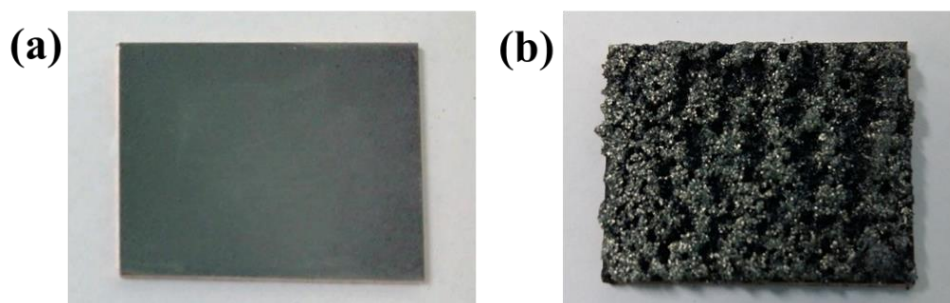


Figure 12 Electrodeposited zinc at (a) 2 A/dm<sup>2</sup> and (b) 4 A/dm<sup>2</sup>.



Figure 13 Defect sample

A closer look on the surface morphology of the zinc coating layers by SEM is depicted in Fig.14. The morphology of the surface at  $2 \text{ A/dm}^2$  consists of sub-micron zinc rods that are intertwined and formed clusters of granules and a dendrite structure is clearly seen at  $4 \text{ A/dm}^2$ .

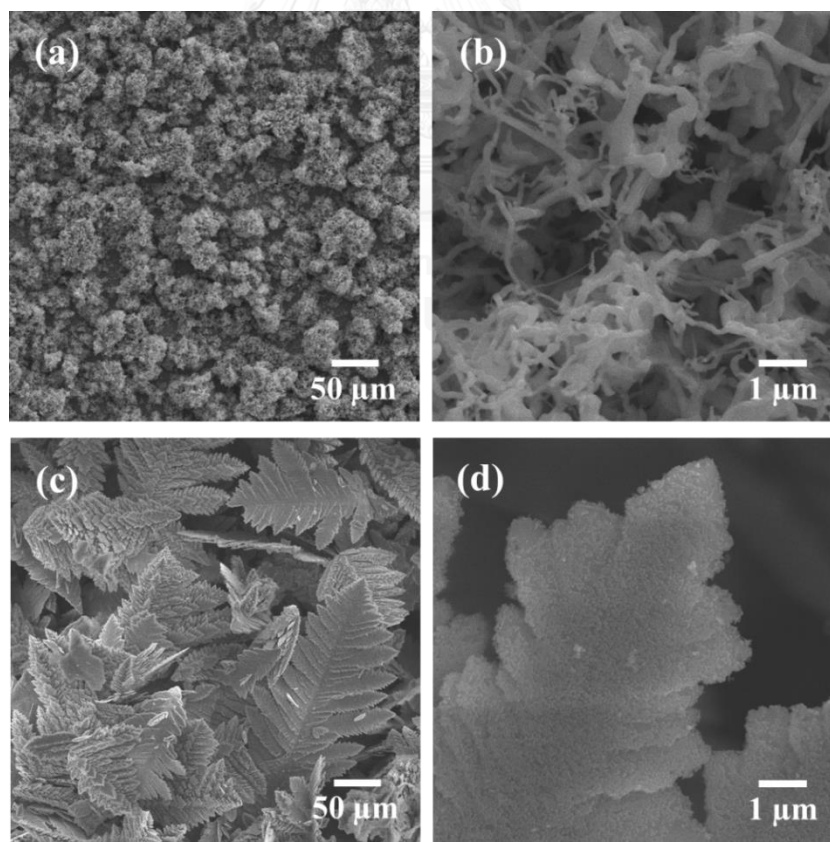


Figure 14 SEM image of electrodeposited zinc at  $2 \text{ A/dm}^2$  (a) 200x and (b) 10000x and at  $4 \text{ A/dm}^2$  (c) 200x and (d) 10000x.

The morphologies developed as an effect of current density may be explained as in Fig. 15. The Zn ions are driven by applied potential to combine with electrons to form cluster of deposits. According to Faraday's law, higher current result in higher deposition rate. As the deposition time increase, Zn grains gradually developed. Without additive, nonuniform deposits (peaks and valleys) developed area with high localized current density. For higher current density at  $4 \text{ A/dm}^2$  (Fig.15(b)), the same concept applied but with a faster deposition rate. High deposition rate at the highly localized current density area result in surface irregularities.

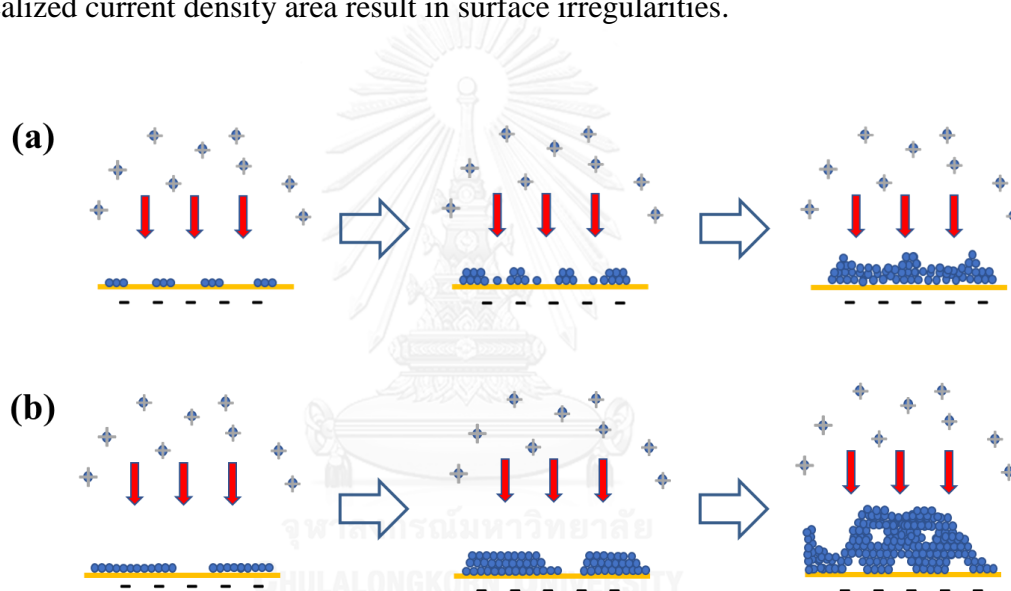


Figure 15 Effects of current density (a)  $2 \text{ A/dm}^2$  and (b)  $4 \text{ A/dm}^2$  on nucleation and growth

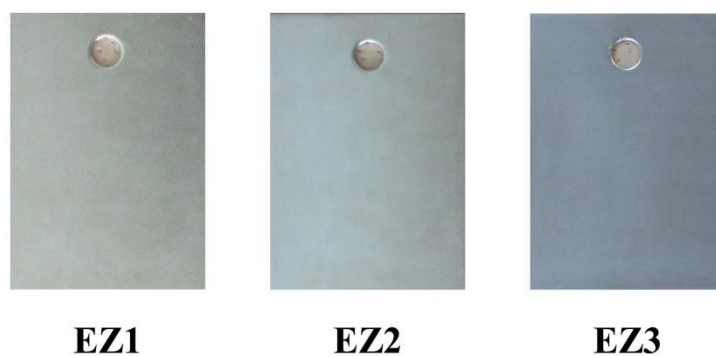


Figure 16 Electrodeposited zinc samples with additives.

For bath containing additives, a bright deposit with good surface uniformity is obtained as seen in Fig. 16. Additives are generally added to electroplating baths to improve the quality and uniformity of the deposits [68]. Additives play a role in influencing the nucleation and grain growth of the deposits as shown in Fig.17. Particularly, additives serve as adsorbates, which are selectively transferred from the electrolyte to a cathode surface. Often, the additive molecules are preferentially adsorbed at rapid growth sites and locally hinder the reduction of metal ions, resulting in a decrease of an overall growth rate of a deposit [69]. Adsorption of the additives also contributes to a reduction of the mean free path of the adions, and in effect influences the nucleation, grain growth, and texture developments of the crystalline metals [38, 39, 41, 70].

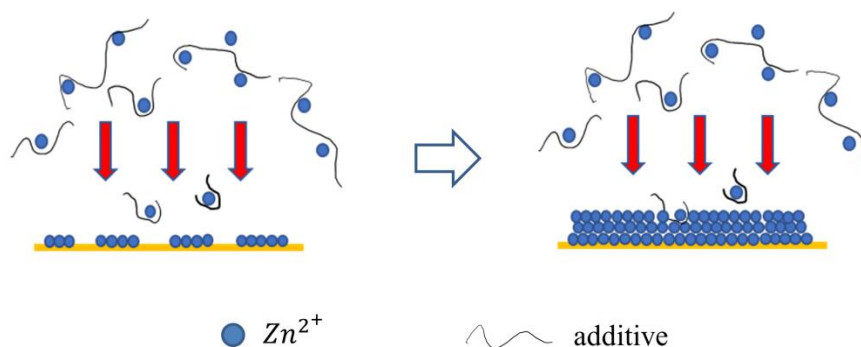


Figure 17 Effects of additives on nucleation and growth.

Comparing to the sample without additives, the SEM images in Fig. 18 show a smoother and more uniform coatings. The addition of additives also leads to a difference in the surface morphologies of the zinc coating layers of different group. EZ1 sample showed a smooth and compact film while EZ2 sample present the coatings with highest surface roughness. However, comparing the sample with additives to EZ0 sample, the film is still very smooth and this showed that additives affect the structure in nanoscale.

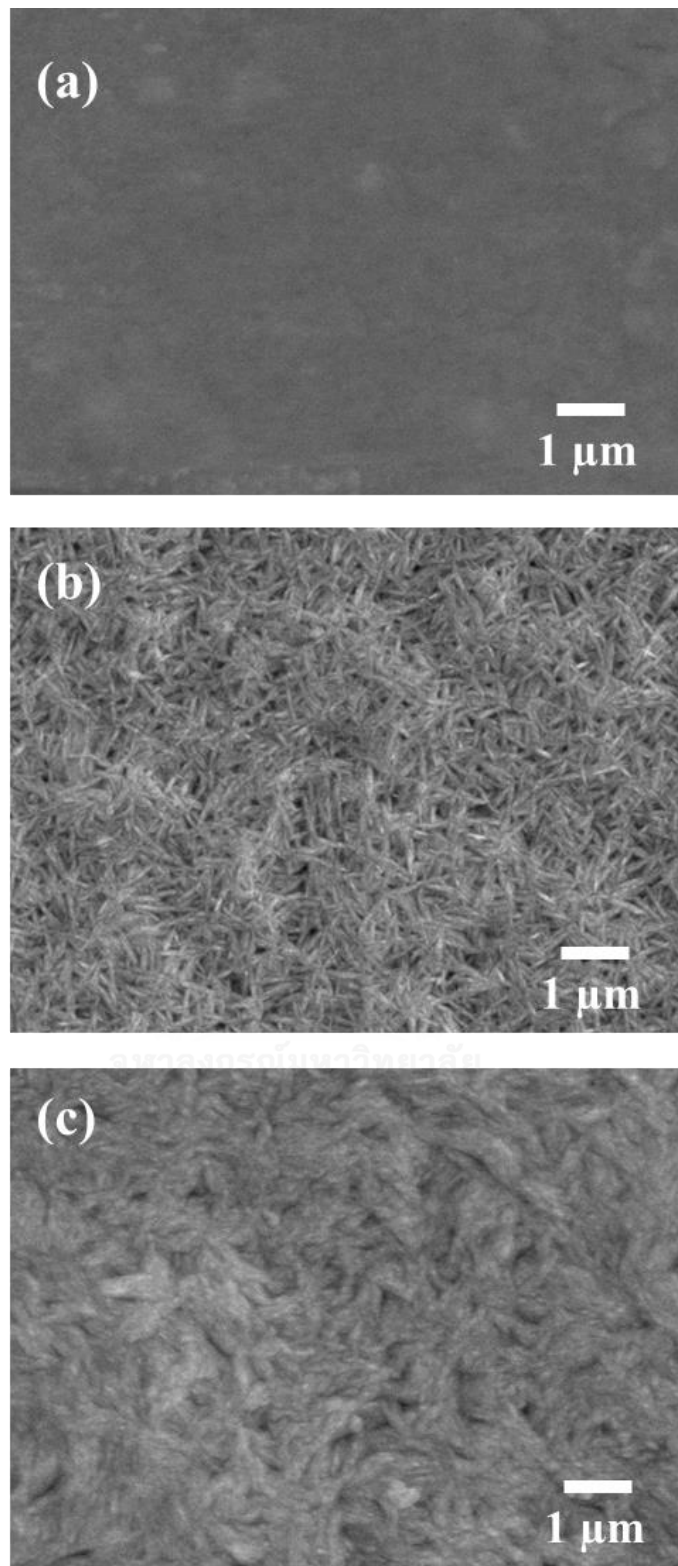


Figure 18 SEM micrographs of electrogalvanized samples: (a) EZ1, (b) EZ2, and (c) EZ3.

With different charge density of the additives, it may result in different deposition rate and the atoms are deposit with different preferred orientations. As shown by the profiles from the XRD measurements in Fig. 19(a), specimens EZ0, EZ1, EZ2 and EZ3 exhibit different crystallographic orientations of zinc grains. This thus underlines the effects of organic additives in controlling the deposits' crystallographic structures. EZ0 showed a preferred orientation in the (002) and (101) plane. (100) and (110) planes appear preferentially orientated perpendicular to the surface normal direction in EZ1 and EZ3, respectively. On the other hand, the surface of EZ2 is dominated by both (100) and (110) planes.

Considering the XRD profiles of EZP2 and EZP3 (Fig. 20(a)) in comparison with their EZ counterparts (Fig. 19(a)), some modifications of crystallographic orientations of the zinc layer via the chromate conversion process is observed. After chromating, (100) and (101) orientations become more preferential in these deposits. Furthermore, the crystallographic structure of the zinc coatings of EZP2 and EZP3 is found comparable, whereas that of EZP1 shows a strong (100) texture.

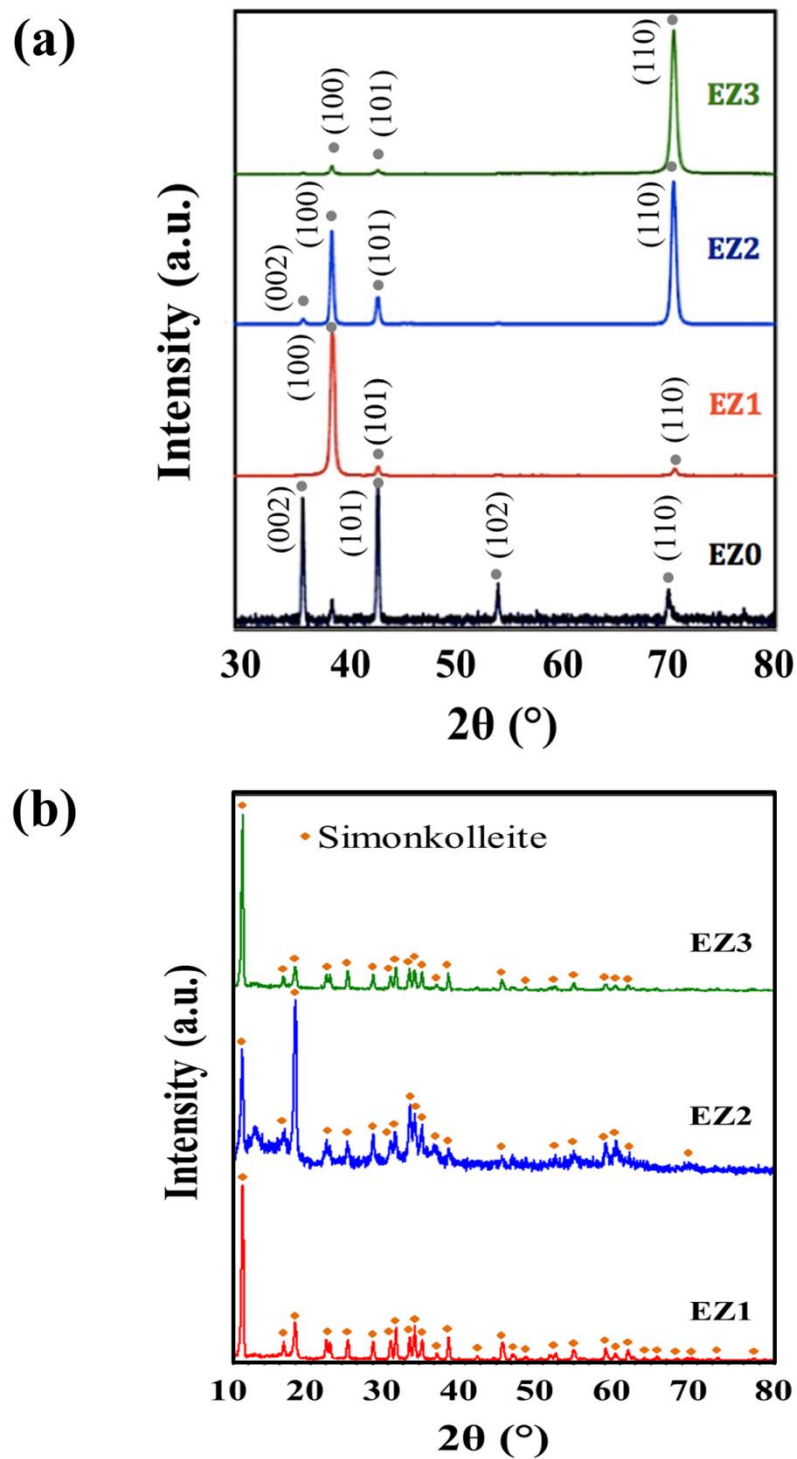


Figure 19 XRD profiles of the zinc samples (a) before and (b) after completion of the 6-week corrosion test.

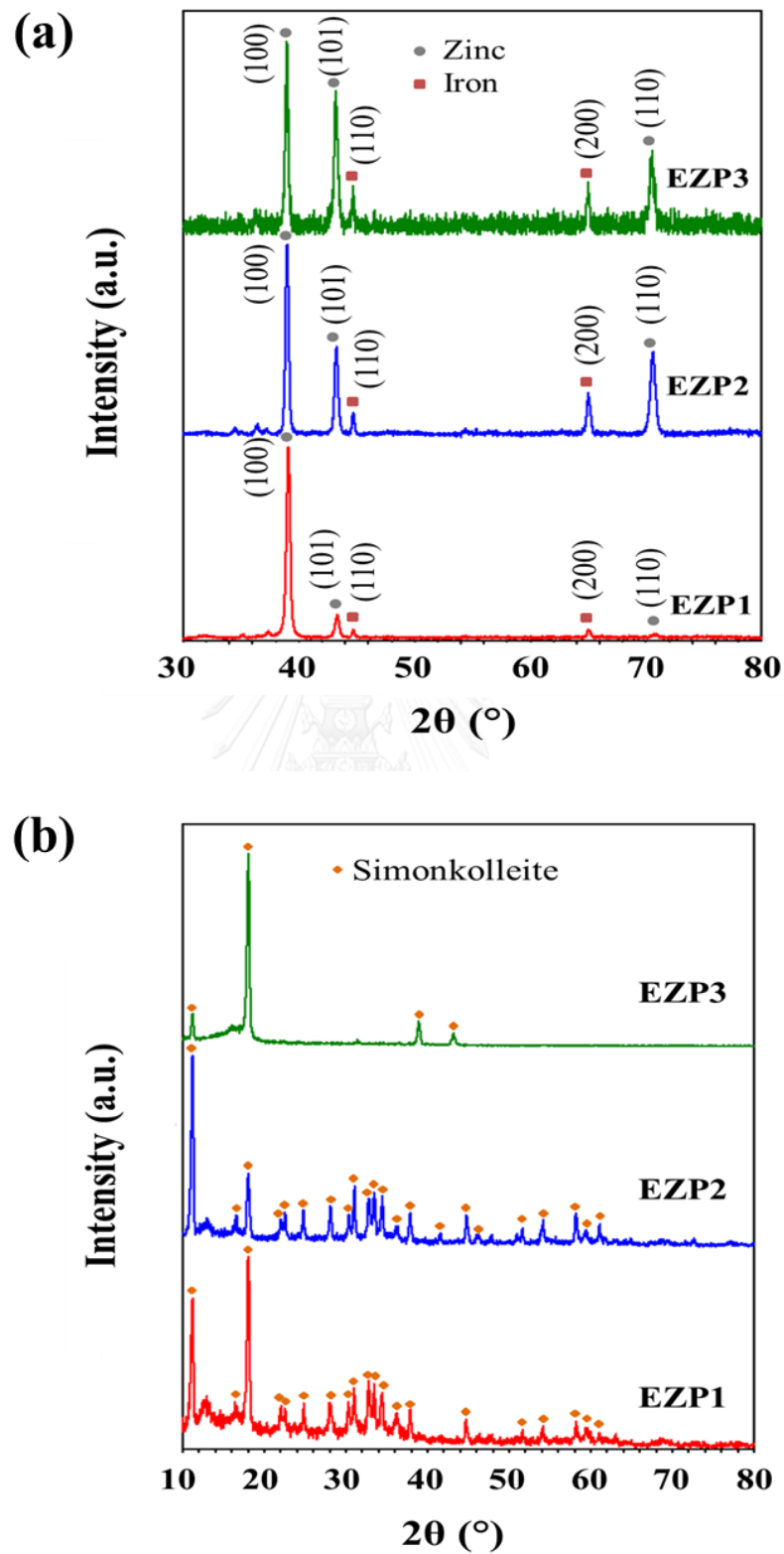


Figure 20 XRD profiles of the chromated samples (a) before and (b) after completion of the 6-week cyclic exposure corrosion test.



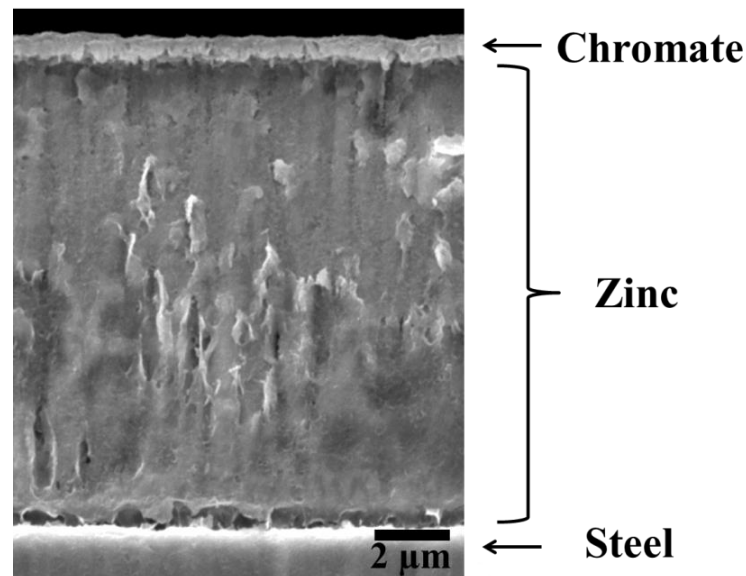


Figure 21 Cross-sectional SEM micrograph of electrogalvanized sample with steel substrate, zinc layer and chromium conversion layer.

Table 2 XRF chromium to zinc content ratio in the top-coat vicinity of the deposit samples

Sample Set	Cr:Zn ratio
EZP1	0.153
EZP2	0.088
EZP3	0.212

Figure 21 shows a representative cross-sectional microstructure of a columnar-grained galvanized deposit, covered with a relatively thin chromate conversion layer (EZP2). The thickness of the zinc and chromate conversion layers of all specimen groups from baths containing additives are approximately  $10 \pm 2 \mu\text{m}$  and  $0.5 \mu\text{m}$  respectively. Whereas zinc is the key component in the galvanized layer, the passivation layer comprises chromium and zinc in the form of oxides and hydroxides [48]. The XRF analysis identifies that, among different EZP groups, the ratio of

elemental chromium and zinc contents in the chromate layer's vicinity varies between 0.08 – 0.21, depending on a type of zinc-bath additives, as shown in Table 2.

#### 4.1.2 Corrosion Behaviors

##### 4.1.2.1 Physical Appearance

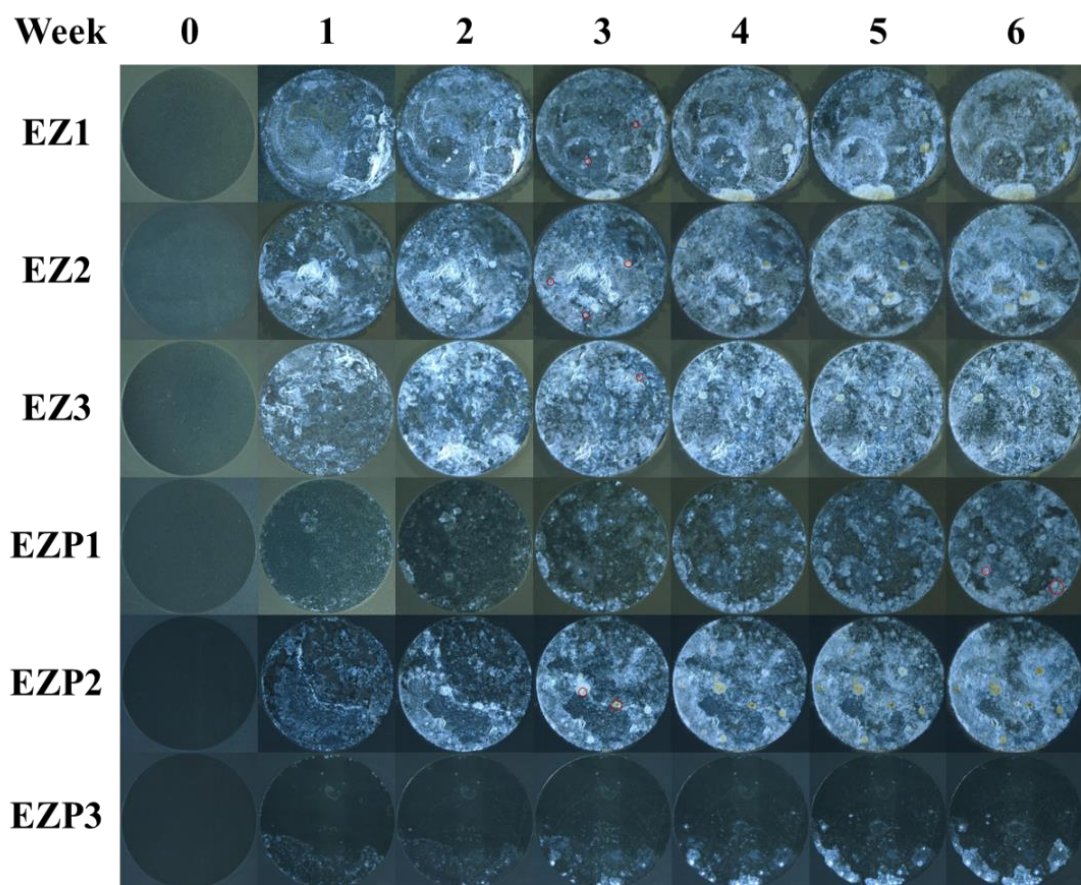


Figure 22 OM images of the samples following each week of the cyclic exposure corrosion test

Figure 22 shows the surface appearance of the test specimens following the cyclic exposure corrosion test at each stage. In general, formations of white rust due to oxidation of zinc, which was indicated to compose mainly of simonkolleite (Fig.19b and Fig.20b), occurred and increase more dispersedly over time.

Subsequently, many of the specimens further developed red rust spots on their surface. All specimens in the EZ groups exhibited white rust formation as early as the 1<sup>st</sup> week of the test, with red rust being developed by the 3<sup>rd</sup> week. On the other hand, the chromated EZP1 and EZP3 are characterized by a relatively slow rate of rust formations. Red rust was developed in the 6<sup>th</sup> week for EZP1 and not visibly present following the test completion for EZP3. The surface of EZP2 however appears comparable to those in the EZ groups in each period, with developments of white and red rust occurred in the early period.

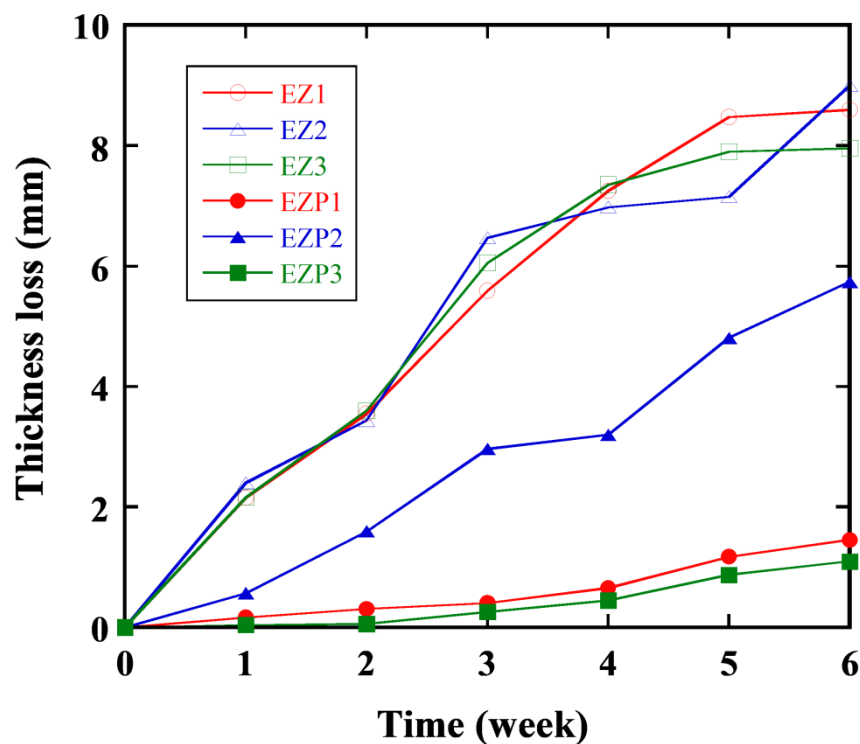


Figure 23 Coating thickness loss of the electrogalvanized samples in each week of the cyclic exposure corrosion test

These visual observations are resonated by the results of the remaining coating thickness measurement by the anodic stripping. As shown in Fig. 23, the determined

corresponding corrosion rates of EZP1 and EZP3 are about 4 times slower than those of the EZ specimens. Furthermore, their corrosion rates appear to be almost negligible in the first few weeks, after which corrosion occurred slightly more rapidly. The coating thickness of all EZ specimens reduced monotonically and comparably. By the 6<sup>th</sup> week, zinc in the coating layer of EZ1 and EZ2 was almost all corroded.

#### 4.1.2.2 Impedance Characteristics

The EIS measurements performed on the test specimens following each week of the cyclic exposure corrosion tests results in the Nyquist and Bode diagrams, as representatively shown in Figs. 24 and 25 for the results from the 1<sup>st</sup> and 6<sup>th</sup> weeks. The Bode diagrams of the test specimens for all six weeks can be seen in the Appendix A. Over time as testing pursued, an impedance amplitude was found to reduce progressively for EZ1 and EZP1, remain fairly stable for EZP3, and gradually increase for EZ2, EZP2, and EZ3. The obtained impedance spectra were found to fit well to one of the two equivalent circuits, shown in Fig. 26. Specifically, the equivalent circuits in Fig. 26a and Fig. 26b correlate to the specimens' characteristic in their early stage and later stage of corrosion, respectively. The corresponding equivalent circuit elements are summarized in Table 3, where  $R_s$  refers to solution resistance,  $R_f$  oxide film resistance,  $C_f$  oxide film capacitance,  $R_{ct}$  charge transfer resistance, and  $C_{dl}$  double layer capacitance.  $R_{ct}$  and  $C_{dl}$  are found to mainly govern the impedance of each specimen in general. Furthermore, the specimens with a chromate conversion layer are characterized by relatively high  $R_{ct}$  and low  $C_{dl}$ , as compared to those without a top coat.

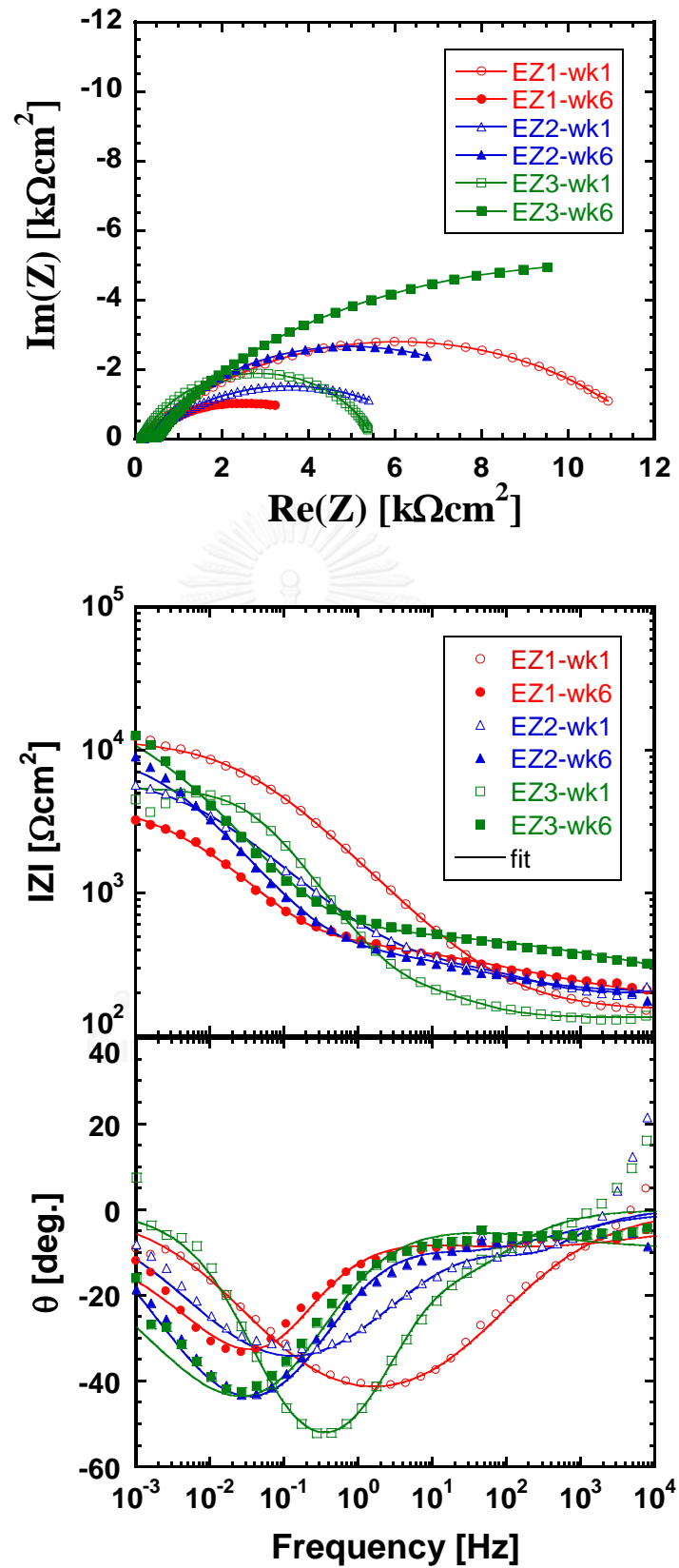


Figure 24 Nyquist, Bode and phase shift plots of the zinc samples from the EIS analysis following the 1st and 6th week of the cyclic exposure test

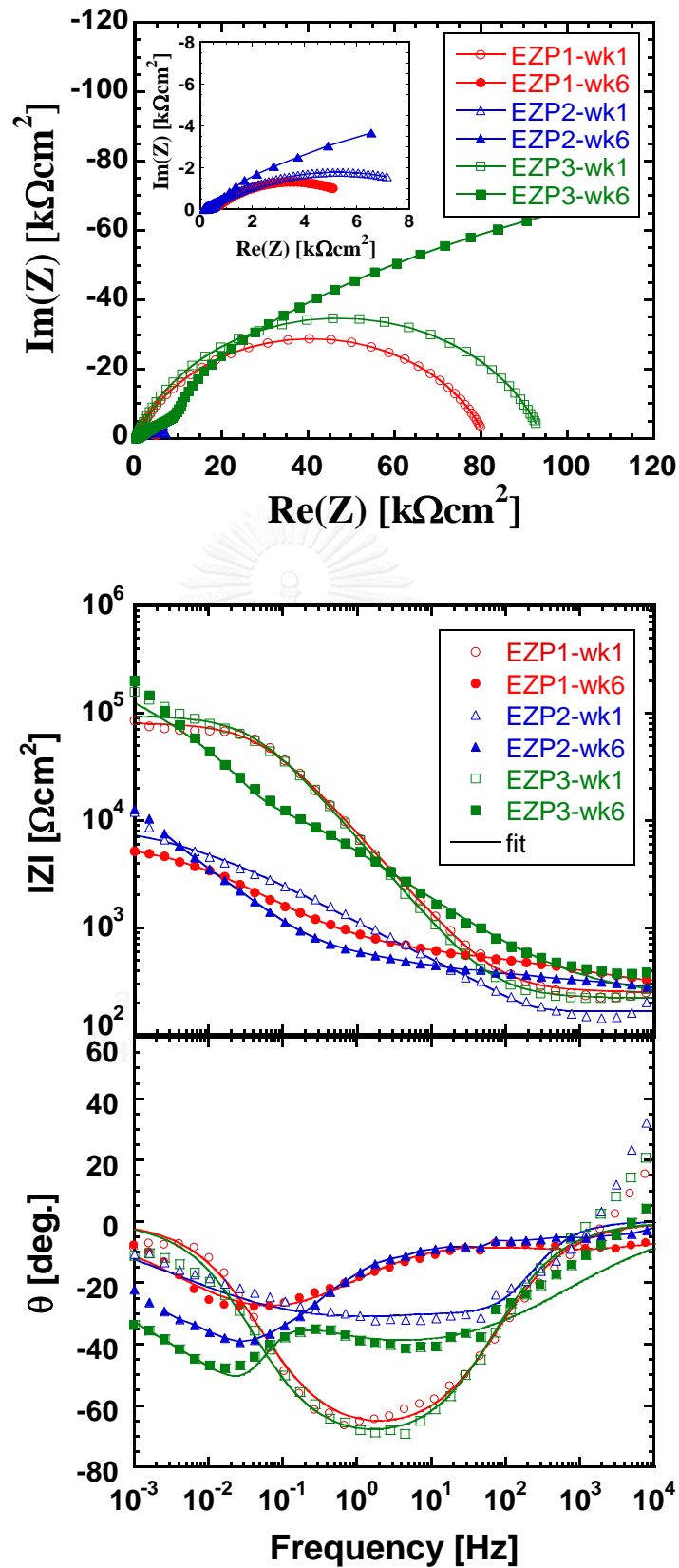


Figure 25 Nyquist, Bode and phase shift plots of the chromated samples from the EIS analysis following the 1st and 6th week of the cyclic exposure test

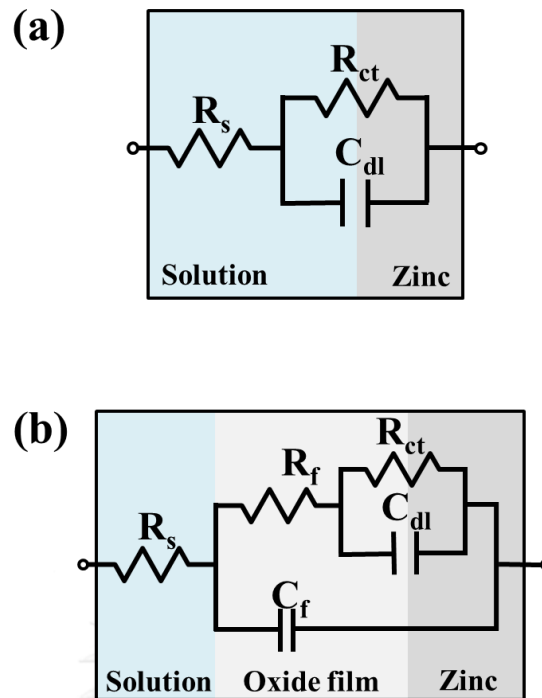


Figure 26 Electrical equivalent circuits of the samples without (a) and with (b) passive oxide film in a saline solution based on the electrochemical impedance spectroscopy (EIS).

Table 3 Numerical data of equivalent circuit elements of the non-chromated and chromated electrogalvanized samples from the EIS analysis following the 1st and 6th week of the cyclic exposure test

Sample		$R_s$ ( $\Omega\text{cm}^2$ )	$R_f$ ( $\Omega\text{cm}^2$ )	$R_{ct}$ ( $\Omega\text{cm}^2$ )	$C_{dl}$ ( $\mu\text{F cm}^{-2}$ )	$C_f$ ( $\mu\text{F cm}^{-2}$ )
EZ1	wk1	150	-	11900	206	-
	wk6	150	400	5660	1940	600
EZ2	wk1	200	90	6590	850	19
	wk6	200	210	9490	1340	360
EZ3	wk1	135	110	5250	400	160
	wk6	135	440	30000	1150	165
EZP1	wk1	250	-	81000	30	-
	wk6	250	370	5900	830	100
EZP2	wk1	168	0.81	10200	2	428
	wk6	168	230	18900	1220	61
EZP3	wk1	220	-	94100	33	-
	wk6	220	34600	335000	109	72

### **4.1.3 Discussions**

#### **4.1.3.1 Effects of additives on corrosion of zinc coatings**

Examining the 3 organic additives, they in fact exhibit different levels of charge density, in an increasing order of polyquaternary amine salt < imidazole and epihalohydrin < polyethyleneimine [37]. It can then be anticipated that their adsorption strength varies correspondingly, and that these additives influence texture development of the deposits in different fashions. Indeed, as presented in Figs.18 and 19, the electrogalvanized coating samples exhibit distinct surface morphologies and texture when different additives were employed.

Despite similar corrosion behaviors of EZ1, EZ2 and EZ3 with respect to the wet-dry cyclic saline environment, it is observed that EZ1 exhibits slightly higher corrosion rate and lower impedance, especially toward the end of the corrosion test (Fig.22 and Fig.24). The lower corrosion resistance of EZ1 could be attributed to its (100) texture which exhibits a relatively low packing density of zinc's crystallographic planes, in agreement with the general understanding of texture and corrosion resistance relationship [71]. On the other hand, the increments of the impedance in EZ2 and EZ3 over time could imply that the crystallographic structure of these deposits, possibly the (110) orientation, may better facilitate a formation of passive films of corrosion products, which in turn equip the coatings with higher corrosion protection.

#### **4.1.3.2 Effects of additives on corrosion of chromated zinc coatings**

A chromate conversion coating layer is formed on a zinc coating surface through the oxidation-reduction process, which comprising of the zinc dissolution and



complex chromium compound film formation steps [46, 47]. Since the surface metal of the electrogalvanized layer directly interacts with chromic acid and chromium salt solutions, and hence primarily involves in these chromating steps, it can be anticipated that the characteristic of the zinc layer would influence the development of a chromate conversion coating layer and hence affect the film's corrosion behavior.

Indeed, it is determined that EZP1, EZP2 and EZP3, which have distinct crystallographic textures and surface morphologies in the zinc coating layer, exhibit marked differences in the levels of the relative Cr content in the film (Table 2) and the corresponding degrees of corrosion resistance, in an increasing order of  $EZP2 < EZP1 < EZP3$ . This is achieved despite using the same chemicals and processing parameters for the chromate conversion treatment in preparation of these materials. EZP3, in particular, exhibited a high charge transfer resistance and low double layer capacitance, which suggest a more protective and stable film formation [58]. The relatively high Cr content in the chromate film of EZP3 could stem from the crystallographic texture of its galvanized layer that facilitates zinc dissolution reaction and chromate conversion reaction [38, 47, 72]. Consequently, EZP3 withstood a corrosion attack relatively well compared to all sets of the specimens throughout the 6-weeks test period. The result therefore underlines that the corrosion resistance of electrogalvanized coatings is critically influenced by the chromate treatment, which is in turn affected by organic additives of the zinc plating baths and the formation of the zinc coating layer.

## 4.2 PART II: Heat treatment of Zinc

### 4.2.1 Sample Characteristics

A set of zinc deposits specimens were successfully fabricated in part I. Zinc is used as the precursor to obtain ZnO after heat treatment. In order to obtain good photocatalytic property, zinc coatings with high roughness and surface area are needed. From part I, it can be noticed that zinc films prepared from bath without additives provide higher surface roughness compared to the films from bath with additives. Hence, the zinc coatings from bath without additives, EZ0 and EZ0', are chosen. However, specimen from the EZ2 group was also taken into consideration. Among the samples from bath with additives, EZ2 specimen shows the surface morphology with the highest surface roughness. Following the heat treatments, the microstructure and chemical composition of the deposits gradually evolved.

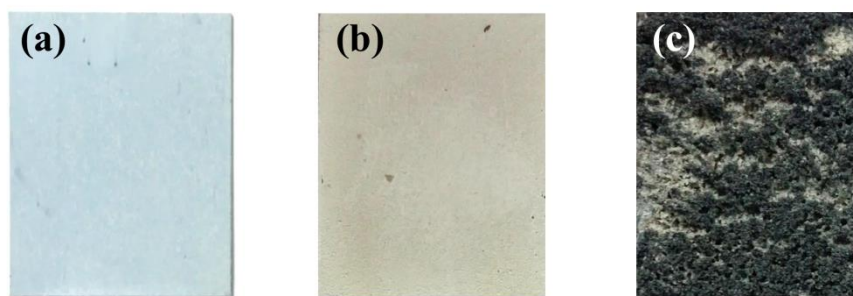


Figure 27 Heat treatment at 500°C of samples (a) EZ2, (b) EZ0, and (c) EZ0'.

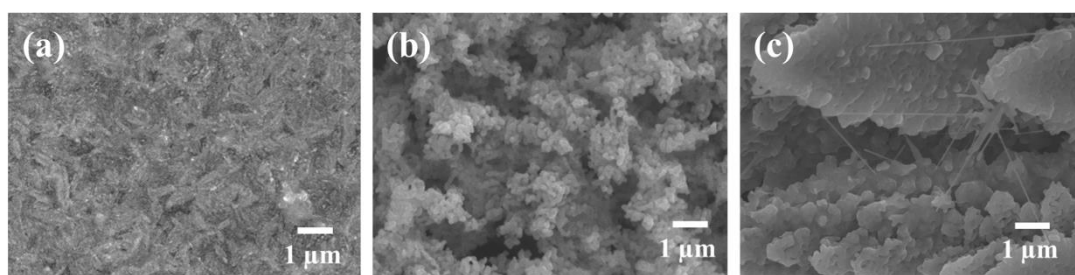


Figure 28 SEM images of heat treated samples (a) EZ2, (b) EZ0, and (c) EZ0'.

Figure 27 shows the resulting ZnO film from heat treatment of zinc film at 500°C. EZ2 and EZ0 samples completely transformed to white ZnO thin film. For EZ0', the zinc film was partially transformed to ZnO. A closer look at the SEM images in Fig.28 showed a grain growth resulting in a smoother surface for EZ2 sample, a formation of ZnO nanospheres on the Zn rod-like structure for EZ0 sample, and an increase in the surface roughness of the dendrites for EZ0' sample. Based on the surface roughness, EZ0 was selected for further investigation due to the high surface area of the sample.

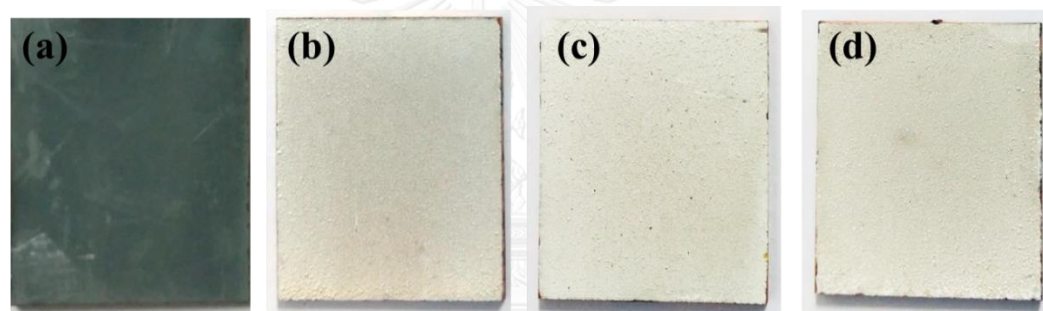


Figure 29 EZ0 samples at different heat treatment temperature (a) 300°C, (b) 400°C, (c) 500°C, and (d) 600°C.

Figure 29 presented EZ0 sample annealed at different temperature of 300°C, 400°C, 500°C, and 600°C. At 300°C, a dull gray color similar to that of Zn deposits was seen. For 400°C, 500°C, and 600°C, white ZnO film was obtained. Further looking at the SEM images (Fig.30), zinc was only partially transformed to zinc oxide with 300°C annealing temperature, and the deposit was found to be flaky and loosely adhere to the substrate. Therefore, this set of specimens was disregarded for the rest of the study. Increasing an annealing temperature to 400°C, a white zinc oxide film that is well-intact to the substrate has now been more uniformly formed.

Interestingly, as observed in Fig. 30(b), zinc oxide was formed and grown using the zinc deposit structure as a template. Specifically, zinc oxide retains the architecture of the prior nanorod-shape zinc deposits, with additions of needle-like ZnO protruded from the intertwined struts. The heat treatment temperature of 500°C again leads to a uniform layer of ZnO. Fig. 30(c) shows that with this higher annealing temperature, the ZnO needles observed in the previous case has been replaced with spherical ZnO particles that agglomerate as parts of the rod structure. The size of these zinc particles increased and their number decreased somewhat after the annealing temperature of 600°C was introduced, albeit the intertwining-rod structure did remain (Fig.30(d)).

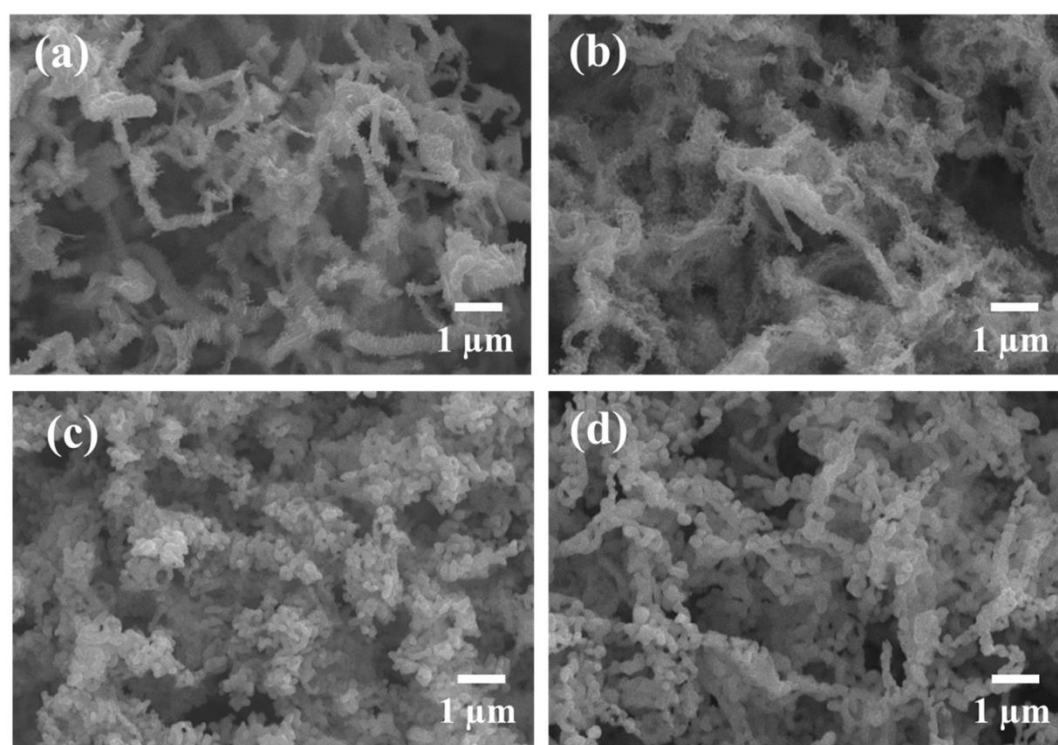


Figure 30 SEM images of heat treated zinc without additive at (a) 300°C, (b) 400°C, (c) 500°C, and (d) 600°C.

#### 4.2.2 Discussions

The formations of the ZnO structure as evolved with the change in annealing temperature may be rationalized as follows. Without polymeric additives so-called levelers, deposition of Zn is promoted at the locally high current density regions such as protruding surface irregularities, resulting in a formation of sub-micron rod, flake, or tree-like shape deposits [73-75]. Subsequently, with heat treatment, Zn deposits react with  $O_2(g)$  to form  $ZnO(s)$ . Depending on the applied temperature with respect to the melting point of Zn ( $420^\circ C$ ), the reaction kinetics and the resulting structure of  $ZnO(s)$  could be different. Indeed, partial reaction is observed in the  $300^\circ C$  case, and at  $400^\circ C$  relatively slow reaction between Zn and  $O_2$  appear to initiate from the surface of the Zn rods resulting in needle-like structures protruded from the intertwined struts. On the other hand, at the higher annealing temperatures of  $500^\circ C$  and  $600^\circ C$ , the Zn rods partially liquified and underwent simultaneous reaction with the exposed  $O_2$  in more rapid rates, inducing a formation of ZnO granules that constitute the rod structure. The high temperature of  $600^\circ C$  appear to promote a formation of larger ZnO particles as driven by a reduction of overall surface energy [64].

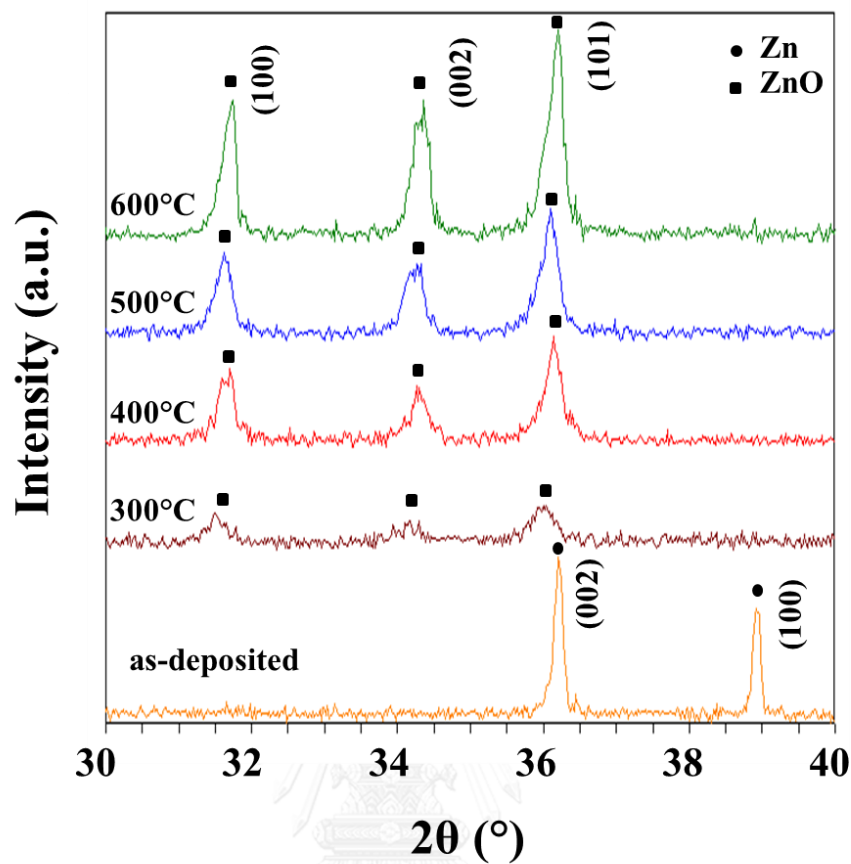


Figure 31 XRD pattern

The XRD pattern of the deposited zinc and oxidized zinc film are presented in Figure 31. The diffraction peaks from zinc film are (002), (100), and (101) showing that the film is polycrystalline. After heat treatment at 300°C, 400°C, 500°C, and 600°C, metallic zinc was transformed to zinc oxide with an increase in the intensity of the peak as the temperature increases. The dominant peaks for zinc oxide composed of (100), (002), and (101) which correspond to the hexagonal wurtzite structure. There is no preferred orientation and the relative intensity of all samples has no significant difference.

From the results, it could be anticipated that Zn has completely transformed to ZnO or the formation of ZnO could be a core-shell Zn-based morphology. The core-shell formation occurred as a result of oxidation on the surface of the Zn rods. The core and the shell can be different materials or the same materials with different structures [76, 77]. The XRD peaks for Zn and ZnO coexisted and this may be due to the core-shell structure. In order to clearly confirm the structure of the film, further analysis could be done.

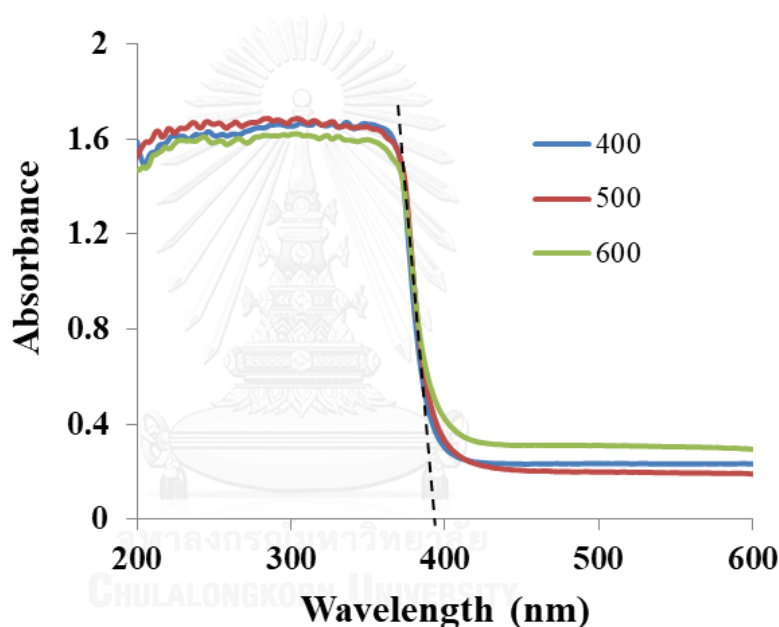


Figure 32 DRS of ZnO at different heat treatment temperature.

Figure 32 shows the diffuse reflectance absorption spectra of the ZnO samples. All three samples exhibit the same absorption edge indicating that they have identical band gap energy (3.15 eV). The stronger absorption intensity in the UV region is a key for good photocatalytic performance.

### 4.3 PART III: Photocatalytic Zinc Oxide

In this part, ZnO thin films from part II were used to study for their photocatalytic activity. The effects of structure and surface morphologies on the photocatalytic activity are investigated. The specimens are ZnO samples annealed at 400°C, 500°C, and 600°C. In addition, the ZnO specimen from EZ2 group was also tested for its photocatalytic activity. For practical use of the ZnO film photocatalyst, the photodegradation efficiency of the film should be maintained after successive test experiments. As the ZnO photocatalyst are irradiated under UV light, the photocorrosion of ZnO could occurred. The photocorrosion of the ZnO specimens are analyzed after the photocatalytic test. The sample characteristics like surface morphology and texture were analyzed as shown in Fig. 33 and 34 respectively. From the XRD results in Fig.34, the texture coefficient is about the same for all samples and there is no preferred orientation. The relative intensity of all samples has no significant difference, hence, the crystal quality of the layers is not the main parameter affecting the photocatalytic property of ZnO film.



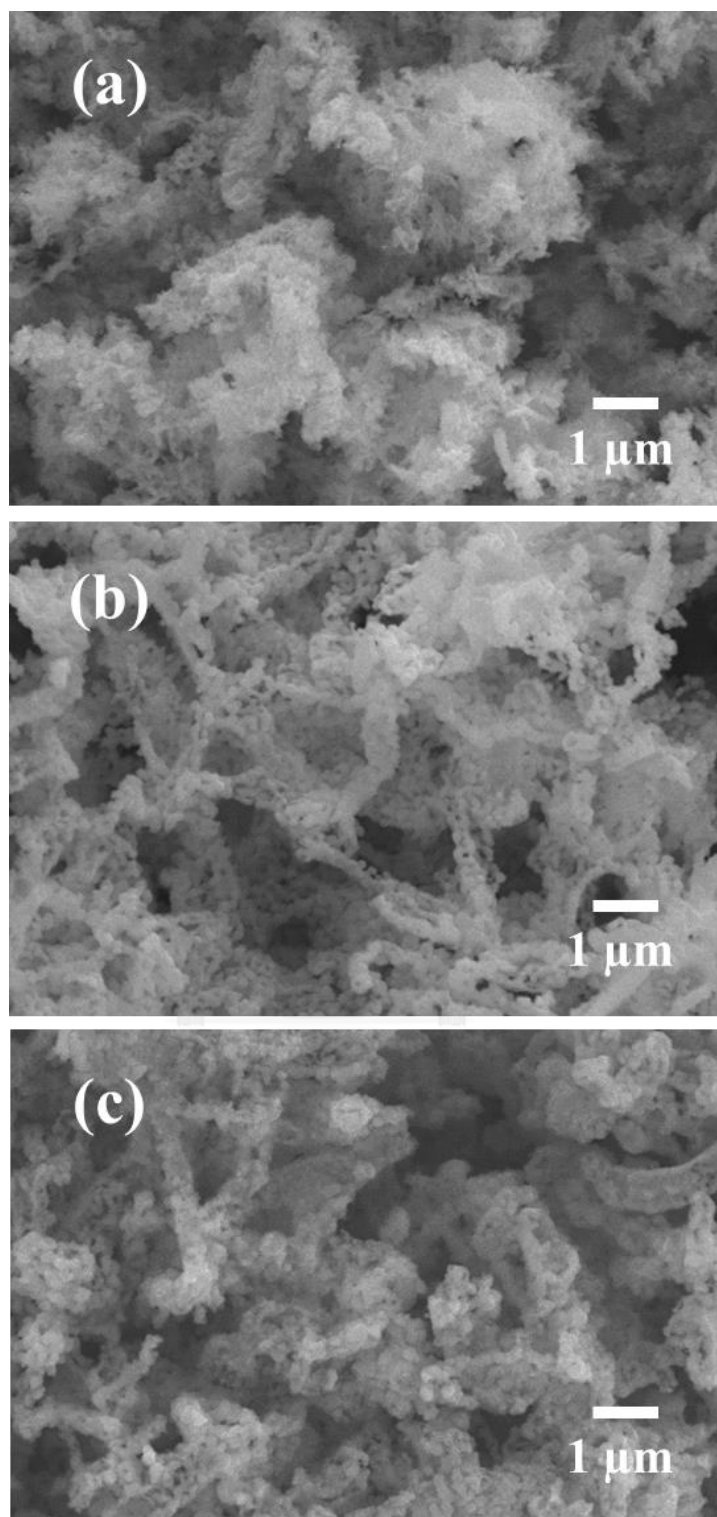


Figure 33 SEM image of ZnO photocatalyst (a) 400°C, (b) 500°C, and(c) 600°C after photocatalytic test.

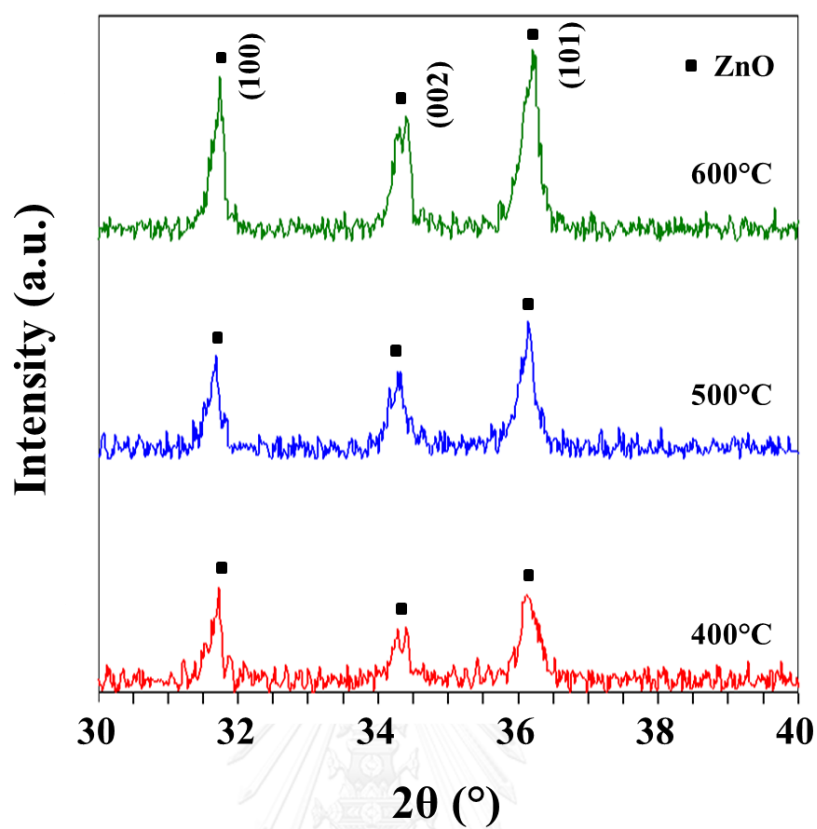


Figure 34 XRD patterns of ZnO after photocatalytic test

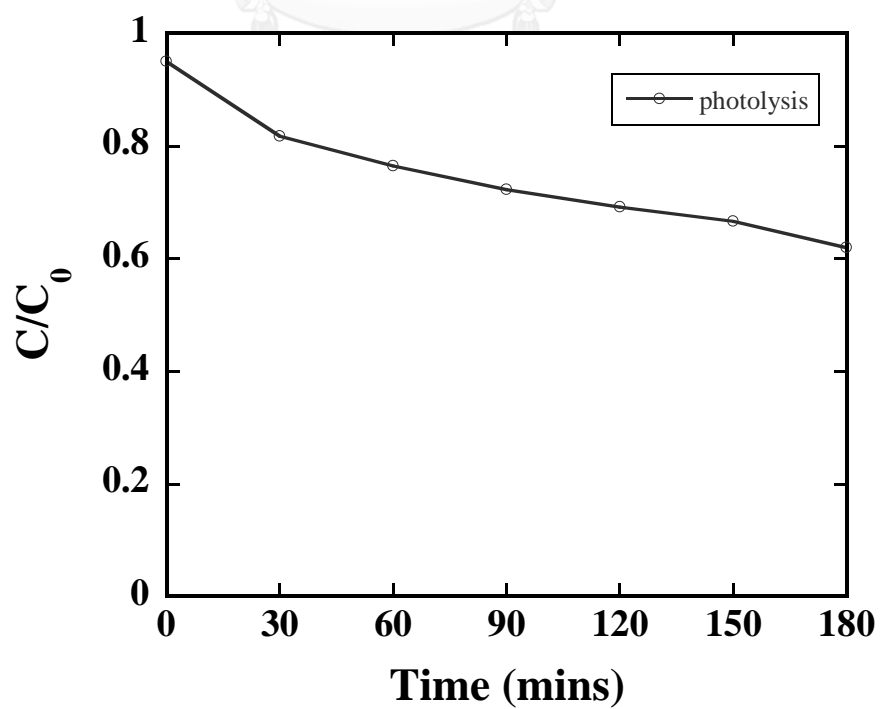


Figure 35 Photolysis test

To confirm the role of ZnO in the photocatalytic test, the degradation test of MB under UV light irradiation with and without photocatalyst were tested. First, UV light was irradiated on the MB solution without ZnO. From Fig. 35, it can be seen that the concentration of MB decreased about 30% after 3 hours.

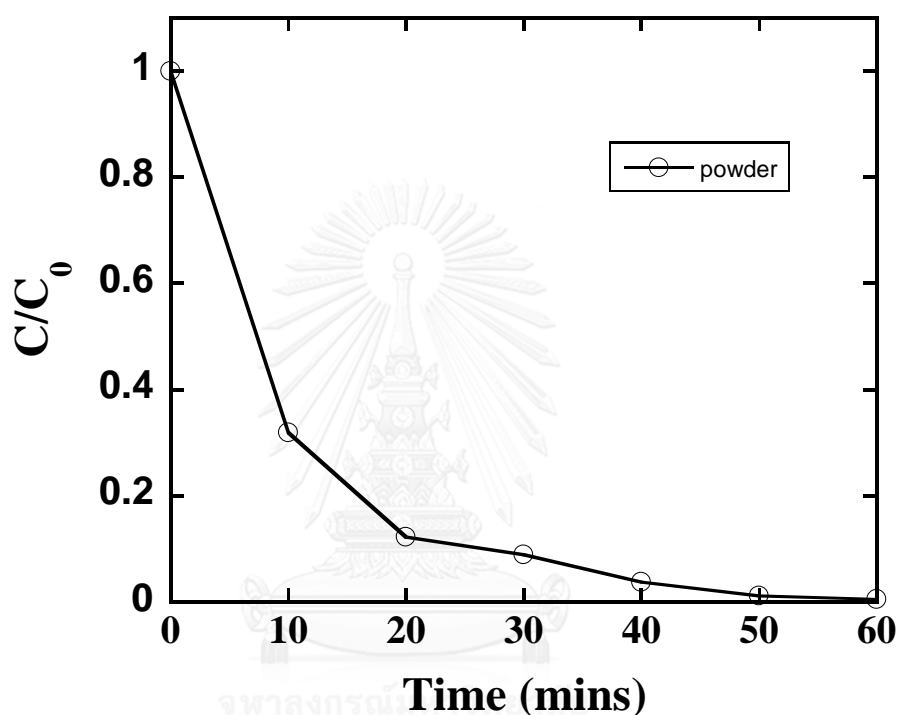


Figure 36 Photocatalytic activity of ZnO powder.

In addition, the photocatalytic activity of the commercial ZnO powder was tested to compare the photodegradation efficiency of the ZnO film. From Fig.36, it can be seen that almost 100% of MB was degraded after 60 mins with the presence of ZnO powder photocatalst under UV light.

The photocatlytic activity for ZnO thin film annealed at 500°C with polyquaternary amine salt and without additives are being tested and compared in Fig.37. It can be seen that the ZnO thin film without additive performed better than

the ZnO thin film with additives. 98.5% of MB was degraded under ZnO thin film without additive while 86.3% of MB was degraded for ZnO thin film with additive.

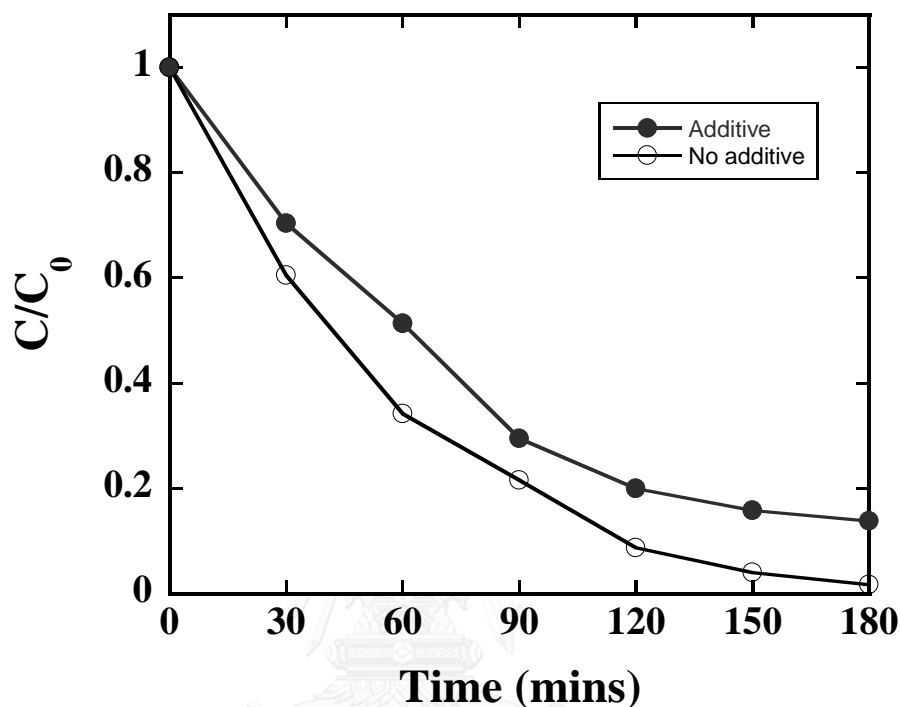


Figure 37 Photocatalytic test of ZnO with and without additives

From this result, the ZnO thin film without additive was further developed to obtain different structure and surface morphology. The different ZnO thin film annealed at different temperature from the previous part are tested for its photocatalytic activity under UV light irradiation with MB as the model dye. During the test, sampling of MB solution was collected to test for the remaining MB concentration in the test solution.

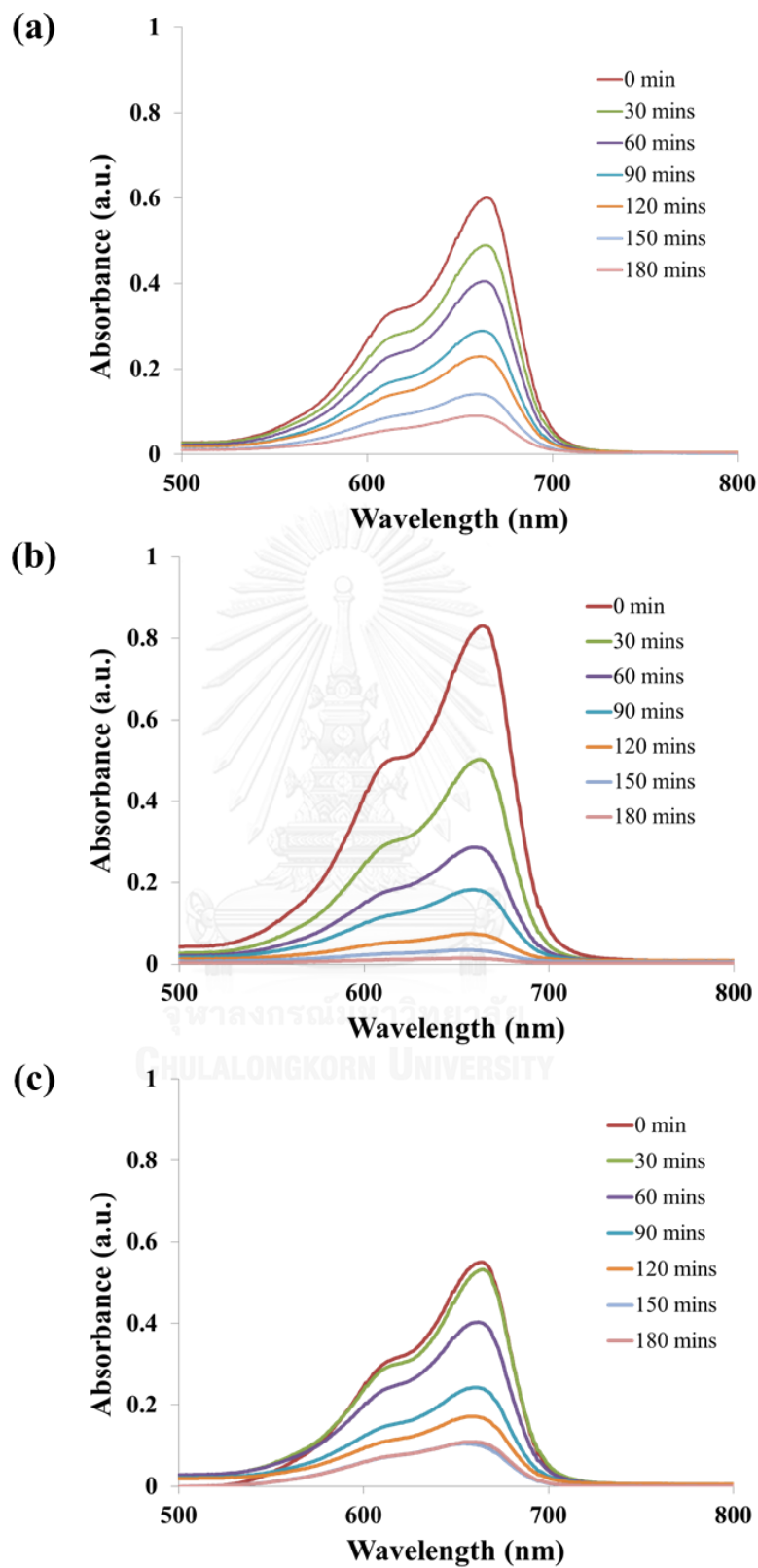


Figure 38 Typical absorbance spectrum of MB solution with sintered ZnO photocatalyst (a) 400°C, (b) 500°C, and (c) 600°C.

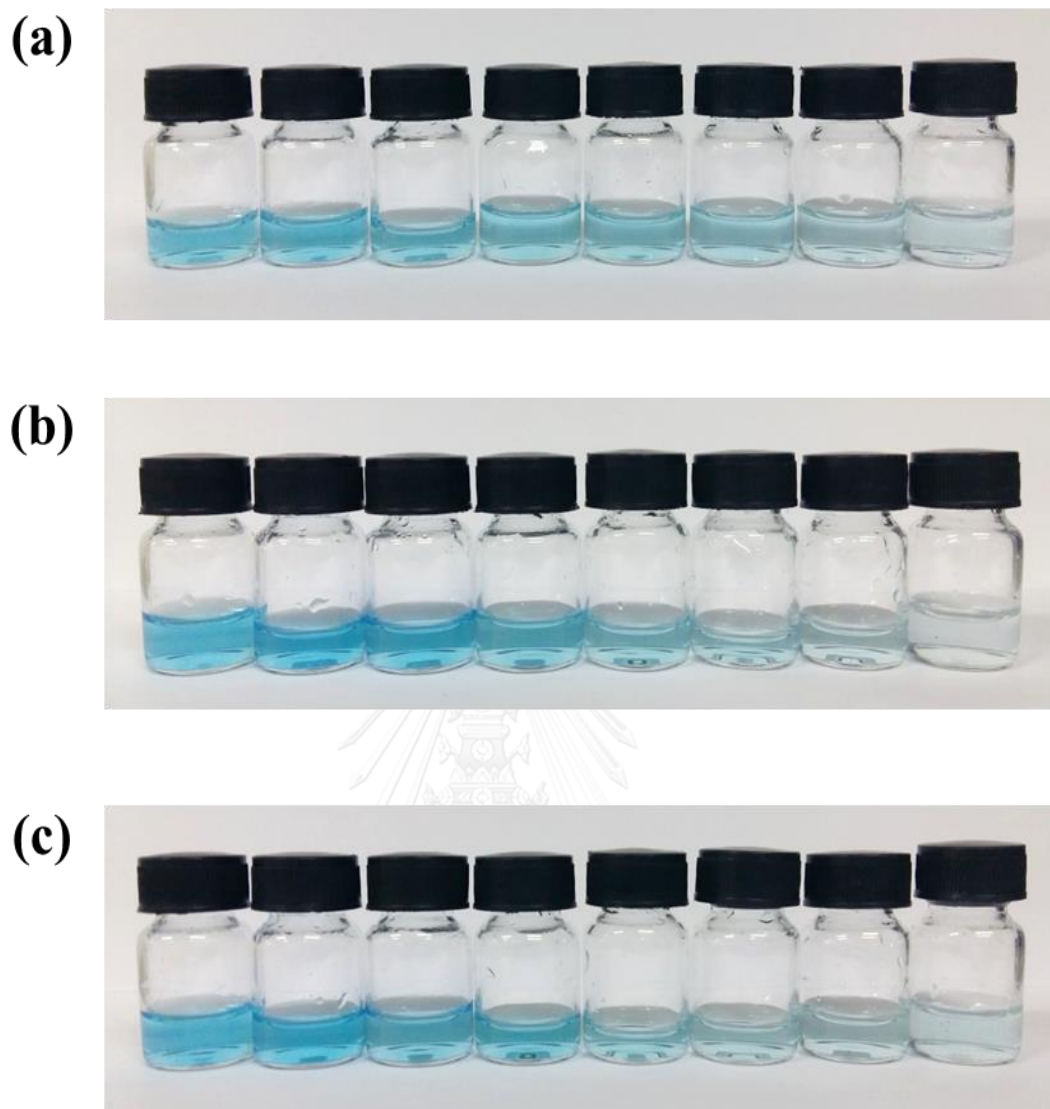


Figure 39 MB solution sampling with ZnO photocatalyst (a) 400°C, (b) 500°C, and (c) 600°C.

Figures 33(a-c) illustrates ZnO films following the tests, indicating that the structures of the samples were generally retained following the tests. Figures 38(a-c) shows the changes of absorbance spectrums of the methylene blue solutions subjected UV light irradiation and immersion of the 3 different sets of ZnO deposits. All 3 groups of the sampling solutions exhibit the characteristic absorbance peaks at 664 nm. Overall, as the immersion duration progressed, the absorbance

levels gradually decreased, reflecting increasing degrees of MB decoloration (Fig.39). Figure 40 shows the normalized concentration of MB from the 3 groups of samples with respect to the reaction time.

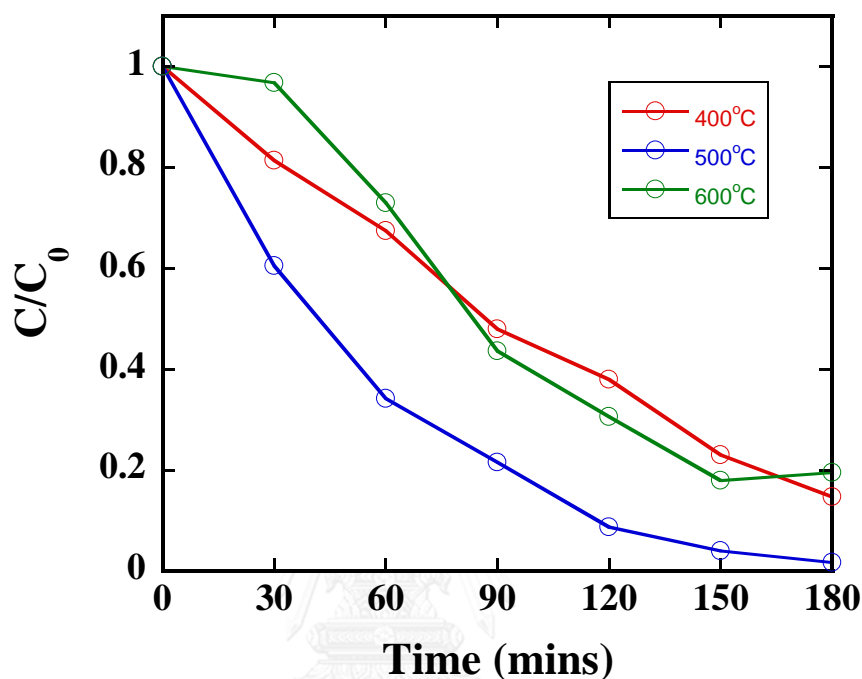


Figure 40 Concentration of MB with respect to irradiation time

The reduction of the concentrations of MB therefore signifies the photocatalytic activity of the ZnO deposits under UV light irradiation. Particularly, electron-hole pairs generated at the surface of ZnO react with water and oxygen to form highly reactive hydroxyl radicals and superoxide radical anions capable of mineralizing the organic substances.

From the concentration profiles in Figure 40, it can be determined that the photodegradation efficiencies of ZnO heat treated at 400°C, 500°C, and 600°C are 86.5%, 98.5%, and 81.3%, respectively. Comparing the photocatalytic activity of ZnO film (Fig.40) to commercial ZnO powder (Fig.36), powder performed better than film due to the higher surface area to volume ratio available for reaction to take place.

However, ZnO films showed good photocatalytic results and can be further improved to be able to compete with powder photocatalyst. The observed variation of the efficiency values suggests that morphology and microstructure of ZnO deposits play important role on photocatalytic activity of the materials. The high surface area in the 500°C samples may provide relatively large effective areas for the radicals to interact with the organic, and vice versa for the 400°C and 600°C samples with lower surface areas. Similar results have been observed in ZnO powder-based catalysts whereby photodegradation efficiency is increased as Zn oxide particles are reduced in size [28].

The determined photodegradation efficiencies are underscored by the EIS Nyquist plots, shown in Fig.41, which are related to the photogenerated charge separation process. The 500°C samples are characterized by relatively small impedance, which suggests an effective separation of the photogenerated electron-hole pair and a more rapid interfacial charge transfer [31]. On the other hand, the plots of the 400°C and 600°C samples have relatively large arc radius reflecting the lower photogenerated charge efficiencies with higher rates of electron-hole pair recombination.



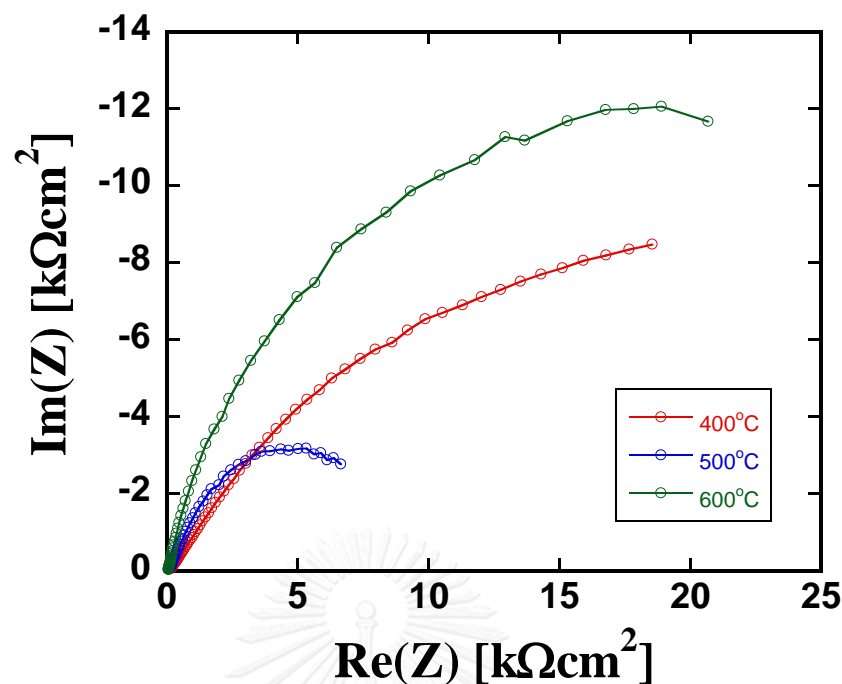


Figure 41 Nyquist plot of EIS for ZnO under UV light irradiation

Having the highest photodegradation efficiency, the 500°C heat treated samples were selected for the stability test. Figure 42 show the reductions of the concentration of MB over the 3 cycles of UV irradiation. The results present small reductions of the photocatalytic activity of the materials following each test cycle. This thus demonstrates that the photocorrosion effect [32], whereby ZnO degrades when interact with positive holes, is minimal. The result is in fact in line with decent stabilities of their microstructure and chemical profile as depicted in Figs. 33 and 34. The photocatalytic ZnO films that are fabricated by zinc electrodeposition and subsequent heat treatment are therefore well-reusable at fairly high photodegradation efficiencies.

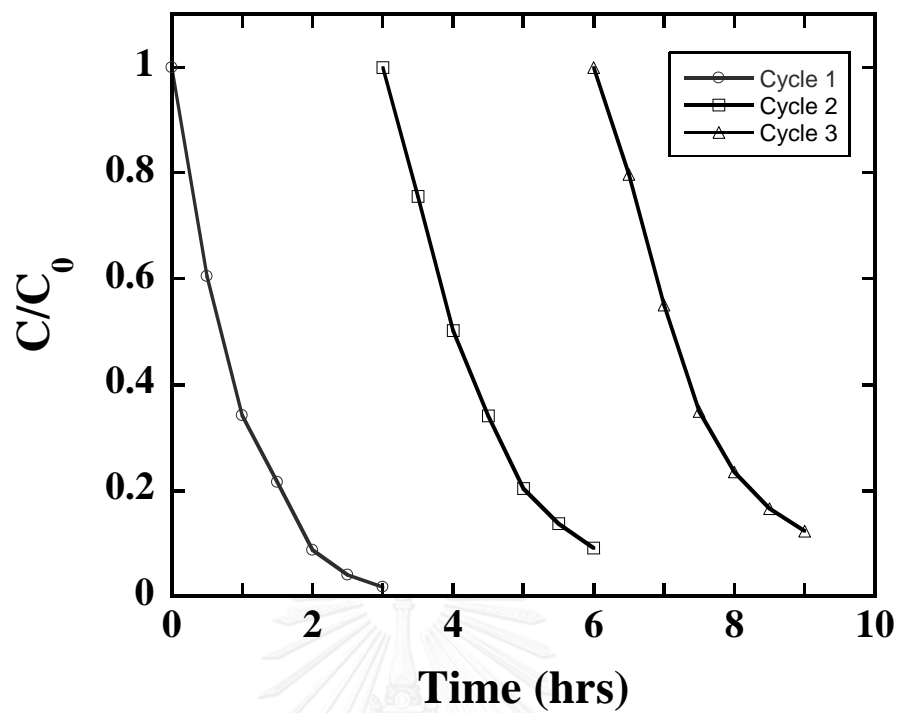


Figure 42 Repeated experiments of ZnO photocatalyst sintered at 500°C.

## CHAPTER V

### CONCLUSION

Nanostructured ZnO thin films were successfully fabricated via the electrodeposition and heat treatment process. The structure of both Zn and ZnO thin films can be influenced by the processing parameters. An effective pure ZnO photocatalyst with good photostability was obtained. The successive studies provide important findings:

#### **Part I: Influence of process variables on structure and property of zinc**

The organic additives in the electrodeposition of zinc coatings play an important role in controlling the structure of the zinc layer. Additives also influence the formation of the chromate conversion film. This subsequently influences a level of corrosion resistance in the coatings, as observed under the wet-dry cyclic saline environment. Among the organic additives in the polyamine group under investigation, polyethyleneimine provided a relatively high level of corrosion resistance for both the zinc layer and its adjacent conversion layer. The high chromium content in the chromate conversion coating layer and a structure of the zinc layer that promotes a formation of passive films of corrosion products are among possible key factors responsible for the improved corrosion resistance.

The current density also plays an important role in controlling the structure of zinc and in the formation of zinc oxide film. At high current density without additive, protruding surface irregularities and a higher

thickness of coating layers are formed. There is an optimum current density value to obtain a good deposit.

### **Part II: Heat treatment of zinc**

ZnO nanostructured thin films were synthesized via heat treatment of electrodeposited zinc films. The structure and surface morphology of the ZnO film can be controlled from the structure of the zinc precursor and oxidation temperature. The oxidation reaction of zinc can occur above and below the melting point of zinc metal. At 300°C, zinc was only partially transformed to zinc oxide. The total transformation of zinc oxide occurred at ZnO films annealed at 400°C, 500°C, and 600°C. A needle-like structure was formed and grown using the zinc deposit structure. For higher heat treatment temperature of 500°C and 600°C, ZnO nanosphere was observed and with a larger size with increasing temperature.

### **Part III: Photocatalytic ZnO**

ZnO thin films at 500°C can effectively degrade MB dye from the water under UV light irradiation and only about 10% of MB dye remained after the film was used for three successive cycles. From SEM and XRD results, the obtained pure ZnO film showed good photostabilization. The microstructure and charge recombination of the photoinduced electrons and holes play a role in affecting the photocatalytic activity. The increase in the surface area enhanced the photocatalytic activity.

Finally, from the experiments conducted in this research, nanostructured ZnO thin film with good photocatalytic property can be synthesized from electrodeposition and heat treatment method. The electrodeposition system is simple and can be done at

low temperature. The process can control the film thickness and morphology accurately. The understanding achieved from each part may be generalized for other synthesis method and applications.



## REFERENCES

1. Lee, K.M., et al., *Recent developments of zinc oxide based photocatalyst in water treatment technology: A review*. Water Research, 2016. **88**: p. 428-448.
2. Fujishima, A., T.N. Rao, and D.A. Tryk, *Titanium dioxide photocatalysis*. Journal of Photochemistry and Photobiology C: Photochemistry Reviews, 2000. **1**(1): p. 1-21.
3. Khedr, M.H., K.S. Abdel Halim, and N.K. Soliman, *Synthesis and photocatalytic activity of nano-sized iron oxides*. Materials Letters, 2009. **63**(6-7): p. 598-601.
4. Shukla, S., et al., *Surfactant functionalized tungsten oxide nanoparticles with enhanced photocatalytic activity*. Chemical Engineering Journal, 2016. **288**: p. 423-431.
5. Kodihalli, G.C. and V.V. Thimmappa, *Electrochemical Synthesis and Photocatalytic Property of Zinc Oxide Nanoparticles*. Nano-Micro Letters, 2012. **4**(1): p. 14-24.
6. Anderson, J. and G.V.d.W. Chris, *Fundamentals of zinc oxide as a semiconductor*. Reports on Progress in Physics, 2009. **72**(12): p. 126501.
7. Daneshvar, N., D. Salari, and A.R. Khataee, *Photocatalytic degradation of azo dye acid red 14 in water on ZnO as an alternative catalyst to TiO<sub>2</sub>*. Journal of Photochemistry and Photobiology A: Chemistry, 2004. **162**(2-3): p. 317-322.
8. Hariharan, C., *Photocatalytic degradation of organic contaminants in water by ZnO nanoparticles: Revisited*. Applied Catalysis A: General, 2006. **304**: p. 55-61.
9. Hong, R., et al., *Synthesis and surface modification of ZnO nanoparticles*. Chemical Engineering Journal, 2006. **119**(2-3): p. 71-81.
10. Hong, R.Y., et al., *Synthesis, surface modification and photocatalytic property of ZnO nanoparticles*. Powder Technology, 2009. **189**(3): p. 426-432.
11. Li, D. and H. Haneda, *Morphologies of zinc oxide particles and their effects on photocatalysis*. Chemosphere, 2003. **51**(2): p. 129-137.

12. Kagaya, S., et al., *Separation of titanium dioxide photocatalyst in its aqueous suspensions by coagulation with basic aluminium chloride*. Water Research, 1999. **33**(7): p. 1753-1755.
13. Wang, H., et al., *Microstructures and photocatalytic properties of porous ZnO films synthesized by chemical bath deposition method*. Applied Surface Science, 2012. **258**(10): p. 4288-4293.
14. Pung, S.-Y., W.-P. Lee, and A. Aziz, *Kinetic Study of Organic Dye Degradation Using ZnO Particles with Different Morphologies as a Photocatalyst*. International Journal of Inorganic Chemistry, 2012. **2012**: p. 9.
15. Pauporté, T. and J. Rathouský, *Electrodeposited Mesoporous ZnO Thin Films as Efficient Photocatalysts for the Degradation of Dye Pollutants*. The Journal of Physical Chemistry C, 2007. **111**(21): p. 7639-7644.
16. Wu, J.J. and S.C. Liu, *Low-Temperature Growth of Well-Aligned ZnO Nanorods by Chemical Vapor Deposition*. Advanced Materials, 2002. **14**(3): p. 215-218.
17. Toumiat, A., et al., *Effect of nitrogen reactive gas on ZnO nanostructure development prepared by thermal oxidation of sputtered metallic zinc*. Nanotechnology, 2006. **17**(3): p. 658-663.
18. Jongnavakit, P., et al., *Surface and photocatalytic properties of ZnO thin film prepared by sol-gel method*. Thin Solid Films, 2012. **520**(17): p. 5561-5567.
19. S., I., C. Y., and C. M., *Preparation and characterization of ZnO thin films deposited by sol-gel spin coating method*. Vol. 10. 2008, Bucuresti: INOE 2000. 2578-2583.
20. Yan, H., et al., *Growth and photocatalytic properties of one-dimensional ZnO nanostructures prepared by thermal evaporation*. Materials Research Bulletin, 2009. **44**(10): p. 1954-1958.

21. Fouad, O.A., et al., *Zinc oxide thin films prepared by thermal evaporation deposition and its photocatalytic activity*. Applied Catalysis B: Environmental, 2006. **62**(1–2): p. 144-149.
22. Postels, B., et al., *Electrodeposition of ZnO nanorods for device application*. Applied Physics A: Materials Science & Processing, 2008. **91**(4): p. 595-599.
23. Luisa Peraldo Bicelli, B.B., Claudio Mele, Lucia D'Urzo, *A Review of Nanostructural Aspects of Metal Electrodeposition*. Int. J. Electrochem. Sci., 2008. **3**: p. 356-408.
24. Gupta, R.K., N. Shridhar, and M. Katiyar, *Structure of ZnO films prepared by oxidation of metallic Zinc*. Materials Science in Semiconductor Processing, 2002. **5**(1): p. 11-15.
25. Yu, W. and C. Pan, *Low temperature thermal oxidation synthesis of ZnO nanoneedles and the growth mechanism*. Materials Chemistry and Physics, 2009. **115**(1): p. 74-79.
26. Bouhssira, N., et al., *Influence of annealing temperature on the properties of ZnO thin films deposited by thermal evaporation*. Applied Surface Science, 2006. **252**(15): p. 5594-5597.
27. Vu, T.T., et al., *Fabrication of wire mesh-supported ZnO photocatalysts protected against photocorrosion*. Applied Catalysis B: Environmental, 2013. **140–141**: p. 189-198.
28. Dodd, A.C., et al., *Effect of Particle Size on the Photocatalytic Activity of Nanoparticulate Zinc Oxide*. Journal of Nanoparticle Research, 2006. **8**(1): p. 43.
29. Ali, M.A., M.R. Idris, and M.E. Quayum, *Fabrication of ZnO nanoparticles by solution-combustion method for the photocatalytic degradation of organic dye*. Journal of Nanostructure in Chemistry, 2013. **3**(1): p. 36.
30. Wang, M., G. Fei, and L. De Zhang, *Porous-ZnO-Nanobelt Film as Recyclable Photocatalysts with Enhanced Photocatalytic Activity*. Nanoscale Research Letters, 2010. **5**(11): p. 1800-1803.



31. Chen, Y.J., et al., *Controlled growth of zinc nanowires*. Materials Letters, 2007. **61**(1): p. 144-147.
32. Paunovic, M., et al., *Fundamentals of electrochemical deposition*. 2006, Wiley: Hoboken, N.J. .:
33. Al-Bat'hi, S.A.M., *Electrodeposition of Nanostructure Materials*, in *Electroplating of Nanostructures*, M. Aliofkhazraei, Editor. 2015, InTech: Rijeka. p. Ch. 01.
34. Güler, E.S., *Effects of Electroplating Characteristics on the Coating Properties*, in *Electrodeposition of Composite Materials*, A.M.A. Mohamed and T.D. Golden, Editors. 2016, InTech: Rijeka. p. Ch. 02.
35. Vagramyan, T., J.S.L. Leach, and J.R. Moon, *The structures of zinc electrodeposits formed at low current densities*. Journal of Materials Science, 1979. **14**(5): p. 1170-1174.
36. Geduld, H., *Zinc plating*. 1988: Finishing Publications.
37. Hsieh, J.-C., C.-C. Hu, and T.-C. Lee, *Effects of polyamines on the deposition behavior and morphology of zinc electroplated at high-current densities in alkaline cyanide-free baths*. Surface and Coatings Technology, 2009. **203**(20–21): p. 3111-3115.
38. Nayana, K.O. and T.V. Venkatesha, *Synergistic effects of additives on morphology, texture and discharge mechanism of zinc during electrodeposition*. Journal of Electroanalytical Chemistry, 2011. **663**(2): p. 98-107.
39. Ortiz-Aparicio, J., et al., *Effects of organic additives on zinc electrodeposition from alkaline electrolytes*. Journal of Applied Electrochemistry, 2013. **43**(3): p. 289-300.
40. Shanmugasigamani and M. Pushpavanam, *Role of additives in bright zinc deposition from cyanide free alkaline baths*. Journal of Applied Electrochemistry, 2006. **36**(3): p. 315-322.

41. Chandrasekar, M.S., S. Srinivasan, and M. Pushpavanam, *Structural and textural study of electrodeposited zinc from alkaline non-cyanide electrolyte*. Journal of Materials Science, 2010. **45**(5): p. 1160-1169.
42. Martyak, N.M., *Grain refinement in electrogalvanized coatings*. Materials Characterization, 2003. **50**(4-5): p. 269-274.
43. Ortiz-Aparicio, J.L., et al., *Effects of organic additives on zinc electrodeposition from alkaline electrolytes*. Journal of Applied Electrochemistry, 2013. **43**(3): p. 289-300.
44. Lan, C.J., C.Y. Lee, and T.S. Chin, *Tetra-alkyl ammonium hydroxides as inhibitors of Zn dendrite in Zn-based secondary batteries*. Electrochimica Acta, 2007. **52**(17): p. 5407-5416.
45. Diggle, J.W. and A. Damjanovic, *The Inhibition of the Dendritic Electrocrystallization of Zinc from Doped Alkaline Zincate Solutions*. Journal of The Electrochemical Society, 1972. **119**(12): p. 1649-1658.
46. Pirnát, A., L. Mészáros, and B. Lengyel, *Study of the formation of chromate layer on zinc by impedance technique*. Electrochimica Acta, 1990. **35**(2): p. 515-522.
47. Gigandet, M.P., J. Faucheu, and M. Tachez, *Formation of black chromate conversion coatings on pure and zinc alloy electrolytic deposits: role of the main constituents*. Surface and Coatings Technology, 1997. **89**(3): p. 285-291.
48. Eppensteiner, F.W. and M.R. Jenkind, *Chromate conversion coatings*. Metal Finishing, 2007. **105**(10): p. 413-424.
49. Lowenheim, F.A., *Modern Electroplating*. 2 ed. 1963, New York: John Wiley & Sons.
50. Wark, I.W., *The electrodeposition of zinc from acidified zinc sulphate solution*. Journal of Applied Electrochemistry, 1979. **9**(6): p. 721-730.

51. Kobya, M., et al., *Treatments of alkaline non-cyanide, alkaline cyanide and acidic zinc electroplating wastewaters by electrocoagulation*. Process Safety and Environmental Protection, 2017. **105**: p. 373-385.
52. Ramesh Babu, K.G.N., G. Devaraj, and J. Ayyapparaj, *Studies on non-cyanide alkaline zinc electrolytes*. Journal of Solid State Electrochemistry, 1998. **3**(1): p. 48-51.
53. Titova, V. and A. Javich, *Studies on electrodeposition of zinc from alkaline electrolyte with surfactants*. Bulletin of Electrochemistry(India), 2000. **16**(9): p. 425-429.
54. Nishikata, A., et al., *An electrochemical impedance study on atmospheric corrosion of steels in a cyclic wet-dry condition*. Corrosion Science, 1995. **37**(12): p. 2059-2069.
55. Nishikata, A., Y. Ichihara, and T. Tsuru, *An application of electrochemical impedance spectroscopy to atmospheric corrosion study*. Corrosion Science, 1995. **37**(6): p. 897-911.
56. El-Mahdy, G.A., A. Nishikata, and T. Tsuru, *Electrochemical corrosion monitoring of galvanized steel under cyclic wet-dry conditions*. Corrosion Science, 2000. **42**(1): p. 183-194.
57. Yadav, A.P., A. Nishikata, and T. Tsuru, *Electrochemical impedance study on galvanized steel corrosion under cyclic wet-dry conditions—influence of time of wetness*. Corrosion Science, 2004. **46**(1): p. 169-181.
58. Bellezze, T., G. Roventi, and R. Fratesi, *Electrochemical study on the corrosion resistance of Cr III-based conversion layers on zinc coatings*. Surface and Coatings Technology, 2002. **155**(2-3): p. 221-230.

59. Palli, S. and S.R. Dey, *Theoretical and Experimental Study of Copper Electrodeposition in a Modified Hull Cell*. International Journal of Electrochemistry, 2016. **2016**: p. 13.
60. Mccolm, T.D. and J.W. Evans, *A Modified Hull Cell and its Application to the Electrodeposition of Zinc*. Journal of Applied Electrochemistry, 2001. **31**(4): p. 411-419.
61. Dargis, R. *The Hull Cell: Key to Better Electroplating - Part I*. 2005.
62. Choopun, S., N. Hongsoth, and E. Wongrat, *Metal-Oxide Nanowires by Thermal Oxidation Reaction Technique*, in *Nanowires*, P. Prete, Editor. 2010, InTech: Rijeka. p. Ch. 05.
63. Ren, S., et al., *Catalyst-free synthesis of ZnO nanowire arrays on zinc substrate by low temperature thermal oxidation*. Materials Letters, 2007. **61**(3): p. 666-670.
64. Rusu, G.G., M. Rusu, and N. Apetroaei, *On the structural changes during thermal oxidation of evaporated Zn thin films*. Thin Solid Films, 2007. **515**(24): p. 8699-8704.
65. Wen, X., et al., *ZnO Nanobelt Arrays Grown Directly from and on Zinc Substrates: Synthesis, Characterization, and Applications*. The Journal of Physical Chemistry B, 2005. **109**(32): p. 15303-15308.
66. Liu, Y., et al., *Synthesis of one-dimensional ZnO nanoneedles using thermal oxidation process in the air and its application as filed emitters*. Materials Letters, 2008. **62**(17-18): p. 2783-2786.
67. Peng, W.-j. and Y.-y. Wang, *Mechanism of zinc electroplating in alkaline zincate solution*. Journal of Central South University of Technology, 2007. **14**(1): p. 37-41.
68. Boto, K., *Organic additives in zinc electroplating*. Electrodeposition and Surface Treatment, 1975. **3**(2): p. 77-95.
69. Jones, F. and M.I. Ogden, *Controlling crystal growth with modifiers*. CrystEngComm, 2010. **12**(4): p. 1016-1023.

70. Paunovic, M. and M. Schlesinger, *Fundamentals of Electrochemical Deposition*. 2006: Wiley.
71. Ashton, R.F. and M.T. Hepworth, *Effect of Crystal Orientation on the Anodic Polarization and Passivity of Zinc*. *Corrosion*, 1968. **24**(2): p. 50-53.
72. Park, H. and J.A. Szpunar, *The role of texture and morphology in optimizing the corrosion resistance of zinc-based electrogalvanized coatings*. *Corrosion Science*, 1998. **40**(4–5): p. 525-545.
73. Wang, R.Y., D.W. Kirk, and G.X. Zhang, *Effects of Deposition Conditions on the Morphology of Zinc Deposits from Alkaline Zincate Solutions*. *Journal of The Electrochemical Society*, 2006. **153**(5): p. C357-C364.
74. Otani, T., et al., *Morphological evolution of mossy structures during the electrodeposition of zinc from an alkaline zincate solution*. *Electrochimica Acta*, 2016. **206**: p. 366-373.
75. Wang, Y., et al., *Self-assembled urchin-like ZnO nanostructures fabricated by electrodeposition-hydrothermal method*. *Journal of Alloys and Compounds*, 2016. **665**: p. 62-68.
76. Dulle, J., et al., *Sononanostructuring of zinc-based materials*. *RSC Advances*, 2012. **2**(32): p. 12460-12465.
77. Hayes, R., et al., *Core-shell particles: Preparation, fundamentals and applications in high performance liquid chromatography*. *Journal of Chromatography A*, 2014. **1357**: p. 36-52.

## APPENDIX

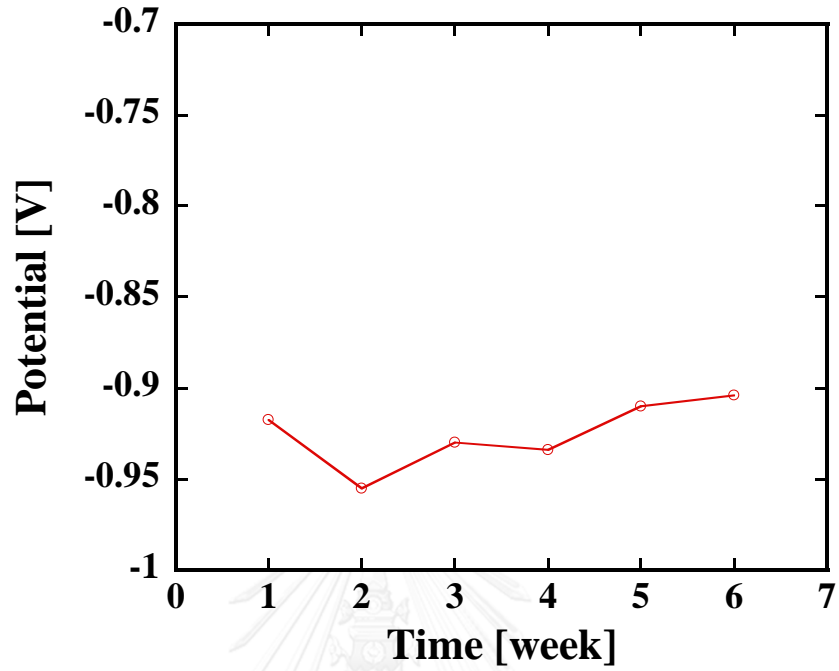


Figure 1 Open-circuit potential measurement for EZ1 sample.

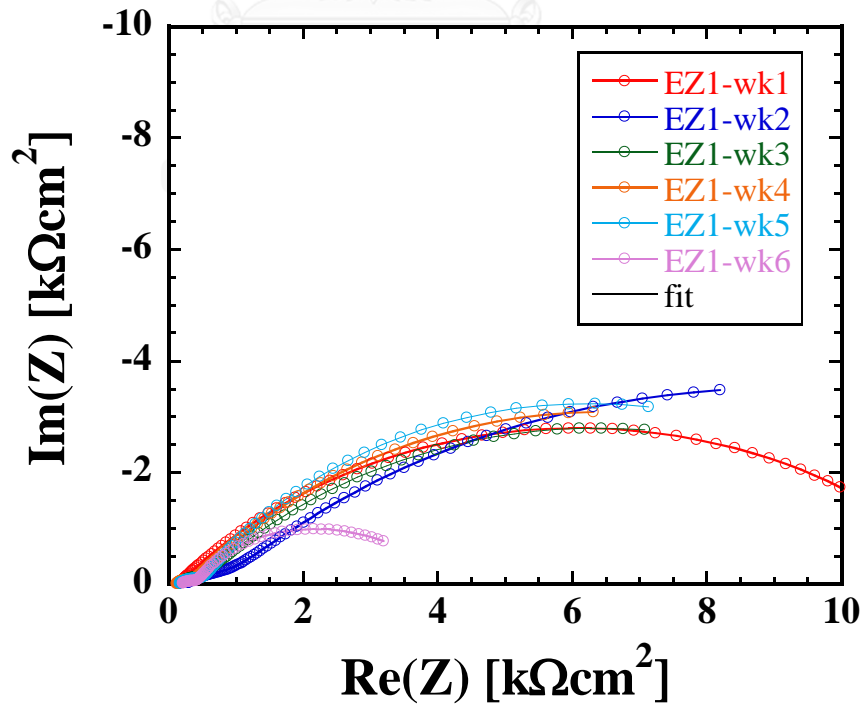


Figure 2 Nyquist plot of EIS for EZ1 sample throughout the six week of cyclic exposure test

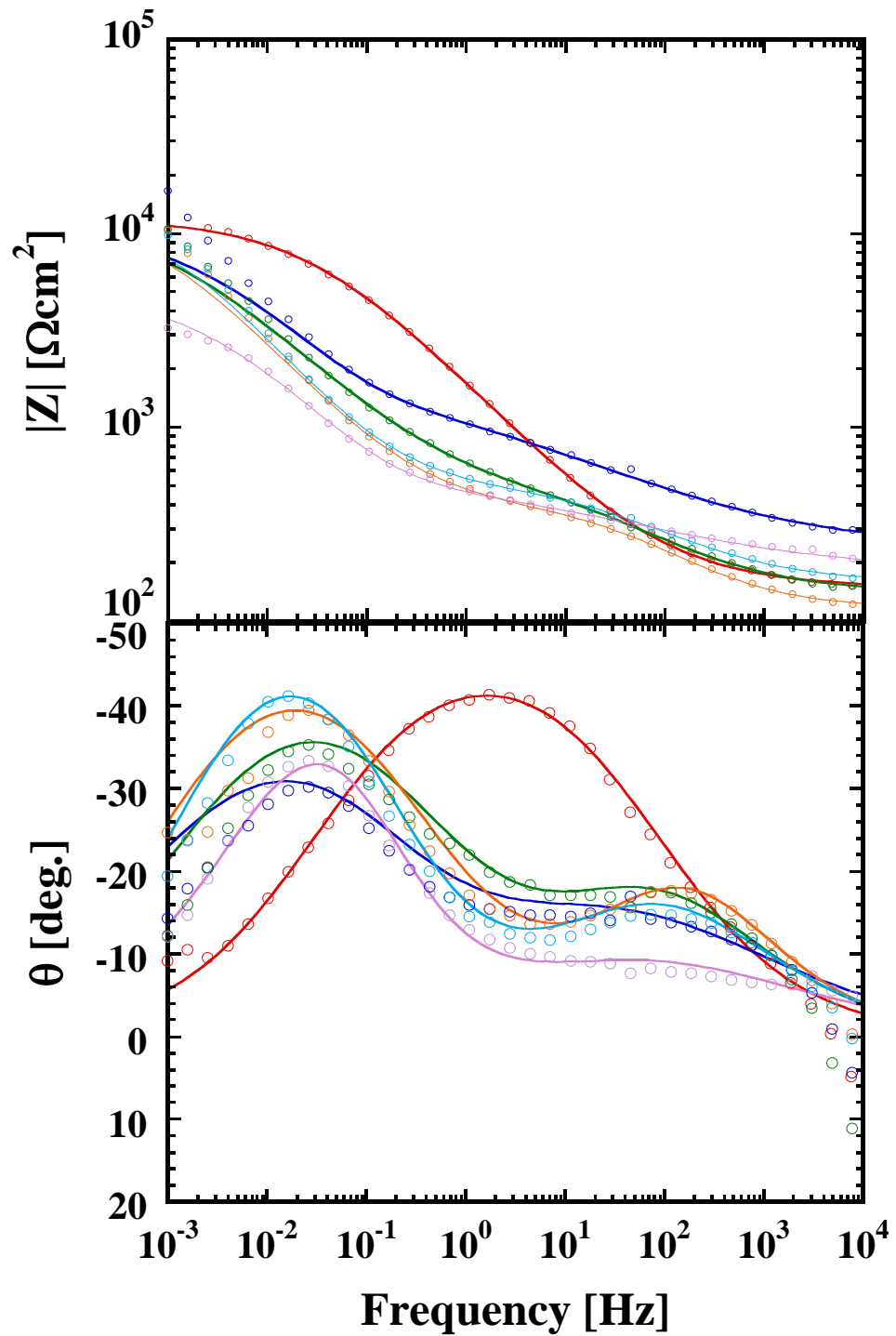


Figure 3 Bode magnitude and phase plot of EIS for EZ1 sample throughout the six week of cyclic exposure test.

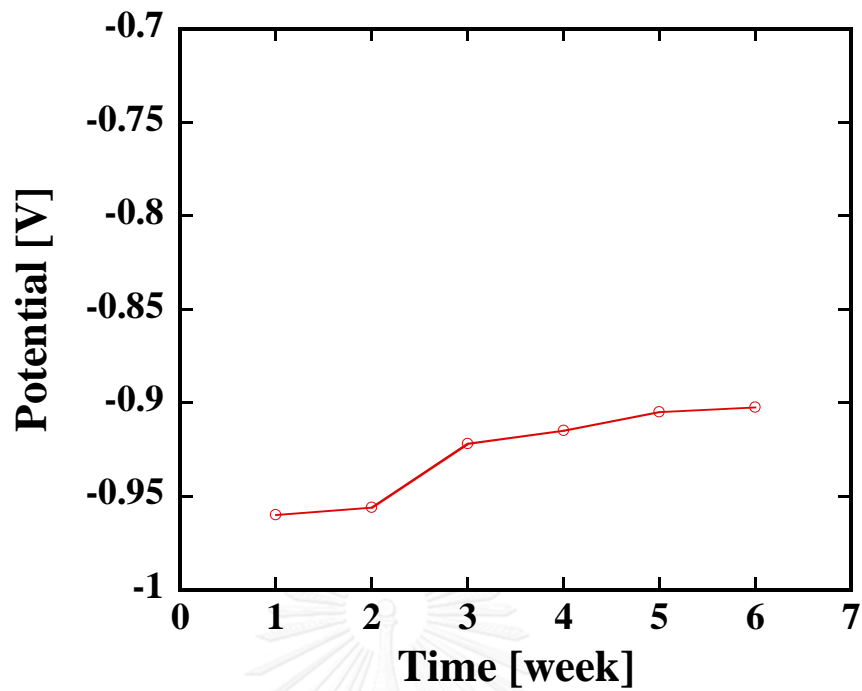


Figure 4 Open-circuit potential measurement for EZ2 sample.

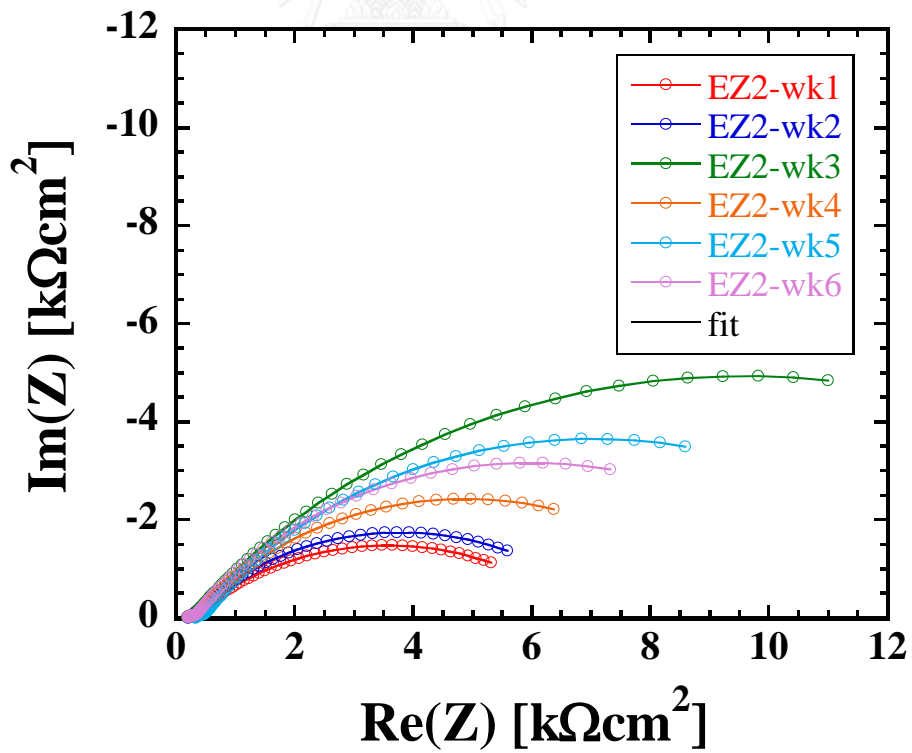


Figure 5 Nyquist plot of EIS for EZ2 sample throughout the six week of cyclic exposure test.



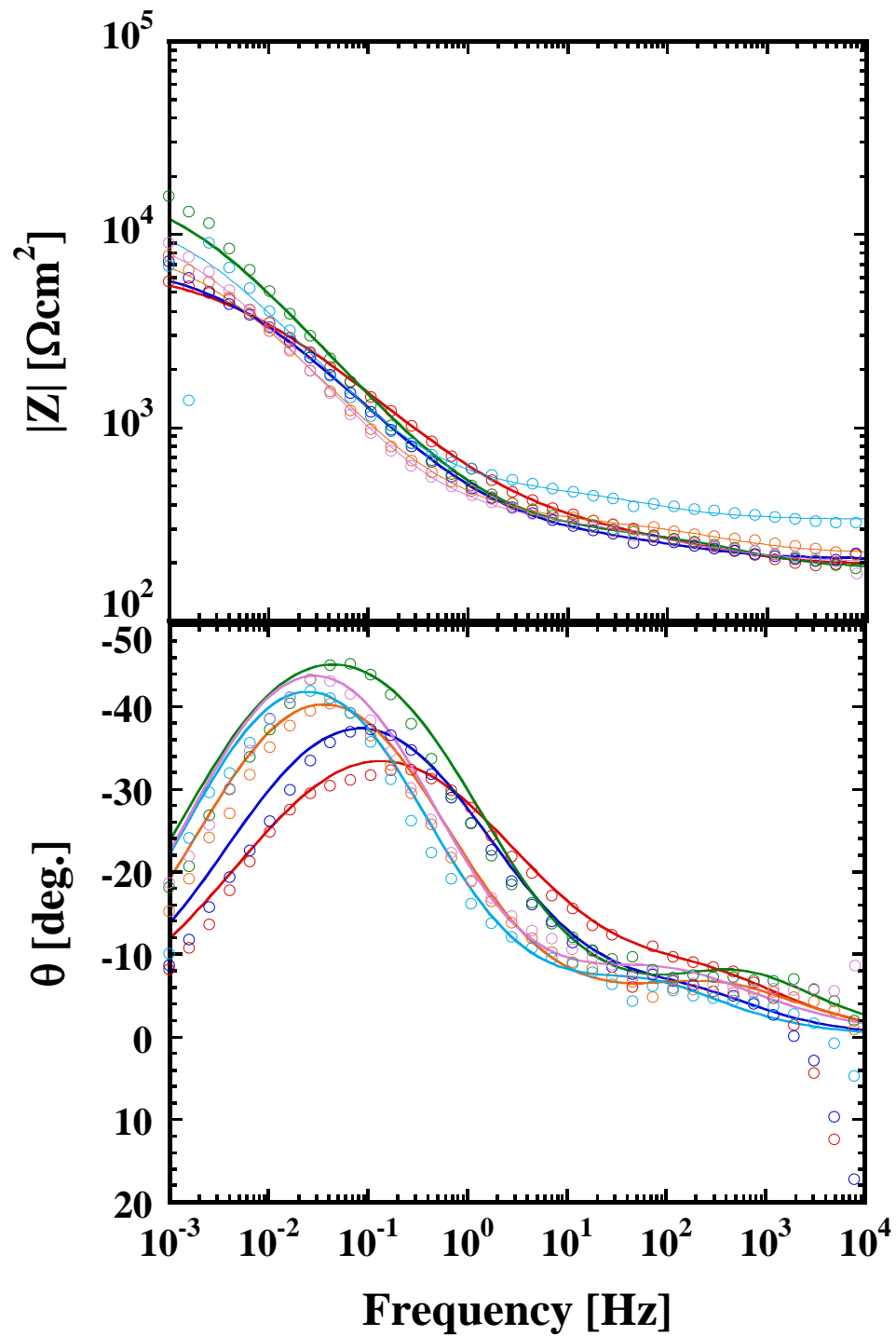


Figure 6 Bode magnitude and phase plot of EIS for EZ2 sample throughout the six week of cyclic exposure test.

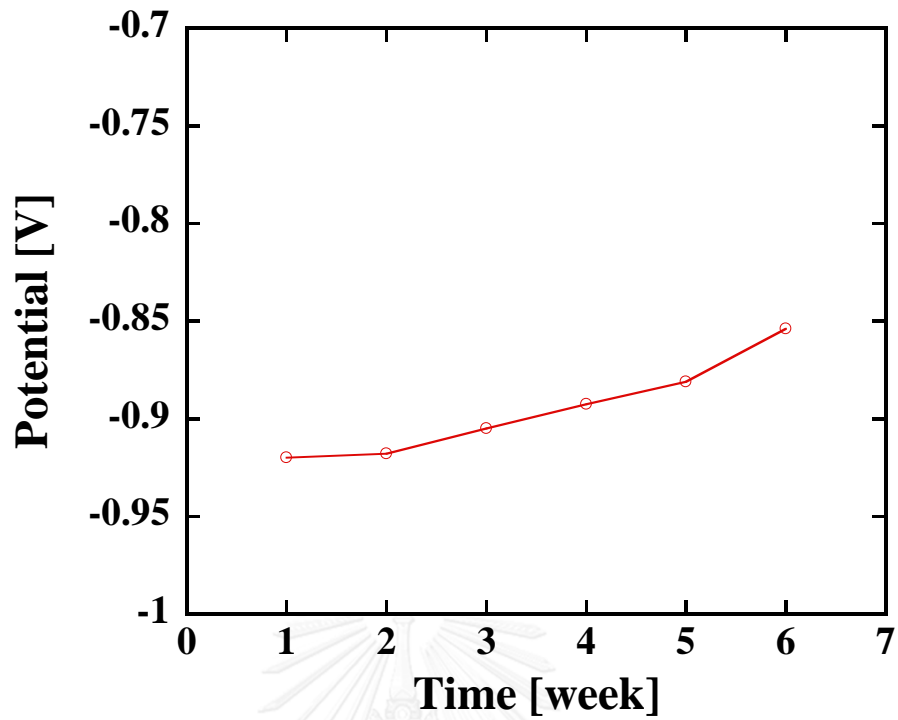


Figure 7 Open-circuit potential measurement for EZ3 sample.

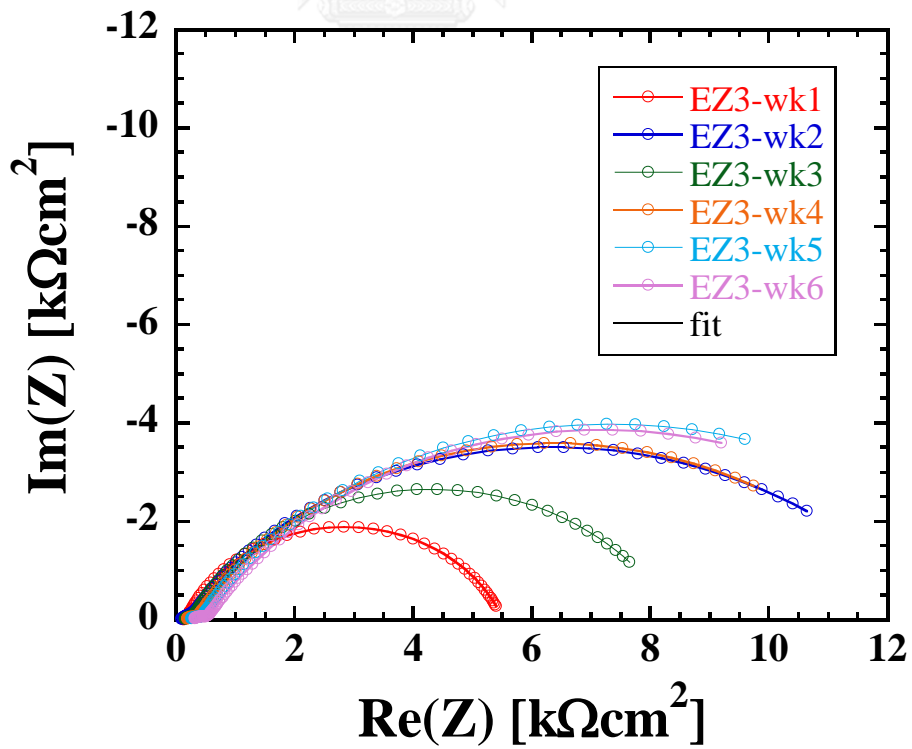


Figure 8 Nyquist plot of EIS for EZ3 sample throughout the six week of cyclic exposure test.

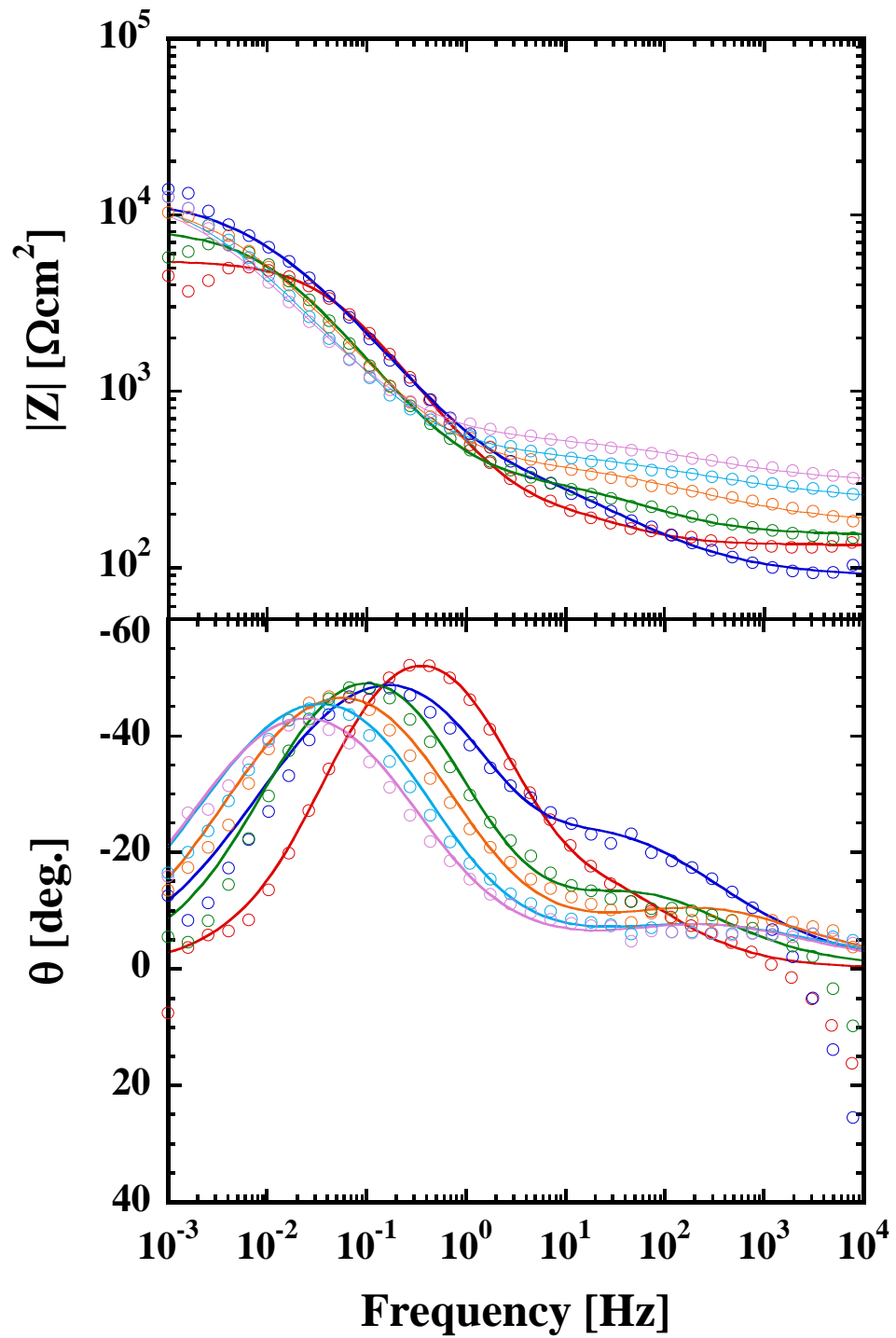


Figure 9 Bode magnitude and phase plot of EIS for EZ3 sample throughout the six week of cyclic exposure test.

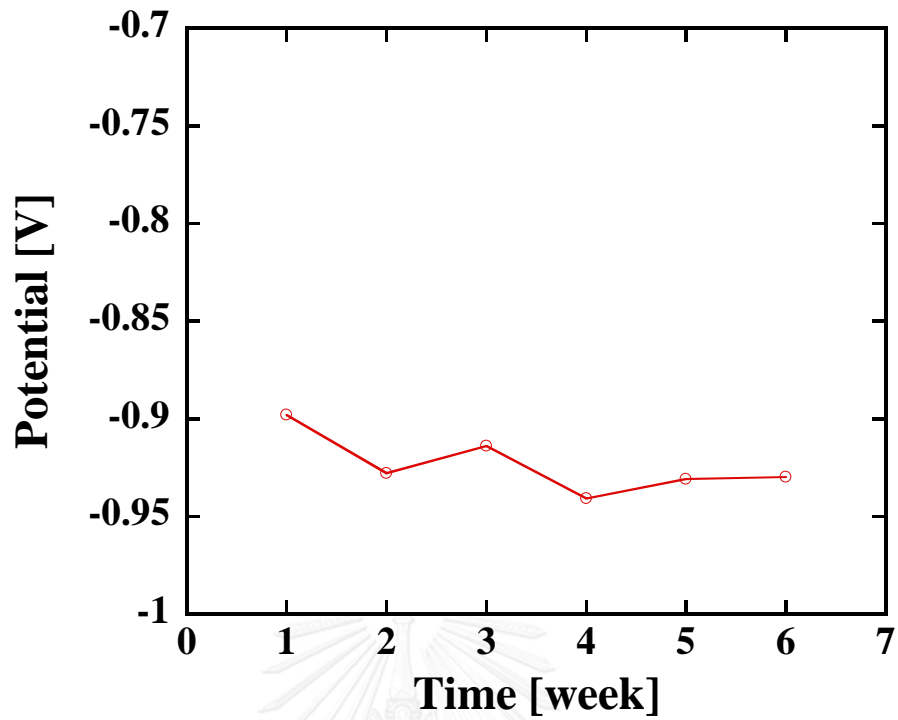


Figure 10 Open-circuit potential measurement for EZP1 sample.

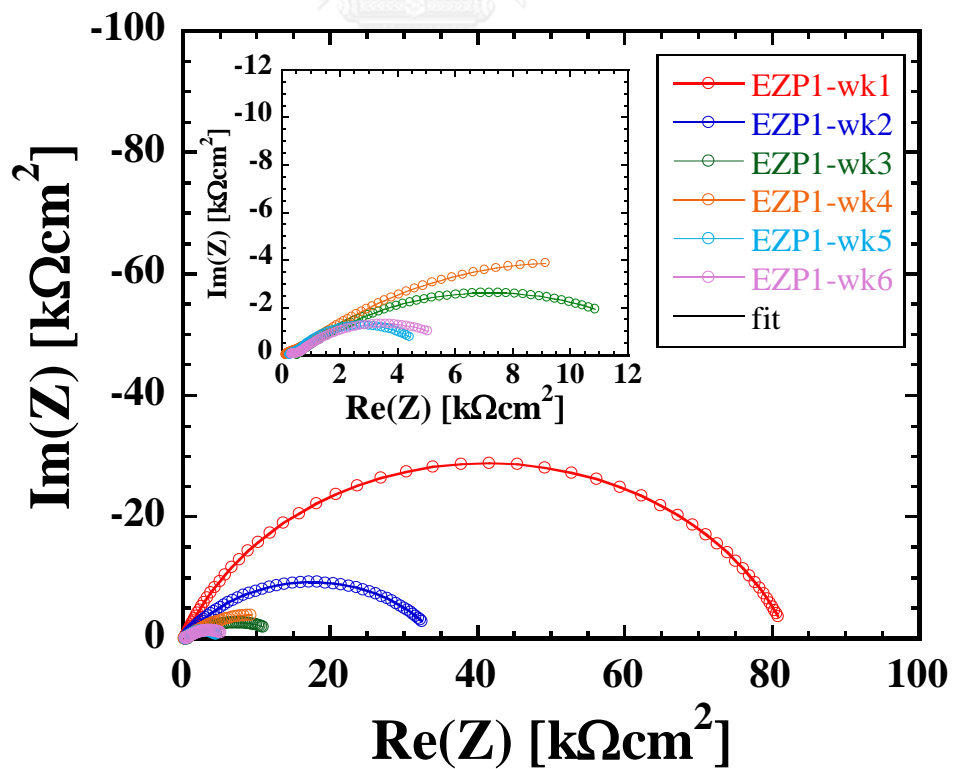


Figure 11 Nyquist plot of EIS for EZP1 sample throughout the six week of cyclic exposure test.

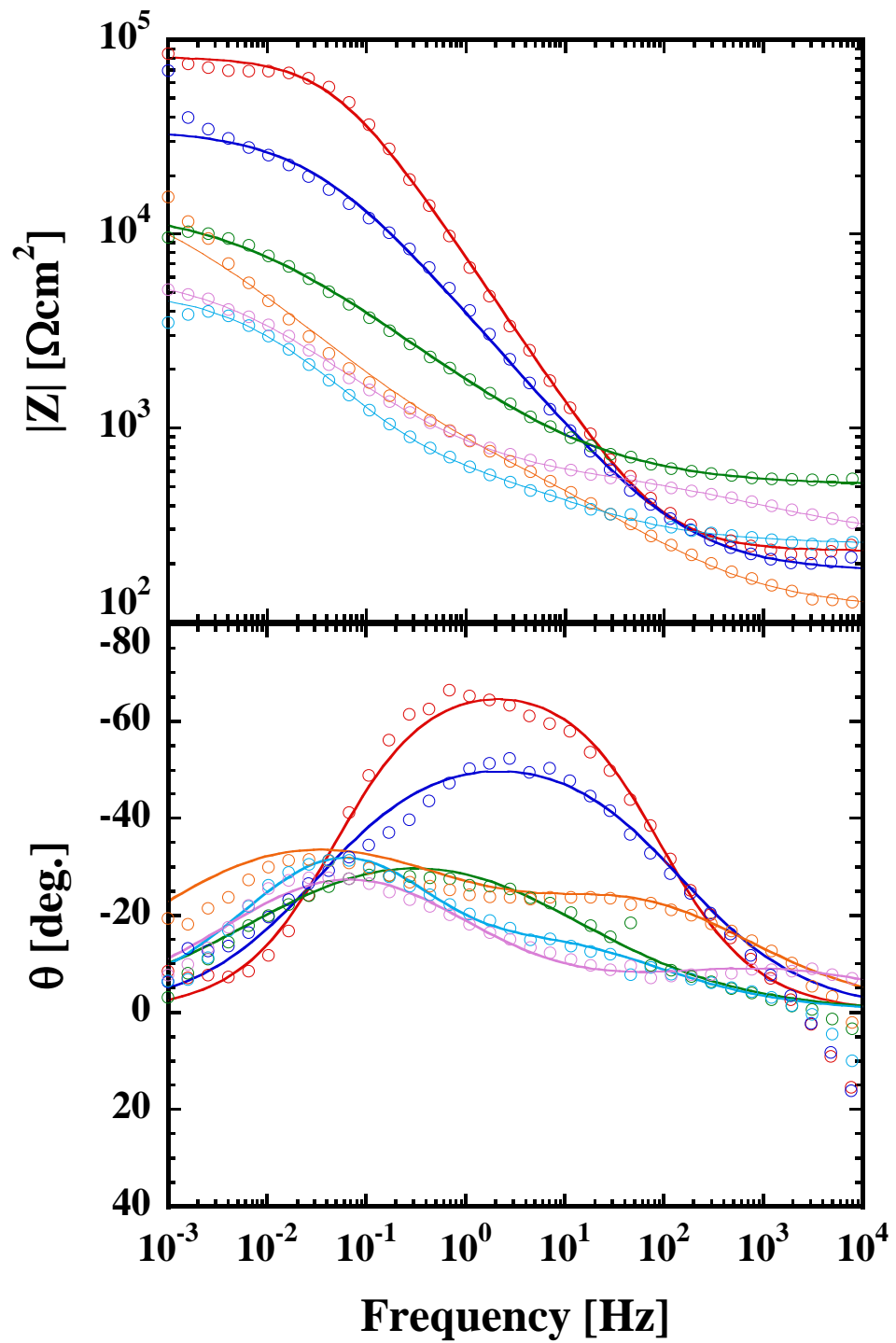


Figure 12 Bode magnitude and phase plot of EIS for EZP1 sample throughout the six week of cyclic exposure test.

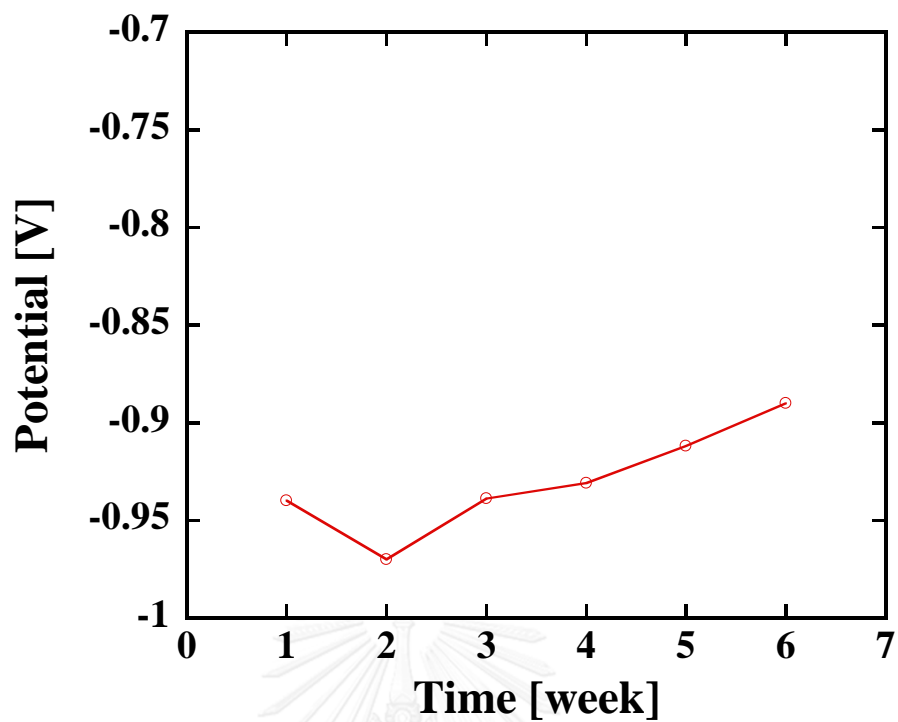


Figure 13 Open-circuit potential measurement for EZP2 sample.

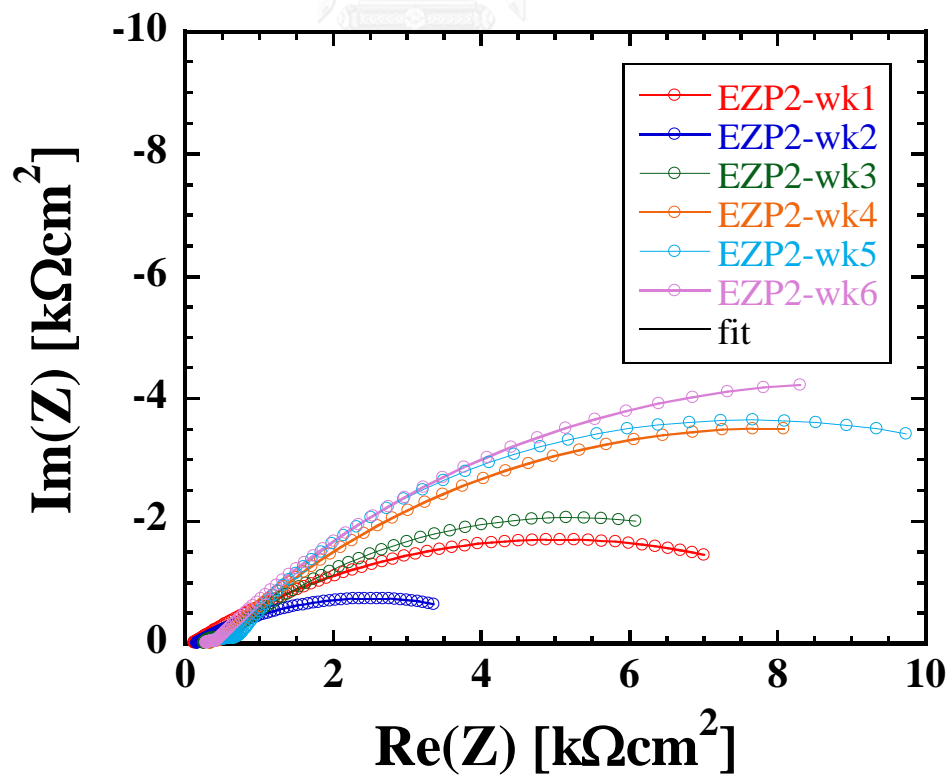


Figure 14 Nyquist plot of EIS for EZP2 sample throughout the six week of cyclic exposure test.

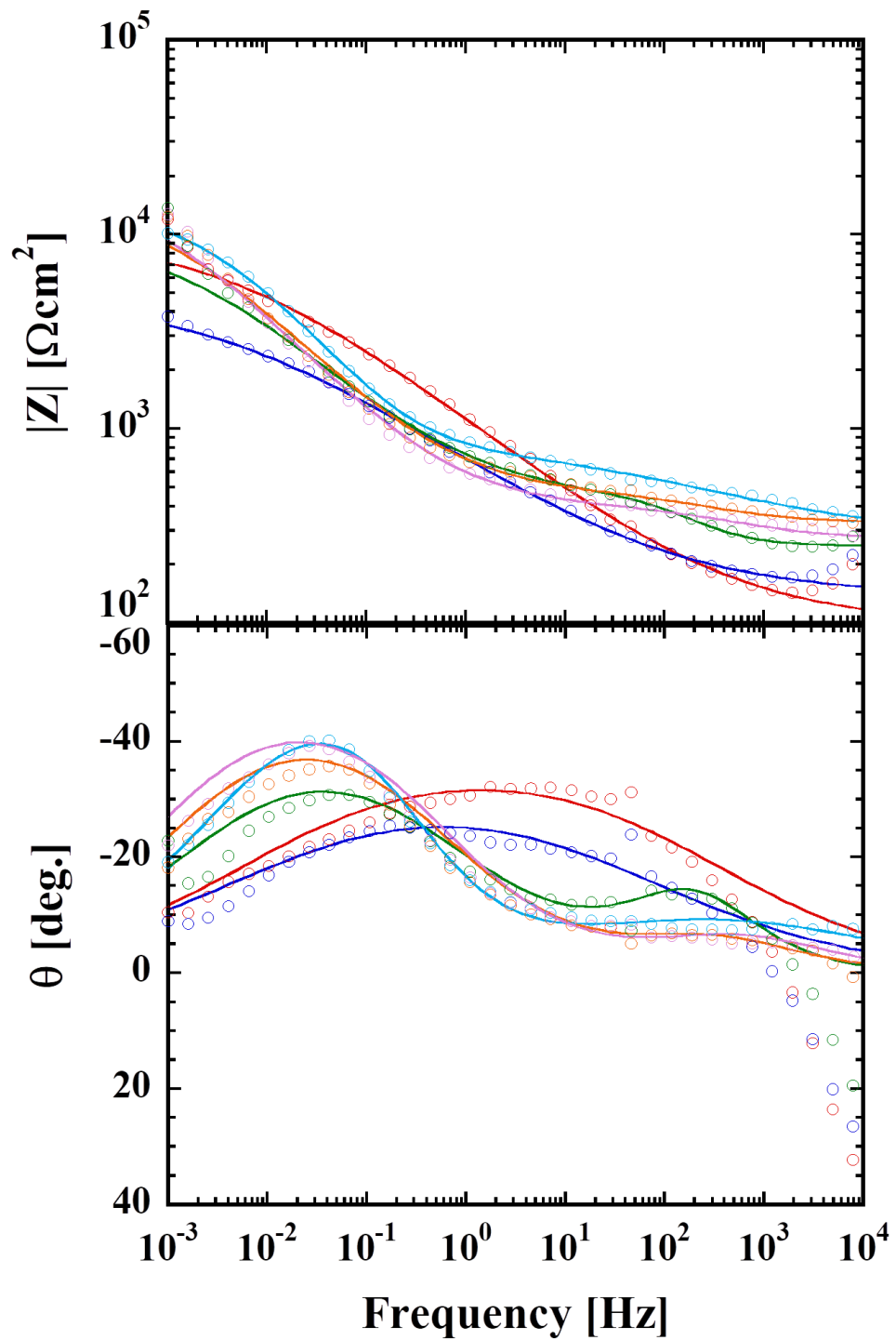


Figure 15 Bode magnitude and phase plot of EIS for EYP2 sample throughout the six week of cyclic exposure test.

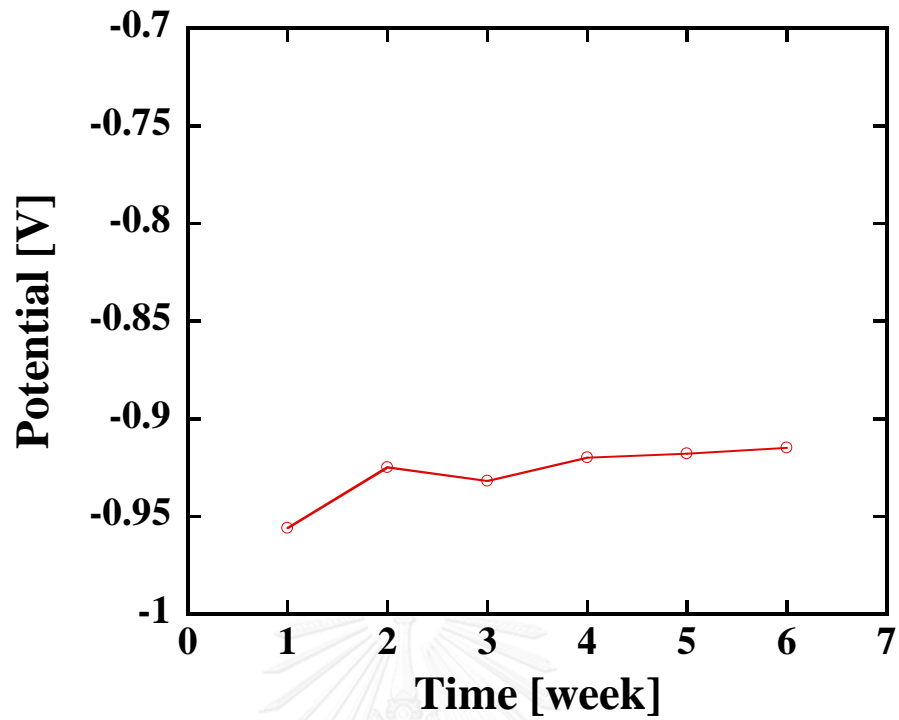


Figure 16 Open-circuit potential measurement for EZP3 sample.

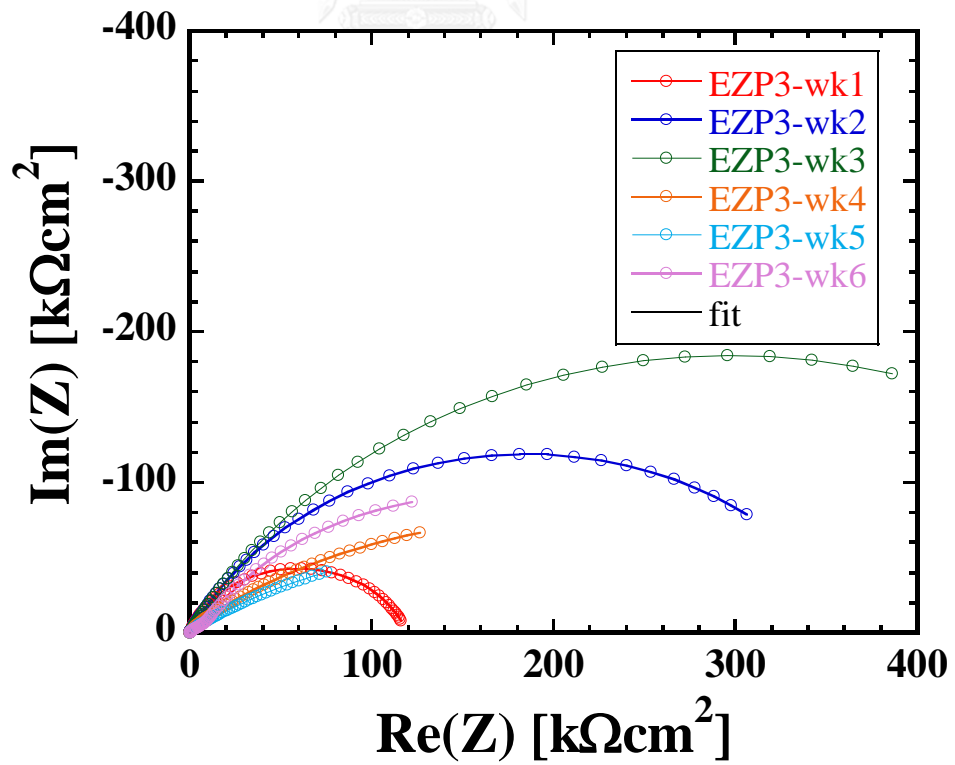


Figure 17 Nyquist plot of EIS for EZP3 sample throughout the six week of cyclic exposure test.



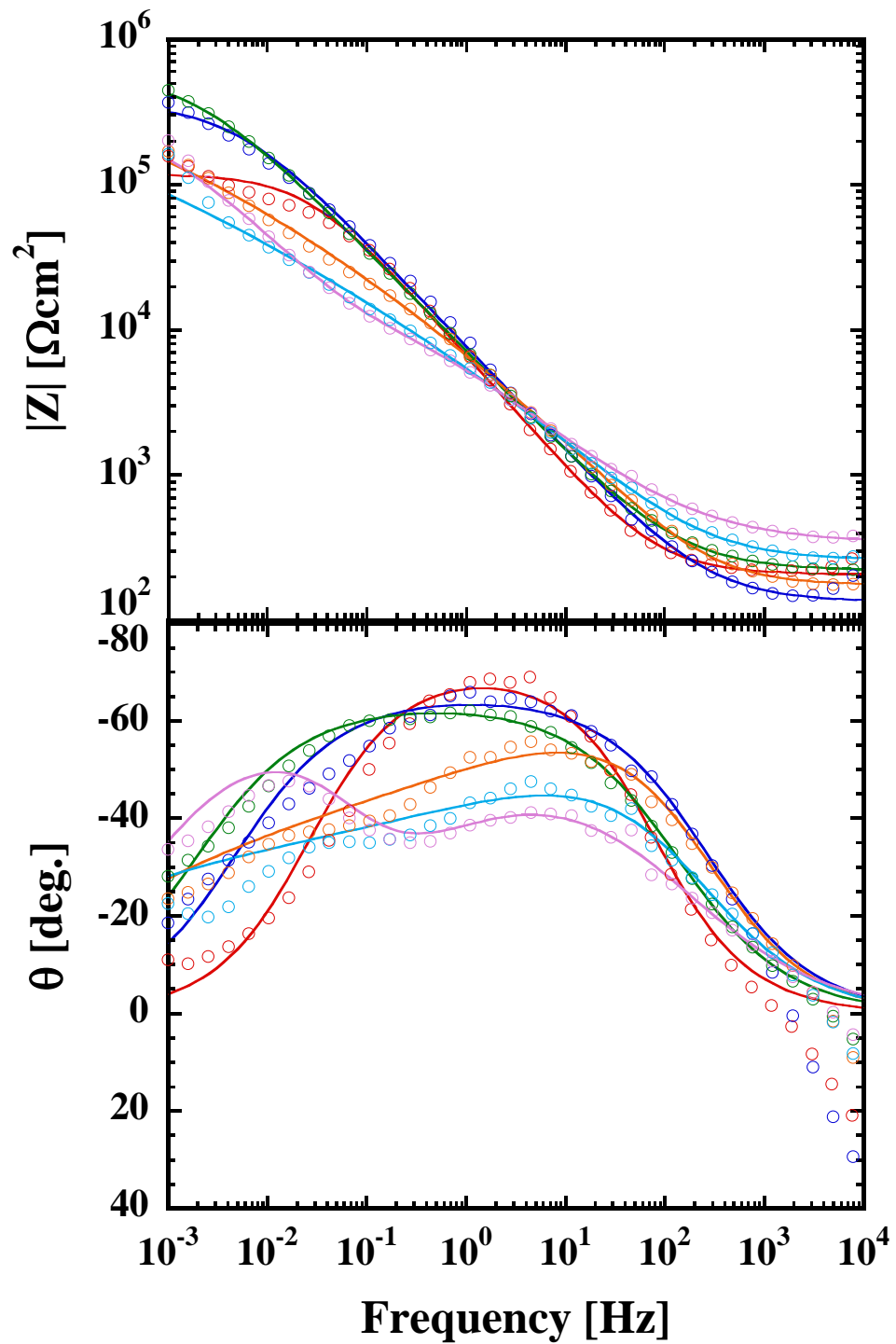


Figure 18 Bode magnitude and phase plot of EIS for EZP3 sample throughout the six week of cyclic exposure test.

**VITA**

Name Miss Thanyalux Wanotayan

Nationality Thai

Date of Birth December 3, 1990

**Education**

2011 Bachelor of Engineering (B.Eng) in Electrical and Electronics Engineering, Asian University, Chonburi, Thailand

2011-present Doctor of Philosophy (Ph.D.) in Nanoscience and Technology Program, Chulalongkorn University, Bangkok, Thailand

2014 Conduct research at Tokyo Institute of Technology, Tokyo, Japan

